Oligomerisation, Localisation and Interaction of the sensor histidine kinases DcuS and CitA in *Escherichia coli*

Dissertation

zur Erlangung des Grades

„Doktor der Naturwissenschaften“

Am Fachbereich Biologie

der Johannes Gutenberg-Universität

in Mainz

vorgelegt von

Patrick Daniel Scheu

geb. am 17.06.1980 in Medellín

Mainz, November 2009

Dekan:

1. Berichterstatter:

2. Berichterstatter:

Tag der mündlichen Prüfung: 11.12.2009

Contents

1. Abstract

The two-component system DcuSR of *Escherichia coli* regulates gene expression of anaerobic fumarate respiration and aerobic C_4-dicarboxylate uptake. C_4-dicarboxylates and citrate are perceived by the periplasmic domain of the membrane-integral sensor histidine kinase DcuS. The signal is transduced across the membrane by phosphorylation of DcuS and of the response regulator DcuR, resulting in activation of DcuR and transcription of the target genes.

In this work, the oligomerisation of full-length DcuS was studied *in vivo* and *in vitro*. DcuS was genetically fused to derivatives of the green fluorescent protein (GFP), enabling fluorescence resonance energy transfer (FRET) measurements to detect protein-protein interactions *in vivo*. FRET measurements were also performed with purified His_6-DcuS after labelling with fluorescent dyes and reconstitution into liposomes to study oligomerisation of DcuS *in vitro*. *In vitro* and *in vivo* fluorescence resonance energy transfer showed the presence of oligomeric DcuS in the membrane, which was independent of the presence of effector. Chemical crosslinking experiments allowed clear-cut evaluation of the oligomeric state of DcuS. The results showed that detergent-solubilised His_6-DcuS was mainly monomeric and demonstrated the presence of tetrameric DcuS in proteoliposomes and in bacterial membranes.

The sensor histidine kinase CitA is part of the two-component system CitAB of *E. coli*, which is structurally related to DcuSR. CitAB regulates gene expression of citrate fermentation in response to external citrate. The sensor kinases DcuS and CitA were fused with an enhanced variant of the yellow fluorescent protein (YFP) and expressed in *E. coli* under the control of an arabinose-inducible promoter. The subcellular localisation of DcuS-YFP and CitA-YFP within the cell membrane was studied by means of confocal laser fluorescence microscopy. Both fusion proteins were found to accumulate at the cell poles. The polar accumulation was slightly increased in the presence of the stimulus fumarate or citrate, respectively, but independent of the expression level of the fusion proteins. Cell fractionation demonstrated that polar accumulation was not related to inclusion bodies formation. The degree of polar localisation of DcuS-YFP was similar to that of the well-characterised methyl-accepting chemotaxis proteins (MCPs), but independent of their presence. To enable further investigations on the function of the polar localisation of DcuS under physiological conditions, the sensor kinase was genetically fused to the flavin-based fluorescent protein Bs2 which shows fluorescence under aerobic and anaerobic conditions. The resulting *dcuS-bs2* gene fusion was inserted into the chromosome of various *E. coli* strains.

Furthermore, a protein-protein interaction between the related sensor histidine kinases DcuS and CitA, regulating common metabolic pathways, was detected via expression studies under anaerobic conditions in the presence of citrate and by *in vivo* FRET measurements.

2. Introduction

2.1 Regulation of anaerobic metabolism in *Escherichia coli*

Prokaryotes sense a large number of external and intracellular stimuli and rapidly adapt their metabolism and cell composition to the prevailing conditions. The gram-negative enteric bacterium *Escherichia coli* is able to grow on a wide variety of carbon and energy sources under either aerobic or anaerobic conditions. Various electron acceptors are used in a hierarchic order to achieve maximal energy conservation. Best growth is obtained by aerobic respiration since oxygen is the most electro-positive electron acceptor. Nitrate or fumarate can function as electron acceptors in anaerobic respiration. Fermentation takes place in the absence of external electron acceptors. The induction of the appropriate metabolic pathway is transcriptionally regulated, ensuring an economic utilisation of the available substrates.

In the absence of oxygen, the global regulatory two-component system ArcBA (aerobic respiration control) represses genes of the aerobic metabolism (Iuchi and Lin, 1988; Iuchi *et al.*, 1989), while the global regulator FNR (fumarate/nitrate regulator) activates gene expression of anaerobic pathways (Shaw and Guest, 1982). The regulation of nitrate and nitrite respiration is governed by the homologous two-component systems NarXL and NarQP (Stewart, 1993). Thereby, genes essential for nitrate and nitrite respiration are induced, while genes of energetically less favourable anaerobic systems, such as fumarate respiration or fermentation, are repressed.

Adaptation of bacteria to the environmental conditions is frequently accomplished by two-component systems consisting of a membrane-bound sensory histidine kinase and the corresponding response regulator (West and Stock, 2001; Mascher *et al.*, 2006). Gene expression is thereby regulated by a phosphorelay cascade. Perception of the signal leads to autophosphorylation of a conserved histidine residue in the kinase domain of the sensor protein. The resulting phosphoimidazole is chemically adequate for donating the phosphoryl group to a conserved aspartate residue of the response regulator. The phosphorylated response regulator binds as transcriptional regulator to the DNA, activating the expression of the target genes. The signal is inactivated by cleavage of the phosphoryl group from the aspartate residue of the response regulator. This is mostly accomplished either through an additional phosphatase or by phosphatase activity of the sensor histidine kinase.

The two-component system DcuSR of *E. coli*

DcuSR of *E. coli* represents a typical two-component system regulating gene expression of anaerobic fumarate respiration and aerobic C_4-dicarboxylate transport in response to external C_4-dicarboxylates and citrate (Zientz *et al.*, 1998; Golby *et al.*, 1999; Kneuper *et al.*, 2005). The sensor histidine kinase DcuS is anchored in the membrane by two

transmembrane helices flanking a periplasmic sensory PAS (Per-Arnt-Sim) domain of about 140 amino acid residues. The structure of the periplasmic PAS domain in the liquid state has been solved independently by NMR in the ligand-free state (Pappalardo *et al.*, 2003) and by X-ray crystallography in the malate-bound state (Cheung and Hendrickson, 2008). The involvement of basic and polar amino acid residues in signal recognition was further demonstrated by mutational analysis (Kneuper *et al.*, 2005; Krämer *et al.*, 2007). The second transmembrane domain is followed by a cytosolic PAS domain, which shows a high intrinsic flexibility and presumably plays an important role in signal transduction (Etzkorn *et al.*, 2008). The cytosolic PAS domain is succeeded by a conserved C-terminal histidine kinase domain.

After perception of the external stimulus by the periplasmic PAS domain of DcuS, the signal is transduced across the membrane by conformational changes within the sensor protein, resulting in ATP-dependent autophosphorylation of the conserved histidine residue (His349) in the cytosolic kinase domain (Fig. 1). The phosphoryl group is subsequently transferred to the conserved aspartate residue (Asp56) in the N-terminal receiver domain of the response regulator DcuR.

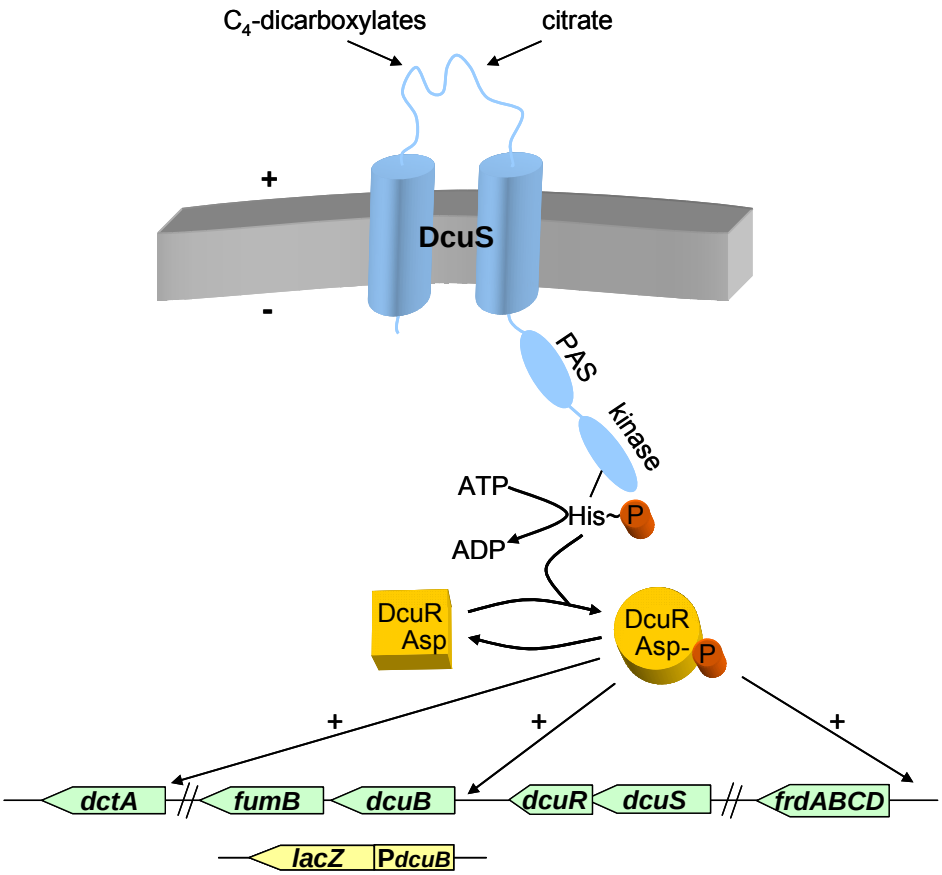

Figure 1: Model of gene regulation mediated by the two-component system DcuSR. The periplasmic domain of DcuS senses external C_4-dicarboxylates and citrate. The signal is transduced across the membrane resulting in autophosphorylation of the conserved histidine residue in the kinase domain. The phosphoryl group is transmitted to the response regulator DcuR. This leads to the activation of DcuR, which thereupon binds as transcriptional regulator to the DNA inducing the target genes.

Phospho-DcuR is active and binds via its C-terminal helix-turn-helix motif to the promoter region of the target genes. DcuSR induces, together with FNR, the expression of genes required for fumarate respiration, i.e. *frdABCD*, *dcuB* and *fumB* (Zientz *et al.*, 1998; Golby *et al.*, 1999). Fumarate is reduced to succinate through the membrane-embedded fumarate reductase FrdABCD. The respiratory chain consisting of a dehydrogenase and of the fumarate reductase establishes a proton gradient. Succinate cannot be further metabolised under anaerobic conditions due to an incomplete citric acid cycle and is transported out of the cell in exchange with fumarate by the antiporter DcuB. The *fumB* gene, encoding the anaerobic fumarase FumB, which converts malate to fumarate, is not directly regulated by DcuR (Tseng, 1997; Golby *et al.*, 1998). The gene is part of the *dcuB-fumB* operon, and *fumB* is partially co-transcribed with *dcuB* and is thus indirectly regulated by DcuSR.

Under aerobic conditions, DcuSR stimulates the expression of *dctA* encoding the C_4-dicarboxylate carrier DctA.

Expression of *dcuB* under anaerobic conditions is strongly dependent on the induction by DcuSR in the presence of C_4-dicarboxylates like fumarate or malate. Thus, expression of a *dcuB'-'lacZ* reporter gene fusion has been used to assay the functional state of DcuS *in vivo* (Zientz *et al.*, 1998; Kneuper *et al.*, 2005).

Citrate fermentation in *E. coli*

E. coli is not able to grow with citrate as sole carbon and energy source. Under aerobic conditions, no citrate uptake system is present. However, some *E. coli* strains have been identified, which express a plasmid-encoded citrate uptake system, allowing the use of citrate as carbon source under aerobic conditions (Ishiguro and Sato, 1985; Sasatsu *et al.*, 1985).

Under anaerobic conditions, *E. coli* is able to ferment citrate in the presence of an oxidisable co-substrate like glucose, glycerol or lactose (Lütgens and Gottschalk, 1980). Citrate is thereby taken up by the anaerobically expressed citrate transporter CitT. The citrate fermentation pathway of *E. coli* (Fig. 2) differs by the lack of oxaloacetate decarboxylase from the well-characterised one of *Klebsiella pneumoniae* (Bott, 1997).

In *E. coli*, citrate is cleaved through citrate lyase into acetate and oxaloacetate (Fig. 2). Oxaloacetate is reduced by malate dehydrogenase to malate, which is subsequently converted to fumarate through fumarase B. Fumarate is finally reduced to succinate by fumarate reductase. The reducing power needed for the stepwise reduction of oxaloacetate to succinate is provided by the oxidation of a co-substrate, such as glucose or glycerol.

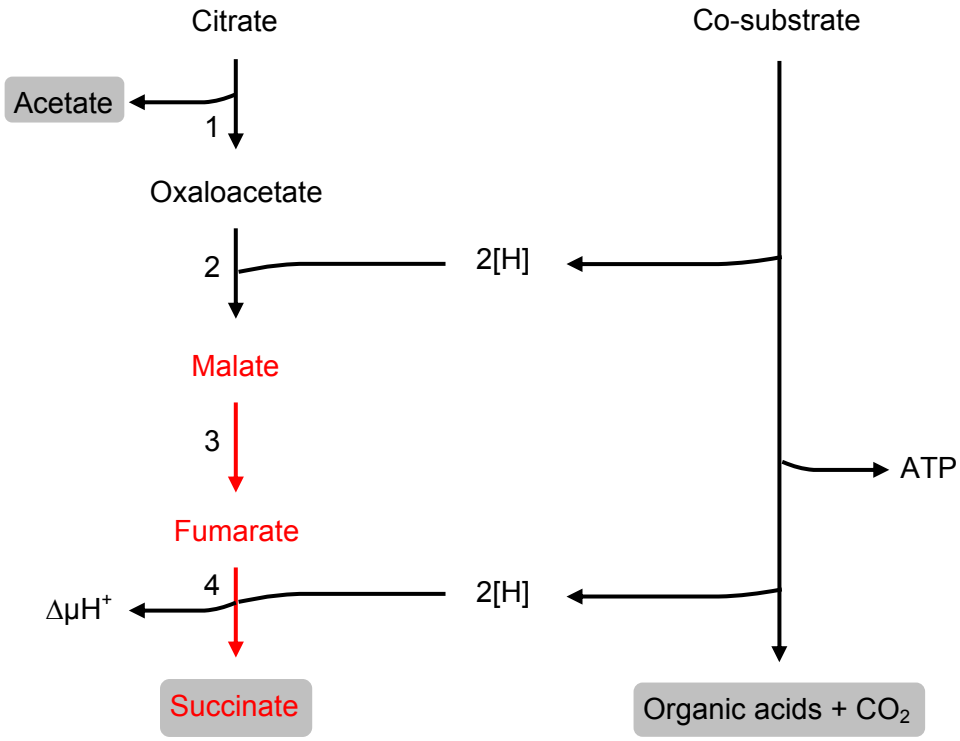

Figure 2: Citrate fermentation pathway of *E. coli*. 1, citrate lyase; 2, malate dehydrogenase; 3, fumarase B; 4, fumarate reductase. Reactions shared with the fumarate respiration pathway are highlighted in red. Final products are marked grey. (Figure derived from Bott, 1997)

The two-component system CitAB of *E. coli*, which is paralogous to DcuSR (Fig. 1), regulates gene expression of citrate fermentation in response to external citrate (Kaspar and Bott, 2002; Yamamoto *et al.*, 2008). CitA represents the sensor histidine kinase, while CitB functions as the cognate response regulator. Under anaerobic conditions and in the presence of citrate, CitAB induces the expression of the *citCDEFXGT* gene cluster, encoding the holo-citrate lyase and the citrate transporter CitT, and *mdh*, which encodes malate dehydrogenase (Yamamoto *et al.*, 2008). Furthermore, the *citAB* operon is positively auto-regulated. In addition to the genes required for citrate fermentation, CitAB induces the *exuTR* operon, encoding the glucuronate and galacturonate transporter and regulator, respectively (Yamamoto *et al.*, 2008).

Because of high similarities in structure, function and overall topology, CitA and DcuS belong to the CitA family of sensor histidine kinases (Pappalardo *et al.* 2003; Reinelt *et al.* 2003). The metabolic pathways regulated by both two-component systems share common reactions during substrate degradation, including fumarate respiration (Fig. 2, highlighted in red). While DcuS senses a broad range of effectors with an apparent K_D of 2 - 13 mM, CitA is a high-affinity citrate-specific sensor with an apparent K_D of 5.5 µM (Kneuper *et al.*, 2005; Kaspar and Bott, 2002).

2.2 Oligomerisation of DcuS

Mechanisms of ligand binding and signal transduction across the cell membrane in membrane-embedded sensor histidine kinases are not fully understood. Structural analyses of the isolated periplasmic PAS domain of CitA from *Klebsiella pneumoniae* and of the full-length chemoreceptor Tar from *Salmonella typhimurium* reveal ligand-induced conformational changes within the periplasmic sensing domain (Sevvana *et al.*, 2008; Ottemann *et al.*, 1998). A piston-type movement of TM2 based on the contraction of the periplasmic sensing domain is suggested. In this way the signal might be transduced to the cytosolic part of the protein.

It is generally assumed that sensor histidine kinases are present in a preformed dimeric state in the membrane (Qin *et al.*, 2000; Gao and Stock, 2009). During trans-autophosphorylation, the catalytic domain of one monomer phosphorylates the conserved histidine residue from the kinase domain in the second monomer by hydrolysis of ATP (Fig. 3). In addition, there are good indications that the processes of signal transduction across the membrane and of signal transduction along cytosolic PAS domains is a mechanical process requiring protein dimers as well (Etzkorn *et al.*, 2008; Sevvana *et al.*, 2008). Therefore the functional state of DcuS is supposed to be a dimer or a higher oligomer. The actual oligomeric state of full-length sensor histidine kinases has not been studied in detail yet.

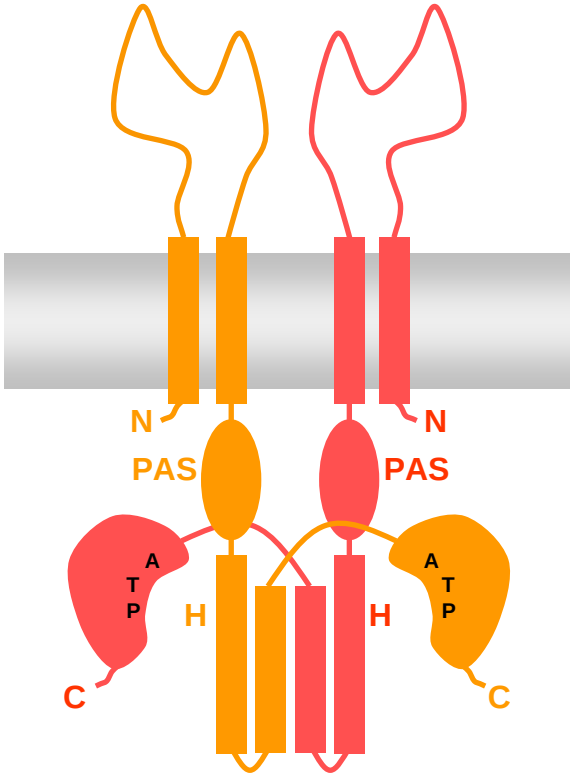

Figure 3: Model of trans-autophosphorylation between two DcuS monomers. After oligomerisation of DcuS, trans-autophosphorylation between two DcuS monomers takes place. Thereby, the catalytic domain of one monomer autophosphorylates the conserved histidine residue in the kinase domain of the second monomer.

Fluorescence resonance energy transfer (FRET)

Fluorescence resonance energy transfer (FRET) techniques are widely used to study protein-protein interactions. The proteins are labelled with different fluorophores and the occurrence of FRET between a donor fluorophore and an acceptor fluorophore is investigated. The emission spectrum of the donor fluorophore overlaps with the excitation spectrum of the acceptor fluorophore, allowing fluorescence resonance energy transfer after excitation of the donor. An excited fluorophore falls back to the ground-level energy state and emits light of longer (less energetic) wavelength. If the fluorophores are in close proximity, the excited donor transfers energy to the acceptor. FRET leads to a decrease of donor emission and an increase of acceptor emission. The energy is transferred in a non-radiative process through dipole-dipole interactions.

Derivatives of the green fluorescent protein (GFP) can be used as FRET pair. The cyan fluorescent protein (CFP), acting as donor, and the yellow fluorescent protein (YFP), acting as acceptor, were each fused to DcuS to study the oligomerisation of DcuS *in vivo* (Fig. 4). If the DcuS-CFP monomer is in a distance greater than 5 nm to the DcuS-YFP monomer, excitation of the donor results in CFP-specific emission, but no energy transfer takes place. If the two monomers are close together due to oligomer formation, excitation of the donor results in decreased CFP-specific emission and most of the energy is transferred to the acceptor leading to YFP-specific emission.

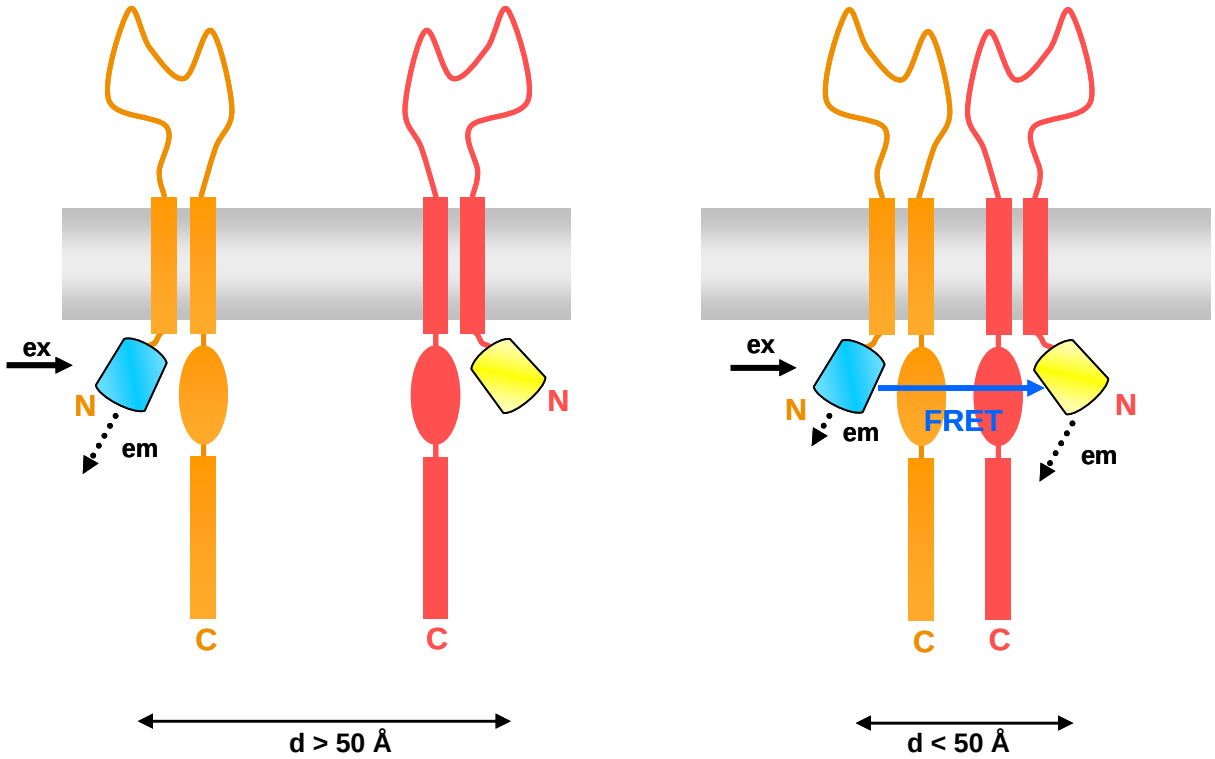

Figure 4: Model of intermolecular FRET between two DcuS monomers. When a DcuS monomer labelled with a donor fluorophore (blue) and a DcuS monomer labelled with an acceptor fluorophore (yellow) associate, the fluorophores come close together. Thereby, the excited donor transfers fluorescence resonance energy to the acceptor. d, distance between the two fluorophores.

2.3 Subcellular localisation of sensor histidine kinases

Bacteria reveal a remarkably complex internal organisation. Many sensor histidine kinases involved in the regulation of asymmetric processes like cell division, development and virulence exhibit an uneven subcellular distribution within the cell membrane according to their site of function (Shapiro *et al.*, 2002). For example, in *Caulobacter crescentus* the antagonistic PleC and DivJ kinases are localised at opposite cell poles. The kinases coordinate cell-cycle progression with polar differentiation (Paul *et al.*, 2008). The WalK sensor histidine kinase from *Bacillus subtilis* is localised to the division septum in growing cells, thereby controlling the synthesis of proteins involved in cell wall remodelling and cell separation (Fukushima *et al.*, 2008).

In contrast, the quorum sensing histidine kinase LuxQ from *Vibrio harveyi* is homogeneously distributed all over the cell membrane, independently of the presence of the auto-inducer AI-2 (Neiditch *et al.*, 2006). A homogeneous distribution within the cell membrane is also shown for the osmosensor kinase KdpD of *E. coli* (Maier *et al.*, 2008). The sensor histidine kinase PhoQ from the PhoQP two-component system, that regulates virulence in *Salmonella enterica*, reveals an even distribution throughout the cell membrane. However, the cognate response regulator PhoP is preferentially localised to one cell pole under inducing conditions, corresponding to its active state (Sciara *et al.*, 2008).

The well-characterised methyl-accepting chemotaxis proteins (MCPs), which have no obvious requirement for an uneven distribution with respect to their site of function, exhibit an asymmetric localisation within *E. coli* cells (Sourjik and Berg, 2000). The MCP clusters, predominantly observed at the cell poles, are believed to support stimulus integration and sensitivity of the sensors (Kentner and Sourjik, 2006; Thiem and Sourjik, 2008). The CitA homologue CitS from *Bacillus subtilis*, controlling aerobic citrate metabolism, also displays an unexpected heterogeneous localisation (Meile *et al.*, 2006).

2.4 Aims of the work

In this work, the oligomerisation of full-length DcuS was studied *in vivo* and *in vitro* by fluorescence resonance energy transfer (FRET) spectroscopy. For *in vivo* studies, DcuS was genetically fused with variants of the green fluorescent protein and expressed in vegetative cells. *In vitro* FRET measurements were performed with purified His_6-DcuS, which was fluorescently labelled with chemical dyes and reconstituted in liposomes. The influence of the presence of effector on DcuS oligomerisation was further investigated *in vivo* and *in vitro*. In addition, the oligomeric state of membrane-embedded His_6-DcuS from bacterial membranes and of reconstituted DcuS was determined by chemical crosslinking.

The cellular distribution of the sensor histidine kinases DcuS and CitA was studied in detail. DcuS and CitA control metabolic processes, i.e. fumarate respiration and citrate

fermentation, respectively, without obvious asymmetric distribution in the bacterial cell. Fusions of DcuS or CitA with the yellow fluorescent protein allowed careful analysis of the distribution of these kinases in the cell membrane of *E. coli* by confocal laser scanning fluorescence microscopy.
A possible interaction of the structurally related sensors DcuS and CitA was investigated by expression studies and by *in vivo* FRET measurements.

FRET measurements and fluorescence microscopy studies were performed in cooperation with the working group of Dr. Wolfgang Erker, WG Prof. Dr. T. Basché (Institut für Physikalische Chemie, Johannes Gutenberg-Universität, Mainz).

3. Materials and methods

3.1 Bacterial strains and plasmids

Table 1: *Escherichia coli* strains and plasmids

Strain	Genotype / Characteristics	Reference
***E. coli* K-12**		
MC4100	F$^-$ *araD139* Δ(*argF-lac*)*U169*, *rpsL150*, *relA1 flbB530 deoC1 ptsF25 rbsR*, Δ*lacZ*	Silhavy *et al.*, 1984
MG1655	CGSC 6300, *fnr*$^-$, λ-F-P1-sensitive	Jensen, 1993
BL21(DE3)	*E. coli* B, F$^-$ *ompT hsdS*$_B$ *gal1 dcm* λ(DE3), with IPTG-inducible chromosomal T7 RNA polymerase, strain for protein over-expression	Studier and Moffatt, 1986
C43(DE3)	Spontaneous mutation of BL21(DE3) for over-expression of membrane proteins	Miroux and Walker, 1996
JM109	F´ *traD36 proAB*$^+$ *lacI*^{q} Δ(lacZ)M15/ Δ(*lac-proAB*) *glnV44 e*$^{14-}$ *gyrA96 recA1 relA1 endA1 thi hsdR17*	Yanisch-Perron *et al.*, 1985
JM109λ*pir*	*pir*$^+$, strain expressing the π protein for replication of plasmids with *R6K* origin	Baba *et al.*, 2006 (Keio Collection, Japan)
IMW205	MC4100 *dcuR::kan*^{r}	Zientz *et al.*, 1998
IMW237	MC4100 λ[Φ(*dcuB'-'lacZ*)hyb *amp*^{r}]	Zientz *et al.*, 1998
IMW238	MC4100 λ[Φ(*dcuB'-'lacZ*)hyb *amp*^{r}] *dcuR::kan*^{r}	Zientz *et al.*, 1998
IMW239	MC4100 λ[Φ(*dcuB'-'lacZ*)hyb *amp*^{r}] *citB::spc*^{r}	Zientz *et al.*, 1998
IMW260	MC4100 λ[Φ(*dcuB'-'lacZ*)hyb *amp*^{r}] *dcuS::cam*^{r}	Zientz *et al.*, 1998
IMW262	MC4100 *dcuS::cam*^{r}	Zientz *et al.*, 1998
IMW279	MC4100 *citA::kan*^{r}	Zientz, 2000
IMW280	MC4100 λ[Φ(*dcuB'-'lacZ*)hyb *amp*^{r}] *citA::kan*^{r}	Krämer *et al.*, 2007
IMW502	MC4100 Δ*dcuB*	Kleefeld, 2006
IMW569	JW1241 carrying a chromosomal *dcuS-bs2-stop* gene fusion, *kan*^{r}	This study
IMW570	MC4100 carrying a chromosomal *dcuS-bs2-stop* gene fusion	This study
BW25113	CGSC6159, F$^-$, λ$^-$, *lacI*^{q} *rrnB*$_{T14}$ Δ*lacZ*$_{WJ16}$ *hsdR514* Δ*araBAD*$_{AH33}$ Δ*rhaBAD*$_{LD78}$	Datsenko and Wanner, 2000
JW1241	BW25113 *cls::kan*^{r}	Baba *et al.*, 2006 (Keio Collection, Japan)
UU1250	Δ*tsr-7028* Δ(*tar-tap*)*5201* Δ*trg-100* Δ*aer-1*, *kan*^{r}	Ames *et al.*, 2002
VS100	Δ*cheY*, in-frame *cheY* deletion	Sourjik and Berg, 2000

Plasmid	Genotype / Characteristics	Reference
pBAD18-Kan	Expression vector; pBR322 *ori*, arabinose-inducible P_{BAD} promoter, *kan*^{r}	Guzman *et al.*, 1995
pBAD30	Expression vector; pACYC *ori*, arabinose-inducible P_{BAD} promoter, *amp*^{r}	Guzman *et al.*, 1995
pET28a	Over-expression vector; pBR322 ori, IPTG-inducible T7 promoter, His-tag, *kan*^{r}	Novagen
pECFP	Vector containing enhanced GFP-variant CFP, *amp*^{r}	Clontech
pEYFP	Vector containing enhanced GFP-variant YFP, *amp*^{r}	Clontech
pGlow-Bs2-stop	Vector containing flavin mononucleotide-based fluorescent protein Bs2, *amp*^{r}	Evocatal evoglow, Drepper *et al.*, 2007
pDS132	*R6K ori*, *cam*^{r}, *sacB*, *mobRP4*; suicide vector enabling gene insertion into the chromosome via homologous recombination	Philippe *et al.*, 2004
pUC18	pUC *ori*, *amp*^{r}	Yanisch-Perron *et al.*, 1985
pACYC184	pACYC184 *ori*, *cam*^{r}, *tet*^{r}	Chang and Cohen, 1978
pMW99	*dcuB'-'lacZ* in pJL29	Zientz *et al.*, 1998
pMW151	*dcuS* in pET28a, for over-expression with N-terminal His-tag, *kan*^{r}	Janausch *et al.*, 2002
pMW181	*dcuS* with its own promoter in pET28a, *kan*^{r}	Janausch *et al.*, 2002
pMW324	pMW151 but DcuS C199S, *kan*^{r}	Kneuper, 2005
pMW325	pMW151 but DcuS C471S, *kan*^{r}	Kneuper, 2005
pMW336	pMW151 but DcuS C199S C471S, *kan*^{r}	Kneuper, 2005
pMW446	pMW151 but DcuS R147A C199S, *kan*^{r}	This study
pMW452	pMW151 but DcuS C199S C471S Q83C, *kan*^{r}	This study
pMW384	*dcuS-yfp* in pET28a, pMW391 derivative, *kan*^{r}	Scheu *et al.*, 2008
pMW385	*yfp-dcuS* in pET28a, pMW392 derivative, *kan*^{r}	Scheu, 2005
pMW386	*dcuS-cfp* in pET28a, pMW393 derivative, *kan*^{r}	Scheu, 2005
pMW387	*cfp-dcuS* in pET28a, pMW394 derivative, *kan*^{r}	Scheu, 2005
pMW388	*yfp-dcuS* in pBAD30, *amp*^{r}	Scheu, 2005
pMW389	*cfp-dcuS* in pBAD18-Kan, *kan*^{r}	Scheu, 2005
pMW391	*'yfp* in pET28a, *kan*^{r}	Scheu *et al.*, 2008
pMW392	*yfp'* in pET28a, *kan*^{r}	Scheu, 2005
pMW393	*'cfp* in pET28a, *kan*^{r}	Scheu, 2005
pMW394	*cfp'* in pET28a, *kan*^{r}	Scheu, 2005
pMW407	*dcuS-yfp* in pBAD30, *amp*^{r}	Scheu *et al.*, 2008

Plasmid	Genotype / Characteristics	Reference
pMW408	*dcuS-cfp* in pBAD18-Kan, *kan*^{r}	This study
pMW442	*citA-yfp* in pBAD30, *amp*^{r}	Scheu *et al.*, 2008
pMW557	pMW442 with additional *cam*^{r} from pACYC184	Scheu *et al.*, 2008
pMW643	pBAD30-Tet, pBAD30 with additional *tet*^{r}	Graf, 2009
pMW762	*cfp* in pBAD18-Kan, *kan*^{r}	This study
pMW765	*yfp* in pBAD30, *amp*^{r}	This study
pMW766	*cfp-yfp* in pBAD18-Kan, *kan*^{r}	This study
pMW842	*dcuS-bs2-stop-3'dcuS* in pUC18, *amp*^{r}	This study
pMW843	*'dcuS-bs2-stop-3'dcuS* in pDS132, *cam*^{r}	This study
pMW875	*dcuS-bs2-stop* with *dcuS*-promoter in pBAD30-Tet, pMW643 derivative, *amp*^{r}, *tet*^{r}	This study
pDK108	Tar(1-331)-YFP expression plasmid, pBR *ori*, IPTG-inducible pTrc promoter, pTrc99a derivative, *amp*^{r}	Kentner *et al.*, 2006
pVS1	CheY-YFP expression plasmid, pBAD18-Kan derivative, *kan*^{r}	Sourjik and Berg, 2000

3.2 Growth and media

Growth of *Escherichia coli*

For all genetic methods bacteria were grown aerobically in LB broth at 37 °C.

For β-galactosidase assays, cells were grown anaerobically at 37 °C in 10 ml enriched M9 medium supplemented with carbon sources, electron acceptors and effectors as indicated in the individual experiments. The medium was inoculated with 0.75-5 % (v/v) of a 5 ml preculture grown semi-anaerobically overnight in M9 medium. Anaerobic growth of the main culture was performed in sealed infusion bottles (Sovirell). Prior to incubation, the cultures were degassed for 3 x 15 min. Within every 15 min the cultures were gassed with 1.2 atm nitrogen (N_2 5.0, purity >99.999 %, Linde). Subsequently, the cultures were incubated at 37 °C. Cells were grown to an optical density (OD_{578nm}) of 0.5-0.8, corresponding to the mid-exponential phase of growth.

For *in vivo* FRET measurements and fluorescence microscopy studies, cells were grown aerobically in LB broth at 30 °C for 3-4.5 h, corresponding to the mid-exponential phase of growth. The medium was inoculated with 1 or 2 % (v/v) of a preculture grown overnight in LB broth on a rotary shaker. Inducer was added when required, thereby L-arabinose was added from the beginning of incubation at a concentration of 10-333 µM. Aerobic growth was

performed in rotating Erlenmeyer flasks with baffles containing maximally 20 % of the total volume.
Antibiotics were added to the media where appropriate. When two antibiotics were supplied simultaneously, half of the concentrations were added.

Media and buffers for *E. coli*

Complex medium, LB (Luria Bertani) broth (Sambrook and Russell, 2001)

10 g/l Casein (Select peptone no. 140, Gibco)
5 g/l Yeast extract (Servabacter 24540, Serva)
5 g/l NaCl (Roth)

LB agar

LB broth with 15 g/l Agar-Agar (Roth)

Minimal medium, M9 medium (10x), pH 7 (Miller, 1992)

75 g/l Na_2HPO_4 x 2 H_2O (Roth)
30 g/l KH_2PO_4 (Roth)
5 g/l NaCl
10 g/l NH_4Cl (Fluka)

Enrichments (autoclaved separately)

10 ml/l $CaCl_2$ x 2 H_2O (Roth), 10 mM
10 ml/l Acid-hydrolysed caseine (AHC, peptone no. 5, Gibco), 10 %
5 ml/l L-tryptophan (Serva), 1 %
1 ml/l $MgSO_4$ x 7 H_2O (Roth), 1 M

Carbon sources, electron acceptors and effectors (final concentration)

50 mM Glycerol (Fluka)
50 mM Na-gluconate, filter-sterilised (Sigma)
20 mM Dimethylsulfoxide (DMSO) (Fluka)
20 mM Na_2-fumarate (Fluka)
20 mM Na_3-citrate, filter-sterilised (Roth)
20 mM Na-acetate (Roth)

Inducers (stock solution)

1 M Isopropyl-β-D-thiogalactopyranoside (IPTG, Roth)
20 mM L(+)-arabinose (Roth)

PBS buffer (1x) (Sambrook and Russell, 2001)

137 mM NaCl
2.7 mM KCl
10 mM Na_2HPO_4
2 mM KH_2PO_4
adjusted with HCl to pH 7.5

Transformation SOC medium (Sambrook and Russell, 2001)

20 g/l Casein (Select peptone no. 140, Gibco)
5 g/l Yeast extract (Servabacter 24540, Serva)
0.584 g/l NaCl
0.19 g/l KCl (Roth)
2.46 g/l $MgSO_4$ x 7 H_2O
2.03 g/l $MgCl_2$ x 6 H_2O (Fluka)
3.96 g/l Glucose x H_2O (Roth)

Antibiotics (final concentration)

100 µg/ml Ampicillin
50 µg/ml Kanamycin
50 µg/ml Spectinomycin
20 µg/ml Chloramphenicol
15 µg/ml Tetracycline

All media and solutions were autoclaved or filter-sterilised prior to use.

Buffers for protein over-expression

Tris/HCl buffer

2 M Tris (Roth), adjusted with HCl to pH 7.7

Buffer M (Membranes washing buffer)

1 mM Tris/HCl, pH 7.7
3 mM Na_2-EDTA (Roth)

Buffer 1 (Resuspension buffer)

50 mM Tris/HCl, pH 7.7
10 mM $MgCl_2$

Buffer 2 (Homogenisation buffer)

50 mM Tris/HCl, pH 7.7
0.5 M NaCl
10 % Glycerol
10 mM Imidazole (Roth), pH 7

Buffer 3 (Column equilibration and washing buffer)

50 mM Tris/HCl, pH 7.7
0.5 M NaCl
10 % Glycerol
0.04 % N,N-dimethyldodecylamine-N-oxide (LDAO, 30 % w/v, Fluka)
20 mM Imidazole, pH 7

Buffer 4 (Elution buffer)

Buffer 3, but with 500 mM imidazole, pH 7

Buffer 5 (Dialysis buffer)

Buffer 3, but without imidazole

Buffer R (Reconstitution buffer)

50 mM Tris/HCl, pH 7.7
10 % Glycerol

SDS sample buffer (2x) (Laemmli, 1970)

100 mM Tris/HCl, pH 6.8
200 mM Dithiothreitol (DTT, Sigma)
4 % Sodiumdodecylsulfate (w/v) (SDS, Roth)
0.2 % Bromphenol blue (Janssen Chimica)
20 % Glycerol

DcuS-labelling buffer (pH 7.2)

50 mM Tris/HCl, pH7.2
0.5 M NaCl
5 % Glycerol
0.04 % LDAO
5 mM Imidazole, pH 7

Buffers and solutions for semi-dry Western blotting (Towbin *et al.*, 1979)

Cathode buffer

25 mM Tris/HCl, pH 9.4
40 mM 6-amino-caproic acid (Serva)
10 % Methanol (v/v) (Roth)

Anode buffer

0.3 M Tris/HCl, pH 10.4
10 % Methanol

Blocking buffer

1x PBS buffer
3 % Bovine serum albumin (w/v) (BSA, Albumin Fraktion V, Roth)
0.1 % Tween 20 (w/v) (Serva)

Washing buffer

0.1 % Tween 20 in 1x PBS buffer

Developer solution

30 mg 4-Chloro-1-naphtol (Sigma-Aldrich) in 20 ml ethanol (denatured Rotisol, Roth)
80 mM Tris/HCl, pH 7.7
0.015 % H_2O_2 (30 %, Fluka)
Ad dH_2O to 100 ml

Antibody solution

1x PBS buffer
1 % BSA (Albumin Fraktion V, Roth)
0.1 % Tween 20
Antibody dilution

Antibodies (polyclonal)

Primary antibody: Anti-DcuS-PD (from rabbit, Eurogentec), raised against the periplasmic domain of DcuS (Müller, 2007), dilution 1:2000

Primary antibody: Anti-His_5 (from mouse, Qiagen), raised against His-tag, dilution 1:2000

Secondary antibody: Anti-IgG-rabbit, coupled to peroxidase (Sigma-Aldrich), dilution 1:1000

Secondary antibody: Anti-IgG-mouse, coupled to peroxidase (Qiagen), dilution 1:10000

Buffers for DSS crosslinking

Buffer A (CL dialysis buffer)

25 mM KP_i, pH 7.4

300 mM NaCl

10 % Glycerol

0.04 % LDAO

Buffer B (CL reconstitution buffer)

25 mM KP_i, pH 7.4

10 % Glycerol

Buffer C (CL membrane buffer)

20 mM MOPS (Roth), pH 7.2

200 mM NaCl

Buffer D (CL reaction buffer)

20 mM HEPES (Roth), pH 7.4

20 mM KCl

250 mM sucrose

1 mM Na_2-EDTA

Buffer and reagents for β-galactosidase assays (Miller, 1992)

β-Galactosidase reaction buffer (pH 7)

0.1 M KP_i buffer (1 M KH_2PO_4, 1 M K_2HPO_4, pH 7)

10 mM KCl

1 mM $MgCl_2$ (Fluka)

The reaction buffer was autoclaved and 2.7 ml/l 2-mercaptoethanol were added prior to use.

Reagents for the β-galactosidase assay

4 mg/ml o-Nitrophenyl-ß-D-galactopyranoside (ONPG, Fluka)

1 M Na_2CO_3 (Fluka)

Chloroform (Roth)

0.1 % SDS (Roth)

Components for enzymatic kinase tests

Table 2: Components of the enzymatic kinase test in 1 ml reaction mixture.

Component	Volume	Final concentration
His_6-DcuS*	100 µl	20 µg
PHP-phosphatase$^{\Delta}$	2 µl	2 µg
$MgCl_2$ (2 M)	1 µl	2 mM
Phosphoenolpyruvate (200 mM)	5 µl	1 mM
NADH (50 mM)	5 µl	0.25 mM
Pyruvate kinase	2 µl	30 U
$MgSO_4$ (1 M)	5 µl	5 mM
KCl (1 M)	25 µl	25 mM
L-Lactic dehydrogenase	2 µl	25 U
Tris/HCl, pH 7.7	845 µl	50 mM
ATP (50 mM)	8 µl	0.4 mM

*Detergent-solubilised or reconstituted His_6-DcuS.
$^{\Delta}$Protein histidine PHP-phosphatase was obtained from Prof. Dr. S. Klumpp, Münster.

The enzymatic tests were performed at 37 °C. The absorption spectra of NADH were recorded at 365 nm every 5 seconds in a quartz cuvette (Specord UV Vis S10 photometer, Zeiss). For the control measurement, 10 µl glucose (final concentration 20 mM) and 1 µl hexokinase (3 U) were added, but neither DcuS nor phosphatase.

3.3 Molecular genetic methods

Molecular genetic methods such as PCR, restriction and ligation of DNA fragments were performed according to standard procedures (Sambrook and Russell, 2001). Restriction endonucleases and T4 DNA ligase were applied from MBI Fermentas. Prior to ligation, the vector was dephosphorylated through CIAP-phosphatase (Fermentas). The insert was added at a 5-fold excess of the molar mass in respect to the vector. Ligations were incubated for 3 h at 37 °C and precipitated with butanol prior to transformation. Clonings were predominantly performed in *E. coli* JM109. Preparation of electro-competent cells was performed according to Farinha and Kropinski (1990). *E. coli* strains were transformed by electroporation (Dower *et al.*, 1988). When required, two plasmids were successively transformed into one cell. Therefore, the plasmids have to carry different antibiotic resistance genes, and for stable maintenance, additionally harbour different origins of replication (Novick, 1987).

Genomic DNA was isolated with the Nucleospin C+T kit (Macherey & Nagel). Plasmids were isolated using the QIAprep Spin Miniprep kit (Qiagen, Hilden). PCR products and restriction fragments were purified with the QIAquick PCR Purification kit (Qiagen, Hilden). Point

mutations were introduced into plasmid-borne genes using the QuikChange Site-Directed Mutagenesis kit (Stratagene, La Jolla, USA). DNA gel electrophoresis was run with 1 % agarose gels at 90 V for 40 min. The sequences of resulting constructs were verified by DNA sequencing with standard primers T7-prom and T7-term or self-designed primers (Agowa LGC group, Berlin; Genterprise, Mainz).

Polymerase chain reaction (PCR)

The *in vitro* amplification of genes was performed via PCR (Mullis *et al.*, 1986). The reactions were carried out in the iCycler (Bio-Rad), MyCycler (Bio-Rad) or Progene Thermocycler (Techne). The components used in a 50 µl PCR reaction mixture are listed (Tab. 3).
For different purposes, different DNA polymerases were used. The proof-reading polymerases *Pfu*Ultra (Stratagene) or Phusion (Finnzymes) were used for cloning. For control amplifications the *Taq* polymerase (Abgene) was used.

Table 3: Final concentration of the components added to a 50 µl PCR reaction mixture.

Components	Phusion (Finnzymes)	*Pfu*Ultra (Stratagene)	*Taq* (Abgene)
PCR buffer	1x	1x	1x
10 mM dNTP mix	200 µM	250 µM	200 µM
$MgCl_2$	included in the buffer	included in the buffer	1.5-3 mM
Primer	0.5 µM each	0.5 µM each	0.5 µM each
Template DNA	25-100 ng	25-100 ng	25-100 ng
Polymerase	1 U	2.5 U	2.5 U
DMSO	3 % (optional)	1-10 %	1-10 %
bdH_2O	Ad 50 µl	Ad 50 µl	Ad 50 µl

PCR protocols were dependent on the length of the amplified DNA fragments and the melting temperature (T_m) of the primers. The T_m value for each cloning primer was calculated by equation [1].

[1] $T_m = 69.3\ °C + 0.41 \times GC\ \% - 650/n$

n, number of nucleotides; GC %, GC content in %

The optimal annealing temperature was ascertained by step gradient PCR. The protocols used for the amplification of DNA fragments are listed (Tab. 4).

Table 4: PCR protocols for the DNA polymerases used.

Step	Phusion (Finnzymes)	*Pfu*Ultra (Stratagene)	*Taq* (Abgene)
1. Initial denaturation	98 °C, 30 sec	95 °C, 3 min	94 °C, 4 min
2. Denaturation*	98 °C, 10 sec	95 °C, 30 sec	94 °C, 20 sec
3. Annealing*	T_m + 3 °C, 30 sec	T_m - 3 °C, 30 sec	T_m - 3 °C, 30 sec
4. Elongation*	72 °C, 15-30 sec/kb	72 °C, 1 min/kb	72 °C, 1 min/kb
5. Final elongation	72 °C, 10 min	72 °C, 10 min	72 °C, 10 min

*The cycle (steps 2. - 4.) was repeated 30 times.

The primers used for cloning and for site-directed mutagenesis, their melting temperatures and the restriction sites which were inserted by PCR, are listed (Tab. 5).

Table 5: Oligonucleotides were applied from MWG Biotech (Ebersberg; HPSF-purified).

Primers	**Sequence (5'→ 3')**	**T_m [°C]**	**Restriction site**
dcuS petCfor	CGGCAGCCATATGAGACATTC	60	*Nde*I
dcuS petCrev	TGTTCGAGAGCTCCCCGTC	61	*Sac*I
gfpCfor	CCATGGAGCTCAAGGGCGA	61	*Sac*I
gfpCrev	AGCGACCGAAGCTTAGTTGG	59	*Hind*III
citApetCfor	CAACCCGCTAGCAAAACAATG	58	*Nhe*I
citApetCrev	CGTCCTCAGAGCTCAATAGG	59	*Sac*I
for-gfp-NcoI	GGTCGCCACCATGGTGAGC	63	*Nco*I
HindIII-gfp-rev	CACCAGACAAGAAGCTTGTAATGG	61	*Hind*III
BamHI-gfp-for	CTCTAGAGGGATCCCGGGTACC	66	*Bam*HI
rev-BamHI-gfp	GGAATTCTAGAGTCGGATCCGCTATACTTG	67	*Bam*HI
cam-HindIII-for	GTGACGGAAGCTTACTTCGC	59	*Hind*III
cam-HindIII-rev	GTAGCACCAAGCTTCTAAGGG	60	*Hind*III
dcuS-bs2_Eco-for	CACAAAGAGAATTCCAGCG	54	*Eco*RI
dcuS-bs2_Eco-rev	CCTGGGAATTCTGCTACG	56	*Eco*RI
DcuS-N	CACACAAGGAAGCATATGAGACATTC	62	*Nde*I
DcuS-C	ATTAAAAGCTTGATCATCTGTTCGAC	59	*Hind*III
dcuSsurHind3-for	CCTATCAAGCTTAAACGCTCTGG	61	*Hind*III
dcuSsurHind3-rev	GAAGGATGAAGCTTGTGCCAGG	62	*Hind*III
Bs2-stop-for	CGAGCTCCATATGGCGTCG	61	*Nde*I
Bs2-stop-rev	GCATGCCTGCAGTCACTCG	61	*Pst*I
dcuS-Bs2SacI-for	CTACGAGAGCTCCACGCTG	61	*Sac*I
dcuS-Bs2SacI-rev	CAGTGCCGAGCTCGTGCC	63	*Sac*I

dcuS_for	TTCAGCTCCGCGACCATTGC	61	
dcuS_frev	GTCACACAAGGAAGCTGATG	57	
Mutagenesis	**Sequence (5'→ 3')**		**Mutation**
Mut18Kfor	GAAATGCATAAGCTCTTGCCATTCTCACCGG	76	-*Hind*III
Mut18Krev	CCGGTGAGAATGGCAAGAGCTTATGCATTTC	76	-*Hind*III
C199S_nc	CTGATTGGCACCAGCATTCTGGTTAAGG	67	C199S
C199S_cn	CCTTAACCAGAATGCTGGTGCCAATCAG	67	C199S
C471S_nc	GGCTGGCTGCACAGTGAAGTTAATGATG	67	C471S
C471S_cn	CATCATTAACTTCACTGTGCAGCCAGCC	67	C471S
Q83Cmutfor	CCGCAGGAGAGTGGCATCTGCGCCATCGCGGA AGCCGTACGC	66	Q83C
Q83Cmutrev	GCGTACGGCTTCCGCGATGGCGCAGATGCCACT CTCCTGCGG	66	Q83C
R147A-Mut-for	GGCGCAGGCTTTAGCAGTATTTACCCCC		R147A
R147A-Mut-rev	GGGGGTAAATACTGCTAAAGCCTGCGCC		R147A
Mut_puC_NdeI-for	GTATTTCACACCGCACATGGTGCACTCTCAG	78	-*Nde*I
Mut_puC_NdeI-rev	CTGAGAGTGCACCATGTGCGGTGTGAAATAC	78	-*Nde*I
Mut_puC_PstI-for	CTAGAGTCGACCCGCAGGCATGCAAGC	79	-*Pst*I
Mut_puC_PstI-rev	GCTTGCATGCCTGCGGGTCGACTCTAG	79	-*Pst*I
Mut_sur_NdeI-for	GGAGAGGTCGAACAGAGGACATATGTATTAATTA TCGATGACGACGC	77	*Nde*I
Mut_sur_NdeI-rev	GCGTCGTCATCGATAATTAATACATATGTCCTCT GTTCGACCTCTCC	77	*Nde*I
Mut_PstI-for	GTCGAACAGAGGACATATGTATTAATTATCGCTG CAGACGCAATGG	78	*Pst*I
Mut_PstI-rev	CCATTGCGTCTGCAGCGATAATTAATACATATGT CCTCTGTTCGAC	78	*Pst*I

Cloning of gene fusions into inducible expression vectors

For *in vivo* studies, genes encoding fluorescent fusion proteins were cloned into the arabinose-inducible vectors pBAD30 and pBAD18-Kan (Guzman *et al.*, 1995). Due to the lack of a Shine-Dalgarno sequence in the multiple cloning site of these vectors, the gene fusions were first cloned behind the ribosome binding site (RBS) of the pET28a vector and then cloned with the RBS sequence into the respective pBAD vector.

An additional *Hind*III restriction site in the kanamycin resistance gene of pBAD18-Kan was mutated by site-directed mutagenesis of the DNA sequence with primers Mut18Kfor and Mut18Krev. The resulting amino acid sequence remained intact.

Construction of *dcuS-yfp*, *dcuS-cfp*, *citA-yfp* and *cfp-yfp* fusions

The *eyfp* gene was amplified from plasmid pEYFP by PCR with oligonucleotide primers gfpCfor and gfpCrev. The PCR fragment, lacking the sequence of the three N-terminal amino acid residues of EYFP, was cloned via the *Sac*I and *Hind*III sites of the oligonucleotides into pET28a behind the inducible T7 promoter. The resulting construct pMW391 served as the plasmid for cloning EYFP to the C-terminal end of proteins. *dcuS* was amplified by PCR with primers dcuSpetCfor and dcuSpetCrev from pMW151. The PCR fragment was cloned via the flanking *Nde*I and *Sac*I sites into pMW391 at the 5'-end of *eyfp*. The resulting construct pMW384 encoded DcuS(1-539)-(Lys)-EYFP(4-240), hereafter referred to as *dcuS-yfp* or DcuS-YFP. The fusion protein also carried an N-terminal His_6-tag and a thrombin cleavage site. *dcuS-yfp* was subsequently inserted into pBAD30 using restriction endonuclease *Xba*I. The plasmid harbouring the right gene orientation was selected, resulting in pMW407 (Fig. 5, left). The *dcuS-cfp* fusion was constructed in the same way, whereas the *ecfp* gene was amplified from plasmid pECFP and *dcuS-cfp* was finally inserted via *Xba*I into pBAD18-Kan, resulting in pMW408 (Fig. 5, right).

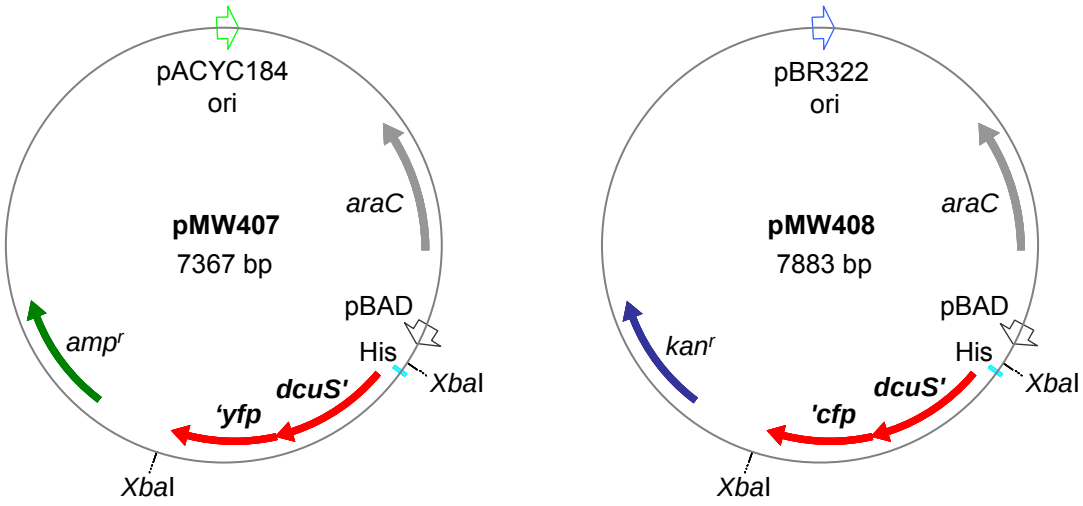

Figure 5: Expression plasmids pMW407 and pMW408 for moderate expression of DcuS-YFP or DcuS-CFP, respectively. *dcuS-yfp* was cloned into pBAD30 (pMW407) and *dcuS-cfp* was cloned into pBAD18-Kan (pMW408) via *Xba*I. Both gene fusions are expressed under the control of the arabinose-inducible P_{BAD} promoter and carry an N-terminal His_6-tag. Due to different antibiotic resistance genes and different origins of replication, both plasmids can be co-expressed in one cell.

citA-yfp was constructed as described for *dcuS-yfp*, whereas the *citA* gene was amplified from genomic DNA of *E. coli* MG1655 by PCR with oligonucleotide primers citApetCfor and citApetCrev. The PCR fragment was cloned via the flanking *Nhe*I and *Sac*I restriction sites into pMW391. The *citA-yfp* fusion was subsequently inserted into pBAD30 via *Xba*I, resulting in pMW442. For functional studies, *cam*^{r} was amplified from pACYC184 with primers cam-

HindIII-for and cam-HindIII-rev and cloned into pMW442 with the *Hind*III restriction site, resulting in pMW557.

For co-expression of *cfp* and *yfp* in one cell for *in vivo* FRET measurements, *ecfp* and *eyfp* were amplified from pECFP or pEYFP, respectively, by PCR with oligonucleotide primers for-gfp-NcoI and HindIII-gfp-rev. Either PCR fragment was subcloned via the flanking restriction sites *Nco*I and *Hind*III into pET28a. *ecfp* and *eyfp* were subsequently cloned into pBAD18-Kan or pBAD30, respectively, using restriction endonucleases *Xba*I and *Hind*III, resulting in pMW762 and pMW765 (Bauer, unpublished).

The *cfp-yfp* fusion was constructed as follows. *ecfp* was amplified from pECFP with primers for-gfp-NcoI and rev-BamHI-gfp, and *eyfp* was amplified from pEYFP with primers BamHI-gfp-for and HindIII-gfp-rev. The *ecfp* fragment was subcloned via *Nco*I and *Bam*HI into pET28a, and the *eyfp* fragment was cloned behind *ecfp* via *Bam*HI and *Hind*III. The e*cfp-eyfp* fusion was subsequently cloned into pBAD18-Kan using restriction endonucleases *Xba*I and *Hind*III. The resulting construct pMW766 encoded ECFP(1-239)-Linker(9 aa)-EYFP(1-239), hereafter referred to as *cfp-yfp* or CFP-YFP (Bauer, unpublished).

CFP or YFP, respectively, were also fused to the N-terminus of DcuS (pMW389, *cfp-dcuS*; pMW388, *yfp-dcuS*) (Scheu, 2005). Most experiments were performed with the C-terminal fusions (pMW407 and pMW408).

Construction of a *dcuS-bs2* fusion

The *dcuS* gene was amplified from genomic DNA of *E. coli* MG1655 by PCR with oligonucleotide primers dcuSsurHind3-for and dcuSsurHind3-rev. The PCR fragment was cloned via *Hind*III into pUC18. The *bs2* gene was amplified from pGlow-Bs2-stop with primers Bs2-stop-for and Bs2-stop-rev and cloned in fusion to *dcuS* via restriction sites *Nde*I and *Pst*I, resulting in pMW842 (Fig. 6). Prior to the cloning of *bs2*, *Nde*I and *Pst*I restriction sites were mutated from pUC18 with complementary primers Mut_puC_NdeI-for and Mut_puC_NdeI-rev, and Mut_puC_PstI-for and Mut_puC_PstI-rev, respectively, by site-directed mutagenesis. A *Nde*I restriction site was then inserted at the 3'-end of *dcuS* by simultaneous mutation of the *dcuS* stop codon with complementary mutagenesis primers Mut_sur_NdeI-for and Mut_sur_NdeI-rev. 13 bp upstream of the inserted *Nde*I site, a *Pst*I restriction site was inserted with complementary mutagenesis primers Mut_PstI-for and Mut_PstI-rev. In this way, *bs2* could be cloned in fusion to *dcuS*.

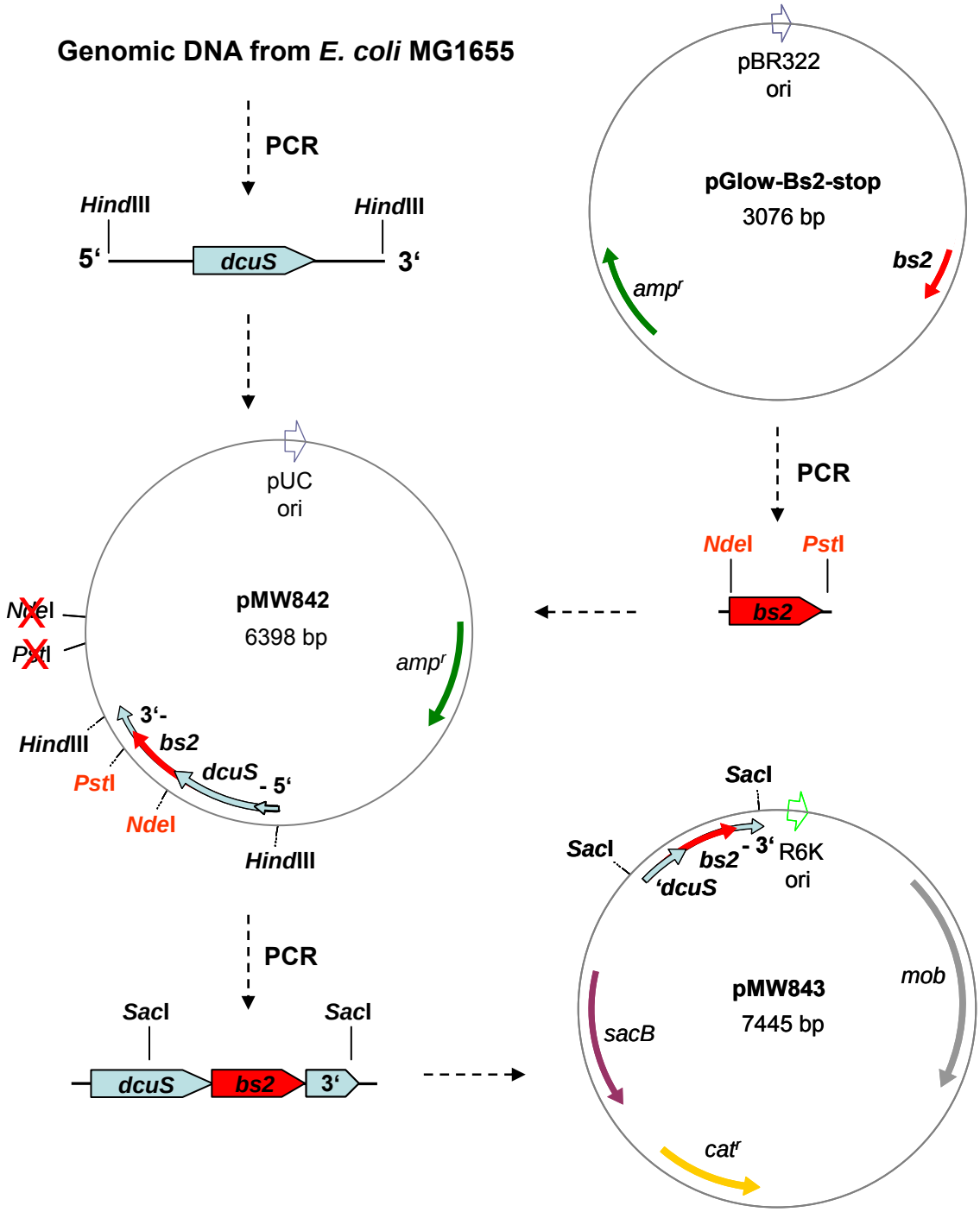

Figure 6: Construction of a *dcuS-bs2* gene fusion and cloning into a suicide vector. *dcuS* was cloned with its adjacent regions into pUC18 and *bs2-stop* was fused to the 3'-end of *dcuS* (pMW842). In the fusion gene, *bs2* is followed by the 3'-end adjacent to *dcuS*. The gene fusion was cloned into the suicide vector pDS132 (pMW843). The vector enables homologous recombination of *dcuS-bs2* into the chromosome of *E. coli* strains via the flanking sequences of *dcuS*. As illustrated in pMW842, restriction sites *Nde*I and *Pst*I were mutated in pUC18 and created in the *dcuS* gene by site-directed mutagenesis, to allow in fusion cloning of *bs2*.

The *bs2* gene and adjacent sequences of *dcuS* upstream and downstream of *bs2*, was amplified from pMW842 with primers dcuS-Bs2SacI-for and dcuS-Bs2SacI-rev and inserted into pDS132 via *Sac*I, resulting in pMW843. Due to the conditional R6K origin of replication of pDS132, which requires the π protein (encoded by the *pir* gene) for replication, cloning

into pDS132 was performed in *E. coli* JM109λ*pir*. The suicide vector was used to insert *dcuS-bs2* into the chromosome of desired *E. coli* strains via homologous recombination.
Besides, *dcuS-bs2-stop* was cloned into the low-copy vector pMW643 under control of the *dcuS* promoter. The gene fusion was amplified from pMW842 with primers dcuS-bs2_Eco-for and dcuS-bs2_Eco-rev and cloned into pMW643 using restriction endonuclease *Eco*RI, resulting in pMW875 (Fig. 7). pMW875 carries a tetracycline resistance gene that allows the selection of the plasmid for studies of the functional state of *dcuS* within the gene fusion. The *dcuS-bs2* fusion encodes DcuS(1-543)-(Gly-His)-Bs2(1-137).

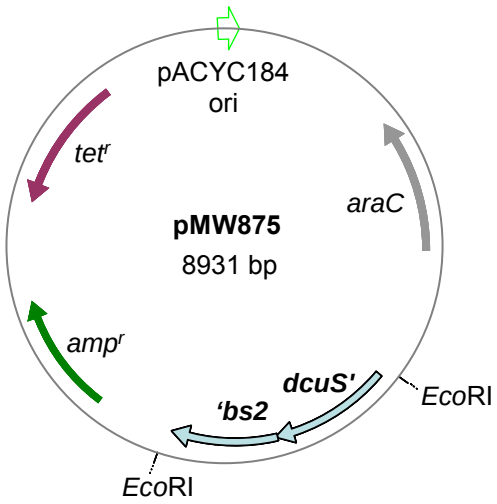

Figure 7: Expression plasmid pMW875 for moderate expression of DcuS-Bs2. *dcuS-bs2* was cloned from pMW842 into the low-copy vector pMW643 and expressed under the control of the *dcuS* promoter.

Homologous recombination into the chromosome of *E. coli* strains

Homologous recombination into the chromosome of *E. coli* was achieved using the suicide vector pDS132 (Philippe *et al.*, 2004). This system includes two recombination steps. Theoretical details are reported in section 4.2.2.
E. coli MC4100 and JW1241, both lacking the *pir* gene, were transformed with pMW843. Transformed cells were plated on LB-chloramphenicol plates to select plasmid integration into the recipient chromosome. After overnight growth at 37 °C, one colony was picked, diluted in 10 mM $MgSO_4$, and serial dilutions were plated on LB agar plates containing 5 % sucrose and without NaCl. This plating step allowed selection of plasmid excision from the chromosome by a second crossover event, leading to allelic exchange. After overnight incubation at 37 °C, 3 colonies were streaked on chloramphenicol-containing LB agar plates and in parallel on LB agar plates with 5 % sucrose and without NaCl. Sucrose-resistant and chloramphenicol-sensitive colonies were stored in a glycerol suspension at -80 °C. Since allelic exchange depends on the location of the second crossover event, picked colonies were screened by PCR in order to identify those carrying the desired allele (statistically 50 %

of the colonies). Omission of NaCl from the medium improves sucrose counter-selection in *E. coli* (Blomfield *et al.*, 1991).

Construction of single and double cysteine mutants of His_6-DcuS for over-expression

Wild-type *dcuS* was amplified from genomic *E. coli* DNA with oligonucleotide primers DcuS-N and DcuS-C and cloned into the over-expression vector pET28a via the flanking restriction sites *Nde*I and *Hind*III (Janausch *et al.*, 2002; Fig. 8). The resulting plasmid pMW151 encodes full-length DcuS (543 aa) with additional 20 amino acid residues derived from the N-terminal His-tag and a thrombin cleavage site. pMW151 served as the template plasmid for construction of single and double cysteine mutants of His_6-DcuS.

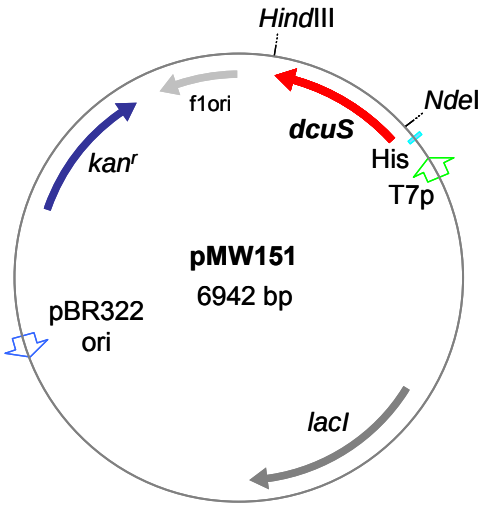

Figure 8: Expression plasmid pMW151 for over-expression of His_6-DcuS. *dcuS* was cloned into pET28a behind the IPTG-inducible T7 promoter and fused to an N-terminal His_6-tag.

Single and double cysteine mutants of His_6-DcuS were generated in pMW151 using complementary mutagenesis primers C199S_cn and C199S_nc, or C471S_cn and C471S_nc. The mutated nucleotide sequence of *dcuS* led to the exchange of cysteine to serine, resulting in pMW324, pMW325 or pMW336 (Kneuper, 2005). A single cysteine mutant at residue 83 in the periplasmic domain of DcuS was generated in pMW336 using complementary mutagenesis primers Q83Cmutfor and Q83Cmutrev, resulting in pMW452. A DcuS binding-defect mutant was generated in pMW324 using complementary mutagenesis primers R147A-Mut-for and R147A-Mut-rev, resulting in the exchange of arginine 147 in the periplasmic domain of DcuS to alanine (pMW446).

3.4 Protein-biochemical methods

Over-expression and purification of His_6-DcuS

Over-expression of His_6-DcuS was performed in *E. coli* C43(DE3) which was freshly transformed with plasmids containing the corresponding recombinant DcuS variant (pMW151, pMW324, pMW325, pMW336, pMW384, pMW446 or pMW452).

380 ml of LB medium, supplemented with 20 ml of 2 M glucose and 400 µl kanamycin, were inoculated with 2 % from an overnight culture of C43(DE3) carrying the desired plasmid. Cells were grown aerobically in 2 l Erlenmeyer flasks on a rotary shaker at 30 °C. Over-expression of the protein was induced by addition of 1 mM IPTG at an optical density (OD_{578}) of 0.5-0.8. Cells were grown for further 3 h at 30 °C and then harvested by centrifugation (6000 rpm, 10 min, 4 °C, Beckman JA-10 rotor). The pellet was washed in 20 ml buffer 1, and after repeated centrifugation resuspended in 20 ml buffer 1. Resuspended cells were broken by 2-3 passages through the French Pressure cell (20000 Psi). Intact cells and cell debris were separated by centrifugation (10000 rpm, 10 min, 4 °C, FiberLite F21B rotor). The supernatant was transferred to ultracentrifugation tubes (polycarbonate; minimal volume 20 ml, maximal volume 25 ml, Beckman). The membrane fraction containing His_6-DcuS was pelleted by ultracentrifugation (45000 rpm, 65 min, 4 °C, Beckman Coulter Optima LE-80K, Kontron TFT 70.38 rotor) and washed twice with buffer M (45000 rpm, 15 min, 4 °C). Subsequently, the membrane pellet was carefully homogenised in buffer 2 (10 ml per 1 g of wet membranes) using Potter S (Braun, Melsungen) and solubilised during homogenisation by the addition of Empigen BB (35 % w/v, Fluka) to a final concentration of 2 % (w/v). For efficient solubilisation, the protein was further stirred for 30 min on ice. Non-solubilised protein and membrane debris were removed by ultracentrifugation (50000 rpm, 55 min, 4 °C). The supernatant was shock-frozen in liquid N_2 and stored at -80°C.

His_6-DcuS was purified by affinity chromatography. Therefore, the solubilised membrane fraction was run by gravity through a Ni^{2+}-nitrilotriacetic acid (NTA)-agarose column (2 ml; Qiagen), which was equilibrated with 25 ml of buffer 3. The sample was added on the column. To obtain high quantities of purified protein, the flowthrough was collected for further purification procedures. The column was washed with 25 ml of buffer 3, and bound His_6-DcuS was eluted with 5 x 1 ml of buffer 4. Elution fractions of 1 ml were collected and analysed by SDS-PAGE. Elution fractions of > 90 % purity were combined and dialysed against buffer 5. Protein concentrations were determined with RotiQuant (Roth) according to Bradford (1976), using bovine serum albumin (BSA) as standard. Samples were shock-frozen in liquid N_2 and stored at -80 °C until further use.

Reconstitution of His_6-DcuS into liposomes

Reconstitution of His_6-DcuS into liposomes was performed, if not otherwise noted, at a phospholipid:protein ratio of 20:1 (w/w), using Triton X-100 as detergent and *E. coli* polar lipid extract (21 mM; Avanti Polar Lipids).

100 mg of *E. coli* phospholipids (20 mg/ml in chloroform) were evaporated and dissolved in 5 ml 20 mM K^+-phosphate buffer pH 7.5 containing 80 mg *N*-octyl-β-D-glucopyranoside (Gerbu). The solution was dialysed overnight against 3 x 1 litre 20 mM K^+-phosphate buffer pH 7.5. The resulting liposome suspension was frozen for three cycles in liquid N_2 and thawed slowly at 20 °C to ensure the formation of unilamellar liposomes.

Liposomes were totally destabilised by the addition of Triton X-100 at an effective detergent:lipid ratio (R_{eff}) of 2.5 (Rigaud *et al.*, 1988; 1995). The total amount of detergent (D_t) for the destabilisation of the lipids was calculated according to Paternostre *et al.* (1988) by equation [2], with D_a being the monomeric detergent concentration in the aqueous phase (0.18 mM for TX-100), and [lipid] the lipid concentration (21 mM).

$$[2] \qquad D_t = D_a + R_{eff}\,[lipid]$$

Purified and detergent-solubilised His_6-DcuS was added to the destabilised liposomes and the solution was stirred gently for 15 min at 20 °C. To remove the detergent, Bio-Beads SM2 (Bio-Rad), which were freshly degassed in 50 mM Tris/HCl pH 7.7, were added at a beads:detergent ratio of 5 (mg/mg) (Holloway, 1973). The suspension was incubated for 2 h at 4 °C, and then the same portion of Bio-Beads was added. After overnight incubation at 4 °C, further 5 mg of fresh Bio-Beads per mg of Triton X-100 were added to the suspension and incubated for one additional hour at 20 °C. The supernatant was removed from the Bio-Beads with a pipette, transferred to an ultracentrifugation tube and filled up to 20 ml with buffer R. The proteoliposomes were pelleted by ultracentrifugation (50000 rpm, 45 min, 4 °C, Kontron TFT 70.38 rotor) and washed twice in 50 mM Tris/HCl pH 7.7 (50000 rpm, 15 min, 4 °C). Finally, the proteoliposomes were resuspended in buffer R to the required protein concentration, frozen for three cycles in liquid N_2 and thawed slowly at 20 °C. After final freezing the proteoliposomes were stored at -80 °C until further use. When required, Na_2-fumarate was added to the buffers to a final concentration of 20 mM.

Chemical crosslinking

Protein subunits within a protein complex can be covalently crosslinked, so that the link remains stable upon SDS-PAGE. Chemical crosslinking was performed with disuccinimidyl suberate (DSS, Sigma-Aldrich). DSS is a homobifunctional, non-cleavable and membrane-permeable crosslinker with a spacer arm length of 11.4 Å (Fig. 9). DSS comprises two NHS esters, which form stable amide bonds after reaction with primary amines of lysine residues.

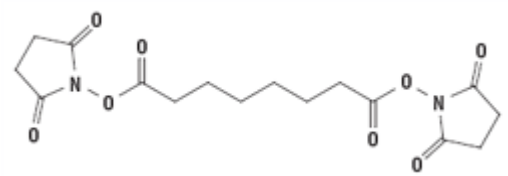

Figure 9: Chemical structure of disuccinimidyl suberate (DSS) crosslinker.

Because DSS is extremely sensitive to hydrolysis, the advices of Thermo Scientific Pierce Protein Research Products (http://www.piercenet.com/Products/) were considered.

DSS was weighed out with a plastic spatula and freshly dissolved in DMSO to a concentration of 25 mM prior to use. For crosslinking with NHS ester-crosslinkers the protein-containing buffer has to be free of Tris or other amine-containing components. Hence, detergent-solubilised His_6-DcuS was dialysed against buffer A, reconstituted His_6-DcuS was resuspended in buffer B, and isolated membranes containing over-expressed His_6-DcuS were homogenised in buffer C prior to crosslinking. For crosslinking reactions, 3 µg of solubilised His_6-DcuS, 6 µg of reconstituted His_6-DcuS, or 30 µg of isolated membranes were mixed with buffer D to a reaction volume of 20 µl. DSS (25 mM) was diluted in DMSO at a ratio of 1:41 (v/v), and 1 µl was added to the reaction mixture to a final DSS concentration of 30 µM. In the control reactions, 1 µl DMSO was added instead of DSS. After the addition of all components, the solution was gently mixed by pipetting. The reaction mixtures were incubated in a microtube thermoshaker (450 rpm, 15 min, 20 °C). The crosslinking reaction was stopped by addition of 1 M Tris/HCl pH 7.7 to a final concentration of 100 mM.

Samples were dissolved in 22 µl 2x SDS sample buffer containing DTT (200 mM), boiled for 5 min and subjected to SDS 10 % polyacrylamide gel electrophoresis (200 V, 70 min; Bio-Rad Mini-PROTEAN Tetra Cell system). Subsequently, the gel was transferred to a nitrocellulose membrane (Towbin *et al.*, 1979), which was treated with rabbit polyclonal antiserum (Eurogentec) raised against the periplasmic domain of DcuS and detected with secondary IgG antibodies coupled to peroxidase (Sigma-Aldrich).

Western blotting (semi-dry)

For the immunostaining of DcuS, protein samples were subject to SDS-PAGE and subsequently blotted for 2 h onto a nitrocellulose membrane (Protran, Schleicher & Schuell) (Towbin *et al.*, 1979).

3 filter layers of Whatman paper were soaked in cathode buffer and put on the cathode. The SDS gel was then put on the filter layers, followed by the nitrocellulose membrane, which was soaked in water. On top, 3 filter layers of Whatman paper were put, which were soaked in cathode buffer. The amperage (I) for blotting was dependent on the area to be transferred, and was calculated by equation [3].

[3] I [mA] = height (membrane) x width (membrane) x 0.8

The amperage (I) was kept constant. After blotting, the membrane was incubated in 20 ml blocking buffer overnight at 4 °C on a tumble shaker, so that the membrane was saturated with BSA. The blotted SDS gel was checked by staining with Coomassie Brilliant Blue (Serva). On the next day, the membrane was incubated with the primary antibody (1:2000 in 10 ml antibody solution) for 2.5 h by agitation at 20 °C. The membrane was washed for 2 x 5 min in 20 ml washing buffer and then incubated for 2 h with the secondary antibody (1:1000 in 10 ml antibody solution). After washing twice, the membrane was developed in 100 ml developer solution and incubated until a colour reaction took place, minimally for 5 min and maximally for 30 min.

The secondary antibody is coupled to peroxidase, which converts the H_2O_2 of the developer solution to O_2 and 2 H_2O. O_2 further oxidises the chlornaphtol, which then becomes visible by a dark blue to black colour.

Determination of β-galactosidase activity

β-Galactosidase activity was measured in permeabilised bacteria (Miller, 1992). Cultures were measured in exponential growth at an optical density (OD_{578}) of 0.5-0.8. The activities reported are the average of at least four independent experiments performed in quadruple. The β-galactosidase activity is given in Miller Units (MU) and was calculated by equation [4], with ΔE_{420nm}, extinction of the sample at 420 nm (blank value subtracted); t, time; V, sample volume; ΔOD_{578nm}, optical density of the sample at 578 nm (blank value subtracted).

[4] $MU = 1000 \times \Delta E_{420nm} / (t\ [min] \times V\ [ml] \times \Delta OD_{578nm})$

Sucrose step-gradient

For the investigation of a possible inclusion bodies formation by the expression of the DcuS-YFP fusion protein, the low-speed supernatant fraction after cell breakage was fractionated in a discontinuous sucrose step-gradient by ultracentrifugation. Thereby, membrane proteins were separated from soluble proteins and protein aggregates according to their different densities.

For the sucrose step-gradient, solutions of 0 %, 10 % and 40 % sucrose were freshly made from a filter-sterilised sucrose stock solution (50 %) in 50 mM Tris/HCl pH 7.7. The sucrose solutions were successively transferred carefully to an ultracentrifuge tube, with the highest concentration at the bottom. It was taken care that the sucrose layers were not mixed. The protein sample, which was also dissolved in 50 mM Tris/HCl pH 7.7, was carefully loaded on top of the layers. The ultracentrifuge was adjusted to slow acceleration and slow deceleration. After ultracentrifugation (45000 rpm, 2 h, 4 °C, Kontron TFT 70.38 rotor),

fractions of 1 ml were carefully collected by pipetting with a syringe successively from the bottom of the layers without whirling up the upper layers. 20 µl of each fraction was subjected to SDS-PAGE to examine the banding of DcuS-YFP in the protein/membrane fraction (10 % sucrose) and in the protein-aggregate fraction (40 % sucrose). Isolated and purified DcuS-YFP (pMW384) was used as a standard on the SDS gel.
Alternatively, a sucrose step-gradient with 10 %, 20 % and 45 % sucrose in 50 mM Tris/HCl pH 7.7 was run in a vertical rotor (VTI 65 vertical rotor, Beckman) by using 4.9 ml gradient tubes (OptiSeal, Beckman). The plastic gradient tubes were pierced at the bottom to collect samples of 0.5-1 ml.

Quantification of fusion protein expression by cell fractionation

Arabinose-induced bacteria expressing DcuS-YFP were harvested, resuspended in 8 ml of buffer 1 and broken using the French press as described previously. The cell homogenate was fractionated by low-speed centrifugation (10000 rpm, 10 min, 4 °C; Sigma 2K15, no. 12139 rotor). Thereby, debris and potential inclusion bodies sedimented in the low-speed pellet and were separated from the soluble fraction and cytosolic membranes, which were contained in the low-speed supernatant. The low-speed pellet was resuspended in 8 ml buffer 1. For semi-dry Western blot analysis, proteins from the low-speed pellet and the low-speed supernatant were separated by SDS-PAGE and transferred to nitrocellulose membranes. Membranes were treated with mouse polyclonal antibodies (Qiagen) raised against the His_6-tag of the fusion protein. Protein bands were detected with secondary IgG antibodies coupled to peroxidase (Sigma-Aldrich). Protein bands of three independent preparations were visualised and quantified by using the Kodak Image Station 440CF and the Kodak Molecular Imaging software.

3.5 Physicochemical methods

FRET spectroscopy

FRET measurements and FRET calculations were performed by Dr. Yun-Feng Liao and Dr. Wolfgang Erker in the working group of Prof. Dr. Basché, Institut für Physikalische Chemie, Johannes Gutenberg-Universität, Mainz.
Absorption and fluorescence spectra were measured in 1 ml quartz semi-microcuvettes at room temperature with a dual-beam UV-VIS spectrophotometer (OMEGA 20, Bruins Instruments, Germany) and a FluoroMax-2 spectrofluorometer (Jobin Yvon-Spex, NJ, USA). Fluorescence spectra were corrected for the wavelength dependence of the fluorometer and the inner filter effect (Lakowicz, 2006).

In vivo FRET measurements

For *in vivo* fluorescence studies, DcuS was genetically fused with derivatives of the green fluorescent protein (GFP). GFP is originated from the jellyfish *Aequorea victoria* (Tsien, 1998). It is non-invasive and can heterogeneously be expressed in many organisms. GFP contains 238 amino acid residues, folding as an 11-stranded β-barrel cylinder, which is threaded by an α-helix running up the axis of the cylinder. Fluorescence of GFP is derived from the oxidisation and cyclisation of three amino acid residues (Ser-Tyr-Gly) forming the chromophore, which is buried deeply in the centre of the β-barrel (Ormö *et al.*, 1996; Yang *et al.*, 1996). Spectral variants of GFP, which were genetically engineered, are available. In this work, the enhanced cyan fluorescent protein (ECFP, containing mutations F64L, S65T, Y66W, N146I, M153T, V163A) was used as the donor fluorophore, and the enhanced yellow fluorescent protein (EYFP, including mutations S65G, V68L, Q69K, S72A, and T203Y) as the acceptor fluorophore in *in vivo* FRET measurements. The Förster distance between the CFP and YFP FRET pair is 4.92 nm ± 0.10 nm (Patterson *et al.*, 2000).

E. coli expressing fluorescent proteins were harvested and washed twice by centrifugation in PBS buffer and finally resuspended in PBS buffer. Absorption spectra were recorded before fluorescence measurements. Cells were diluted to an absorbance of 0.1 at 400 nm to avoid the inner filter effect and signal saturation. Emission spectra were recorded while excited at 433 nm (CFP) or 488 nm (YFP), respectively. The recorded emission spectra were corrected for the wavelength dependence of the fluorometer and intensity fluctuations of the fluorometer lamp. The spectra were considered as a linear superposition of the spectra of donor, acceptor, and background signals. Background consisted of offset, Rayleigh scattering, Raman scattering, and *E. coli* auto-fluorescence. To remove the background from the measured spectrum, a multi-parameter fit was applied (Liao, 2008). Individual spectra of *E. coli* cells without expressing fluorescent protein were recorded at the same day and under the same conditions for each test series. Finally, reference spectra of donor (CFP protein) and acceptor (YFP protein) were determined *in vitro* with purified proteins.

Cytosolic CFP or YFP were purified for reference spectra. Therefore, CFP or YFP protein was expressed from a 20 ml culture of *E.* coli JM109pECFP or JM109pEYFP, respectively, and grown aerobically in LB broth for 4 h after 1 % inoculation of the overnight culture. Cells were harvested by centrifugation (6000 rpm, 10 min, 4 °C), washed twice and resuspended in 20 ml buffer 1. Cell supernatant was prepared by 3 cycles of French Press and cleared by centrifugation (10000 rpm, 10 min, 4 °C) to remove the cell debris. A subsequent ultracentrifugation step (45000 rpm, 45 min, 4 °C) allowed the separation of cytosolic soluble protein fraction from the membrane pellet fraction. The supernatant was subjected to filter centrifugation (Vivascience, molecular weight cutoff 10 kDa) to separate the fluorescent proteins from small disturbing fluorescent molecules. The measured spectra of purified CFP

and YFP, respectively, were normalised to unity for usage as reference spectra of donor and acceptor for *in vivo* FRET measurements. Emission spectra were recorded at an excitation wavelength of 433 nm for CFP and 488 nm for YFP. The spectral shape and the major peak positions at 476 nm for purified CFP and at 527 nm for purified YFP were in good agreement with the literature values (Patterson *et al.*, 2001).

In vitro FRET measurements

For *in vitro* FRET measurements, chemical fluorescent thiol-reactive dyes were used. The FRET pairs Alexa Fluor 488-C_5-Maleimide (donor; Invitrogen) and Alexa Fluor 594-C_5-Maleimide (acceptor; Invitrogen), or 5-IAF (5-Iodoacetamidofluorescein, donor; AnaSpec) and 5-TMRIA (Tetramethylrhodamine-5-iodoacetamide, acceptor; AnaSpec) were used.
Fluorescent dyes (10 mM in DMSO) were freshly diluted with DcuS-labelling buffer. 50 µM or 160 µM of the dye were incubated with 1 mg/ml of purified, detergent-solubilised and dialysed His_6-DcuS in DcuS-labelling-buffer overnight at 4 °C in the dark. Unbound dye was removed using a PD-10 column (Sephadex TMG-25, Amersham Biosciences). Labelled protein was purified and concentrated in a Vivaspin concentrator (Vivascience, MW cutoff 30 kDa) at 4 °C to a volume of 1 ml. The extent of labelling was estimated spectrophotometrically according to the absorption spectrum of labelled His_6-DcuS by measuring dye absorbance and protein concentration. Labelled His_6-DcuS was reconstituted into liposomes. Emission spectra were recorded at an excitation wavelength of 480 nm (Alexa488) or 580 nm (Alexa594), or 480 nm (5-IAF) or 530 nm (5-TMRIA), respectively.

Calculation of FRET efficiency and donor fraction

Background-free spectra of donor and acceptor and mixtures of both were used to calculate fluorophore concentrations, donor fraction (f_D) and FRET efficiency (E) according to Gordon *et al.*, 1998 (Liao, 2008).
The donor fraction (f_D) [5] represents the amount of donor in a sample containing donor and acceptor, and should be approximately 0.5 to allow an accurate determination of the FRET efficiency.

[5] $$f_D = \frac{[D]}{[D] + [A]}$$ with [D], donor concentration; [A], acceptor concentration

The transfer efficiency (E) was determined by equation [6], referred to as Gordon's equation. It includes the determination of the fluorophore concentrations, which is a prerequisite for the calculation of donor fraction and FRET efficiency.

[6] $$E = \frac{F_f - D_f \cdot \frac{F_d}{D_d} - \frac{A_f - F_f \cdot \frac{A_d}{F_d}}{1 - \frac{F_a}{A_a} \cdot \frac{A_d}{F_d}} \left[\frac{F_a}{A_a} - \frac{F_d}{D_d} \cdot \frac{D_a}{A_a} \right]}{G \left[1 - \frac{D_a}{F_a} \cdot \frac{F_d}{D_d} \right] \left[D_f + \frac{F_f - D_f \cdot \frac{F_d}{D_d} - \frac{A_f - F_f \cdot \frac{A_d}{F_d}}{1 - \frac{F_a}{A_a} \cdot \frac{A_d}{F_d}} \left[\frac{F_a}{A_a} - \frac{F_d}{D_d} \cdot \frac{D_a}{A_a} \right]}{G \left[1 - \frac{D_a}{F_a} \cdot \frac{F_d}{D_d} \right]} \left[1 - G \cdot \frac{D_a}{F_a} \right] - \frac{A_f - F_f \cdot \frac{A_d}{F_d}}{1 - \frac{F_a}{A_a} \cdot \frac{A_d}{F_d}} \cdot \frac{D_a}{A_a} \right]}$$

Nomenclature: *G*, factor representing the ratio between the decrease of donor signal and the increase of acceptor signal due to FRET. The *G* factors used in this work were 2.3 for the FRET pair CFP / YFP, 1.3 for Alexa488 / Alexa594, and 0.25 for IAF / TMRIA.

Three filter sets were used, termed by capital letters:

D (Donor filter set), excitation at donor wavelength and detection of donor emission

A (Acceptor filter set), excitation at acceptor wavelength and detection of acceptor emission

F (FRET filter set), excitation at donor wavelength and detection of acceptor emission.

The three filter sets were applied to three types of samples, represented by lower case letters, donor (*d*), acceptor (*a*), or a mixture of donor and acceptor (*f*).

Confocal laser scanning fluorescence microscopy

Confocal laser scanning fluorescence microscopy was performed by Dr. Sven Sdorra and Dr. Wolfgang Erker in the working group of Prof. Dr. Basché, Institut für Physikalische Chemie, Johannes Gutenberg-Universität, Mainz.

For live imaging microscopy, *E. coli* cells expressing fluorescent proteins were harvested, immobilised with poly-L-lysine hydrobromide (Fluka) on backed coverslides and washed with PBS buffer. All measurements were made in PBS buffer under ambient conditions using two different confocal fluorescence microscopes. On the one hand, a custom-built microscope (based on a Zeiss Axiovert 135 TV inverted microscope) was used, which has single-molecule sensitivity (Erker *et al.*, 2005; Kulzer *et al.*, 1999). Images with a typical size of 10 µm x 10 µm and 128 x 128 pixels were recorded with an integration time of 5 ms per pixel (objective: Zeiss Plan-Neofluar 100x / 1.30 oil). An argon-ion laser operating at 488 nm attenuated to a power of 0.5 µW was used for excitation. Emission was split into two beams (50:50), which simultaneously allowed the detection of total intensity (APD: Perkin-Elmer SPCM-AQR-14) and the recording of fluorescence spectra (spectrograph, Acton Spectra Pro-300i; Peltier-cooled CCD-camera, LaVision IM3 QE CAM). Images were recorded by moving the sample via a 3D piezo-scanner (Physik Instrumente P-731.20 and P-721.CLQ PIFOC). Alternatively, a commercial confocal microscope (Leica DM IRE2) with an argon-ion laser (488 nm, 0.4 µW) was used. The recorded images were typically 11.72 µm x 11.72 µm in size with a resolution of 512 x 512 pixels (objective: Leica HCX PL APO 40x / 1.25-0.75 oil). The cellular brightness distributions of individual cells were analysed by line scans and

3D-reconstruction using self-written software based on Igor Pro (Wavemetrics). For 3D-reconstruction, a stack of images was recorded for each cell. The images differed with respect to focus position along the optical axis. Typical z-increments were in the range of 150-200 nm.

Nitroxide spin-labelling of DcuS for EPR measurements

Purified and detergent-solubilised cysteine variants of His_6-DcuS were labelled with methanethiosulfonate spin label (MTSSL, Toronto Research Chemicals) at a 25-fold molar excess. The appropriate amount of MTSSL (25 mM in 25 mM Tris/HCl pH 7.7, 50 % EtOH) was added to the protein solution and allowed to react overnight at 4 °C on a tumble shaker. Excess label was removed by dialysis. The sample was therefore transferred to dialysis bags (MWCO 10 kDa, ZelluTrans Roth) and dialysed two times against 50-100 sample volumes of buffer 5 for 1-2 h. A third dialysis step against 100-200 volumes of buffer 5 was done overnight. Dialysed and labelled protein was shock-frozen in liquid N_2 and stored at -80 °C until further use.

EPR measurements and freeze-fracture electron microscopy

EPR measurements with MTSSL-labelled variants of His_6-DcuS were performed by Dominik Margraf and Dr. Olav Schiemann, WG Prof. Dr. T. Prisner, Institut für Physikalische und Theoretische Chemie, Universität Frankfurt/Main.

Freeze-fracture electron microscopy was performed by Dr. W. Haase, WG Prof. W. Kühlbrandt, Frankfurt/Main. Images were supplied by Dominik Margraf.

3.6 Databases

Literature search

NCBI, PubMed: http://www.ncbi.nlm.nih.gov/pubmed/

Protein information

Swiss-Prot and associated links: http://www.expasy.org/sprot/

Predicted domain organisation of proteins

Programme PSIPRED: http://bioinf.cs.ucl.ac.uk/psipred/

Putative transmembrane helices of proteins

Programme TMHMM: http://www.cbs.dtu.dk/services/TMHMM/

Protein structure information

RCSB Protein Data Bank: http://www.pdb.org/

Virtual Footprint

Programme Prodoric: http://prodoric.tu-bs.de/vfp/

4. Results

4.1 Oligomerisation of DcuS

The DcuSR two-component system of *Escherichia coli* regulates gene expression of anaerobic fumarate respiration in response to external C_4-dicarboxylates (Zientz *et al.*, 1998; Kneuper *et al.*, 2005). The signal is transduced across the membrane resulting in expression of genes essential for fumarate respiration (*dcuB*, *fumB*, *frdABCD*) and aerobic C_4-dicarboxylate transport (*dctA*).

Investigation of membrane-bound sensor histidine kinases like the osmosensors EnvZ and KdpD from *E. coli* as well as the virulence-inducing sensor VirA from *Agrobacterium tumefaciens*, imply that oligomerisation plays an important role in signal transduction across the membrane (Yang and Inouye, 1991; Heermann *et al.*, 1998; Pan *et al.*, 1993).

Little is known about the oligomeric state of membrane-bound sensor histidine kinases. Previous studies were mainly performed with truncated, detergent-solubilised proteins. In this work, the oligomeric state of DcuS was studied *in situ* in its functional environment.

Fluorescent resonance energy transfer (FRET) can be used to detect protein-protein interactions (Truong and Ikura, 2001). Oligomer formation of DcuS was investigated *in vivo* and *in vitro* by FRET. The degree of oligomerisation was determined by chemical crosslinking of DcuS *in situ*.

4.1.1 *In vivo* FRET measurements with DcuS fused to variants of GFP

For *in vivo* FRET measurements, derivatives of the green fluorescent protein (GFP) from the jellyfish *Aequorea victoria* were genetically fused to DcuS. The enhanced variant of the cyan fluorescent protein (ECFP) and the enhanced variant of the yellow fluorescent protein (EYFP) were used as FRET pair. Both fluorophores exhibit enhanced fluorescence intensity due to exchanges of appropriate amino acid residues. For simplicity, they are referred to as CFP and YFP.

The normalised absorption and emission spectra of CFP and YFP are depicted (Fig. 10). The excitation or absorption maximum of CFP is at 433 nm, that of YFP at 513 nm. CFP reveals two emission maxima, a main peak at 475 nm and a minor peak at 501 nm. YFP exhibits an emission maximum at 527 nm. The emission spectrum of CFP overlaps with the absorption spectrum of YFP, allowing fluorescence resonance energy transfer between the two fluorophores. Thereby, CFP acts as donor and YFP as acceptor.

To avoid the interference of the excitation light in the detection of the emission light, YFP was not exactly excited at its absorption maximum, but at a shorter wavelength.

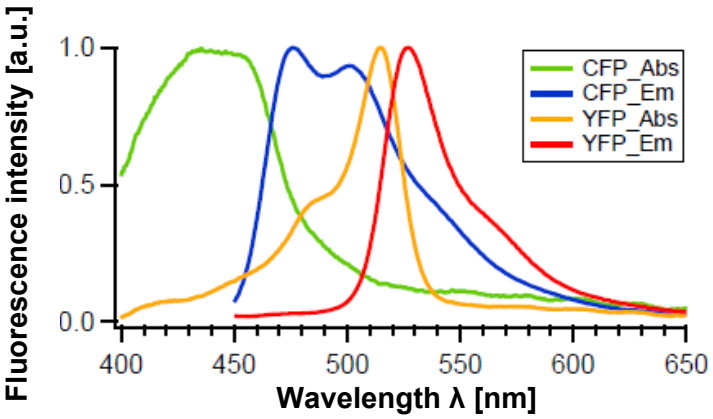

Figure 10: Absorption and emission spectra of purified CFP and YFP. CFP was excited at 433 nm, YFP was excited at 488 nm. Spectra were normalised to unity while setting the highest fluorescence intensity to 1.0. Abs, absorption; Em, emission. (Liao, 2008)

Functional state of DcuS fused to GFP variants

The functional state of DcuS in the fusion proteins was tested *in vivo* by measuring the DcuS-dependent induction of the *dcuB* gene with a *dcuB'-'lacZ* reporter gene fusion in a DcuS-deleted strain (IMW260) grown anaerobically (Tab. 6). Plasmid-encoded DcuS-YFP and DcuS-CFP (pMW384 or pMW386, respectively), carrying YFP or CFP C-terminal to DcuS, restored *dcuB'-'lacZ* expression in the presence of fumarate to a level slightly higher than that obtained with plasmid-encoded wild-type DcuS (pMW151). The fusion proteins with YFP or CFP fused to the N-terminal end of DcuS (pMW385 and pMW387, respectively) complemented *dcuB'-'lacZ* activity to at least 76 **%**. DcuS was thus functional upon fusion with YFP or CFP.

Table 6: Functional test of DcuS-CFP and DcuS-YFP by induction of *dcuB'-'lacZ* expression. *E. coli* IMW260 was grown anaerobically in eM9 medium with 50 mM glycerol and 20 mM DMSO, with and without the addition of 20 mM fumarate as effector.

Strain (relevant genotype)	Expression of *dcuB'-'lacZ* (Miller units)	
	Fumarate	H_2O
IMW260 (*dcuS*)	5 ± 1	8 ± 2
IMW260 pMW151 (*dcuS*$^+$)	279 ± 32	2 ± 1
IMW260 pMW384 (*dcuS-yfp*)	332 ± 33	9 ± 2
IMW260 pMW386 (*dcuS-cfp*)	301 ± 30	6 ± 3
IMW260 pMW385 (*yfp-dcuS*)	234 ± 28	5 ± 2
IMW260 pMW387 (*cfp-dcuS*)	211 ± 38	3 ± 1

The characteristic CFP and YFP fluorescence in the fusion proteins was confirmed by fluorescence spectroscopy. Therefore, DcuS, CFP and YFP were functional in the fusion proteins. Further experiments were predominantly performed with the C-terminal fusion proteins DcuS-CFP and DcuS-YFP.

Qualitative FRET measurements in cells expressing DcuS-CFP and DcuS-YFP

The fusion proteins were expressed in *E. coli* under the control of the *araBAD* promoter. JM109 expressing DcuS-CFP, DcuS-YFP or co-expressing both fusion proteins was excited at 433 nm (Fig. 11A). The emission spectrum of DcuS-CFP (donor) exhibited two peaks characteristic for CFP (Fig. 11B). DcuS-YFP (acceptor) was slightly excited leading to an emission peak characteristic for YFP. Co-expression of both proteins led to a decrease of donor emission and an increase of acceptor emission, giving evidence for fluorescence resonance energy transfer. The observed FRET is indicative for oligomer formation.

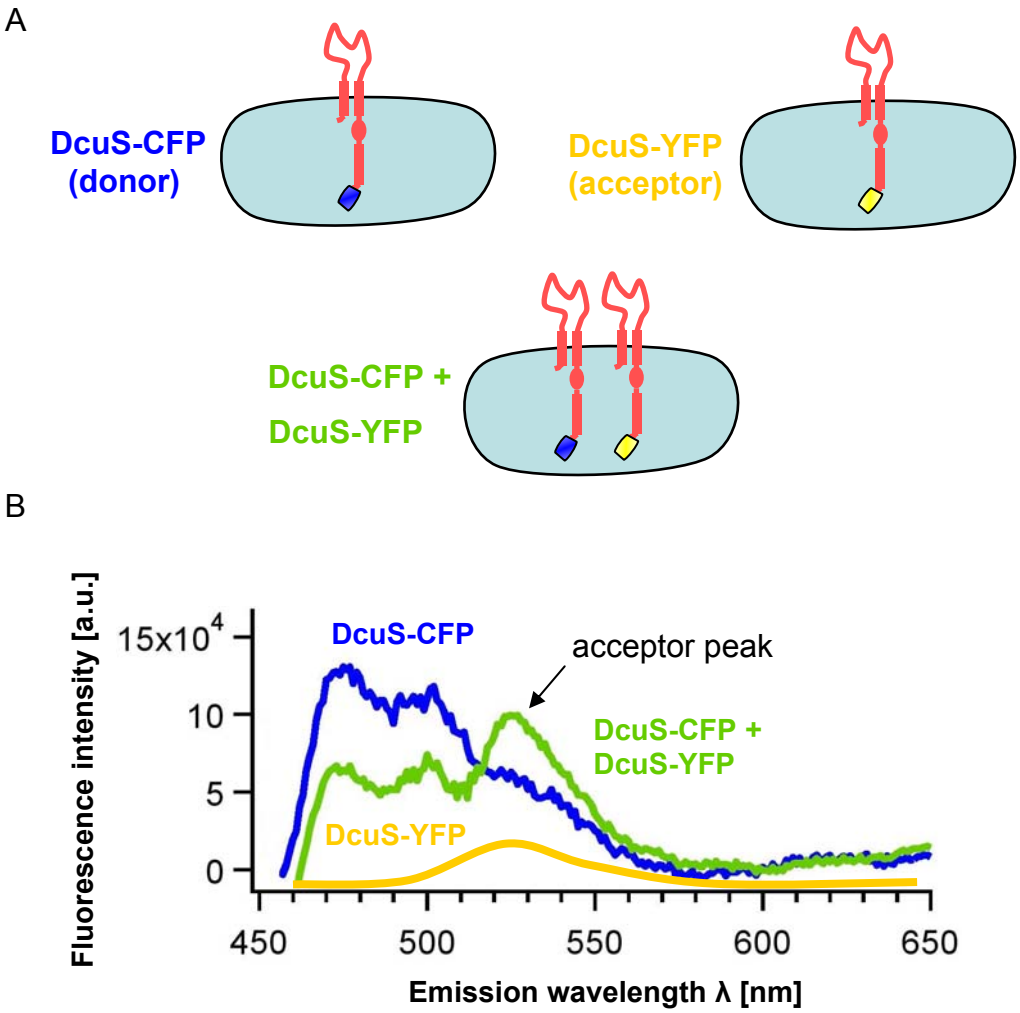

Figure 11: *In vivo* FRET measurements. A, Experimental setup. B, Experimental data. Emission spectra of *E. coli* JM109 expressing DcuS-CFP (pMW408) (blue) or DcuS-YFP (pMW407) (yellow), or co-expressing DcuS-CFP and DcuS-YFP (green) were recorded after excitation at 433 nm and background subtraction. Cells were grown aerobically at 30 °C with 333 µM arabinose as inductor. Prior to measurements, cells were washed and resuspended in 1 ml PBS-buffer, pH 7.5 and further diluted to an absorbance of 0.1 at 400 nm.

Background fluorescence of *in vivo* FRET measurements

In addition to the signals derived from donor and acceptor, measured spectra of *E. coli* cells contained inevitable background signals (Fig 12). Auto-fluorescence of bacteria originated from endogenous fluorophores, such as nicotinamide-adenine dinucleotide (phosphate) (NAD(P)H), flavin mononucleotide (FMN) and flavin adenine dinucleotide (FAD) (Billinton and Knight, 2001). The small cell particles contributed to Rayleigh scattering. Furthermore, a characteristic Raman scattering of water was detected, with an emission peak at 515 nm. A weak constant detector noise was also present.

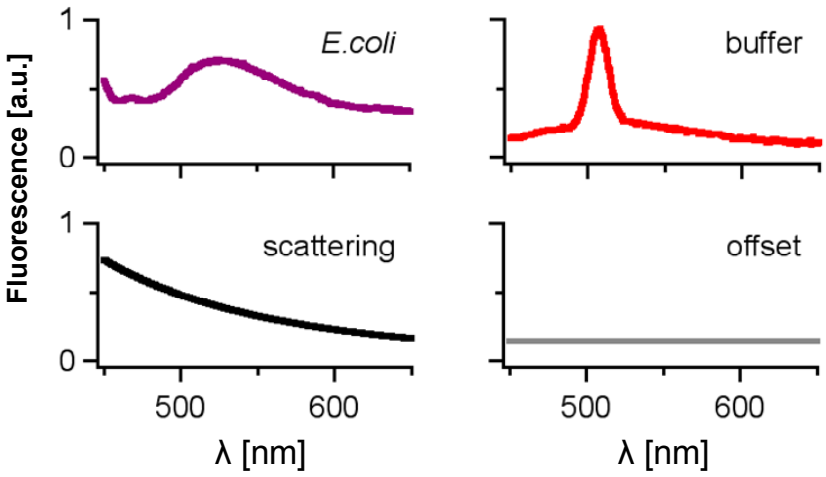

Figure 12: Background fluorescence spectra of *in vivo* FRET measurements after excitation at 433 nm. *E. coli* (JM109) auto-fluorescence (purple), Raman scattering of the buffer (red), Rayleigh scattering from cell particles (black), offset from instrumental noise (grey). (Figure derived from Liao, 2008)

Background spectra were subtracted from all emission spectra measured. Therefore, individual reference spectra from the buffer, and from *E. coli* JM109 grown in parallel to the cells expressing fluorescent proteins were recorded at the same day and under the same conditions for each test series.

Determination of relative FRET efficiencies and control measurements

FRET efficiencies were calculated by Gordon's equation as described in materials and methods (Liao, 2008). The FRET efficiency is dependent on the distance between donor and acceptor, their orientation to each other, and on the Förster distance of the FRET pair. The Förster distance is based on the physical properties of the fluorophores and is characteristic for every FRET pair. It is defined as the distance between donor and acceptor at which 50 % of the excitation energy of the donor is transferred to the acceptor. The Förster distance between CFP and YFP is 4.92 nm (Patterson *et al.*, 2000).

Donor and acceptor should be expressed at similar amounts to allow an accurate determination of the FRET efficiency. The donor fraction represents the amount of donor in a

sample containing both fluorophores. Although the vectors used to co-express two fusion proteins in one cell (pBAD30- and pBAD18-Kan derivatives) exhibit different copy numbers, a donor fraction of about 0.5 was accomplished by growing the cells to the exponential phase. FRET measurements were performed with *E. coli* JM109 harbouring the plasmids indicated.
To determine the maximal FRET efficiency under given experimental conditions, a CFP-YFP fusion protein was constructed (pMW766), containing a linker of 9 amino acid residues between CFP and YFP. Cells expressing cytosolic CFP-YFP fusion protein revealed an average donor fraction of 0.49 ± 0.01 with a FRET efficiency of 0.46 ± 0.1 (26 data points). This represents the maximal FRET efficiency that can be obtained under given experimental conditions and was therefore set as 100 % relative FRET efficiency (Fig. 13).

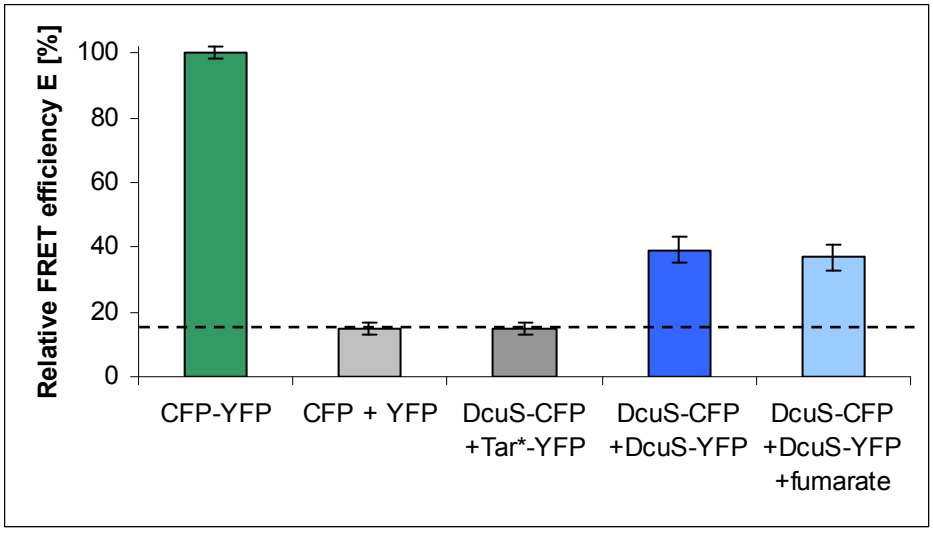

Figure 13: Relative FRET efficiency of cells expressing fluorescent proteins. The relative FRET efficiency of CFP-YFP fusion protein was set as 100 %. Dashed line indicates the threshold value for specific FRET. *Tar(1-331)-YFP.

As a negative control, cytosolic CFP and cytosolic YFP (pMW762 and pMW765) were co-expressed. A donor fraction of 0.4 ± 0.06 with a relative FRET efficiency of 15 % was observed (20 data points). Furthermore, DcuS-CFP (pMW408) was co-expressed with the membrane protein Tar(1-331)-YFP (pDK108), a C-terminal truncated variant of the chemotaxis receptor Tar which is homogeneously distributed in the cell membrane (Kentner *et al.*, 2006) and does not interact with DcuS. Co-expression was performed in the presence of L-arabinose and IPTG. A donor fraction of 0.41 ± 0.01 with a relative FRET efficiency of 15 % was detected (39 data points). The low relative FRET efficiency of 15 % obtained in both control measurements represented a background FRET signal in the experimental system. Specific FRET due to an interaction between the investigated proteins should be clearly above this value, so a relative FRET efficiency of 15 % was set as threshold value (Fig. 13, dashed line). Cells co-expressing DcuS-CFP and DcuS-YFP (pMW408 and pMW407) grown in the absence of effector yielded a donor fraction of 0.41 ± 0.01 with a relative FRET

efficiency of 39 % (44 data points), indicating specific FRET. This can be attributed to specific DcuS-DcuS interaction. When the bacteria were grown in the presence of fumarate, only minor differences were observed, with a donor fraction of 0.45 ± 0.01 and a relative FRET efficiency of 37 % (28 data points). This suggests a constant oligomeric state of DcuS in living cells.

FRET was also observed in cells co-expressing the N-terminal fusions CFP-DcuS and YFP-DcuS. In contrast, cells co-expressing CFP-DcuS (N-terminal fusion) with DcuS-YFP (C-terminal fusion) and vice versa, no FRET was observed (not shown). This could be due to a distance larger than 50 Å between the N-terminus of one DcuS monomer and the C-terminus of another DcuS monomer in the oligomer. However, these results should be considered carefully because an increased expression of the C-terminal fusion proteins compared to the expression of the N-terminal fusion proteins was observed. The unbalanced expression levels led to unbalanced donor fractions which were not adequate to determine an accurate FRET efficiency.

4.1.2 *In vitro* FRET measurements with fluorescently labelled His_6-DcuS

In vitro oligomerisation of DcuS was studied with over-expressed and purified His_6-DcuS after labelling with fluorescent dyes and reconstitution into liposomes.

Alexa-maleimide fluorophores bind to thiol groups of cysteine residues. Alexa488, which reveals an excitation maximum at 493 nm was used as donor, and Alexa594, exhibiting an emission maximum at 615 nm was used as acceptor (Fig. 14). The emission spectrum of the donor overlaps with the excitation spectrum of the acceptor, allowing fluorescence resonance energy transfer.

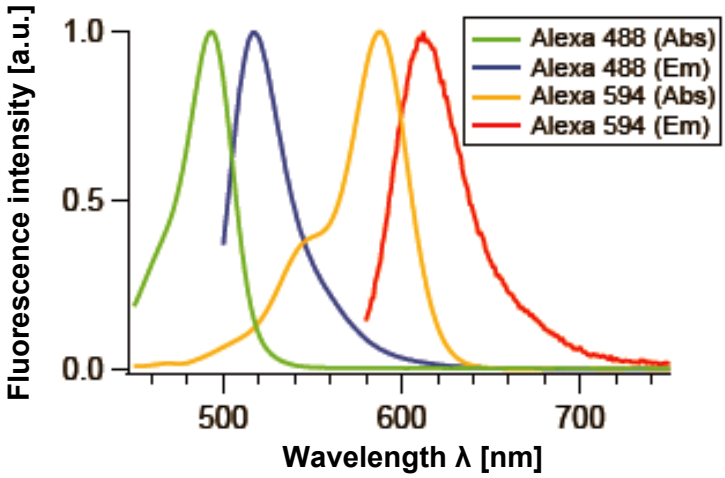

Figure 14: Absorption and emission spectra of Alexa dyes. Alexa Fluor 488-maleimide was excited at 480 nm, Alexa Fluor 594-maleimide was excited at 580 nm. Spectra were normalised to unity while setting the highest fluorescence intensity to 1.0. Abs, absorption; Em, emission. (Liao, 2008)

It turned out that a DcuS mutant lacking cysteine residues was also labelled with the Alexa-fluorophores (Fig. 15). Other fluorophores tested also bound unspecifically to DcuS. Nevertheless, FRET experiments could be performed, since site specific labelling was not essential for qualitative inter-molecular FRET measurements.

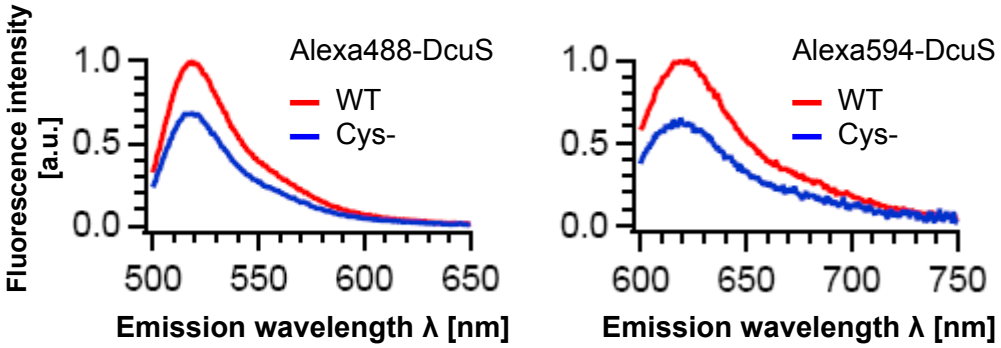

Figure 15: Emission spectra of Alexa-labelled His_6-DcuS. Purified and detergent-solubilised wild-type His_6-DcuS (WT) and a cysteine-less mutant of His_6-DcuS (Cys-) were labelled with Alexa Fluor488-maleimide (left) or Alexa Fluor 594-maleimide (right) and excited at 480 or at 580 nm, respectively. Spectra were normalised to unity while setting the highest fluorescence intensity to 1.0. (Liao, 2008)

Qualitative FRET measurements of labelled His_6-DcuS before and after reconstitution

Purified His_6-DcuS reconstituted into liposomes was reported as functional for fumarate sensing and kinase activity (Janausch *et al.*, 2002; Kneuper *et al.*, 2005). Oligomer formation of His_6-DcuS in proteoliposomes was investigated via FRET.

One aliquot of detergent-solubilised His_6-DcuS was labelled with Alexa-Fluor488, a second aliquot was labelled with Alexa-Fluor594 (Fig. 16A). Both aliquots were mixed and emission spectra were recorded before and after reconstitution into liposomes after excitation at 493 nm. The normalised spectra exhibited the characteristic emission peak of Alexa-Fluor488 (Fig. 16B). In the reconstituted sample a second peak was detected corresponding to Alexa594 emission, which was caused by fluorescence resonance energy transfer.

No significant difference was observed in the presence or absence of fumarate. FRET measurements were also performed with His_6-$DcuS_{R147A}$, a variant of DcuS which was mutated in the binding site to abolish the fumarate-binding ability, but still maintaining the kinase activity (Kneuper *et al.*, 2005). The same results were obtained as for wild-type His_6-DcuS (not shown). The oligomerisation of DcuS seems to be independent of the presence of fumarate, resembling the observation from the *in vivo* FRET measurements.

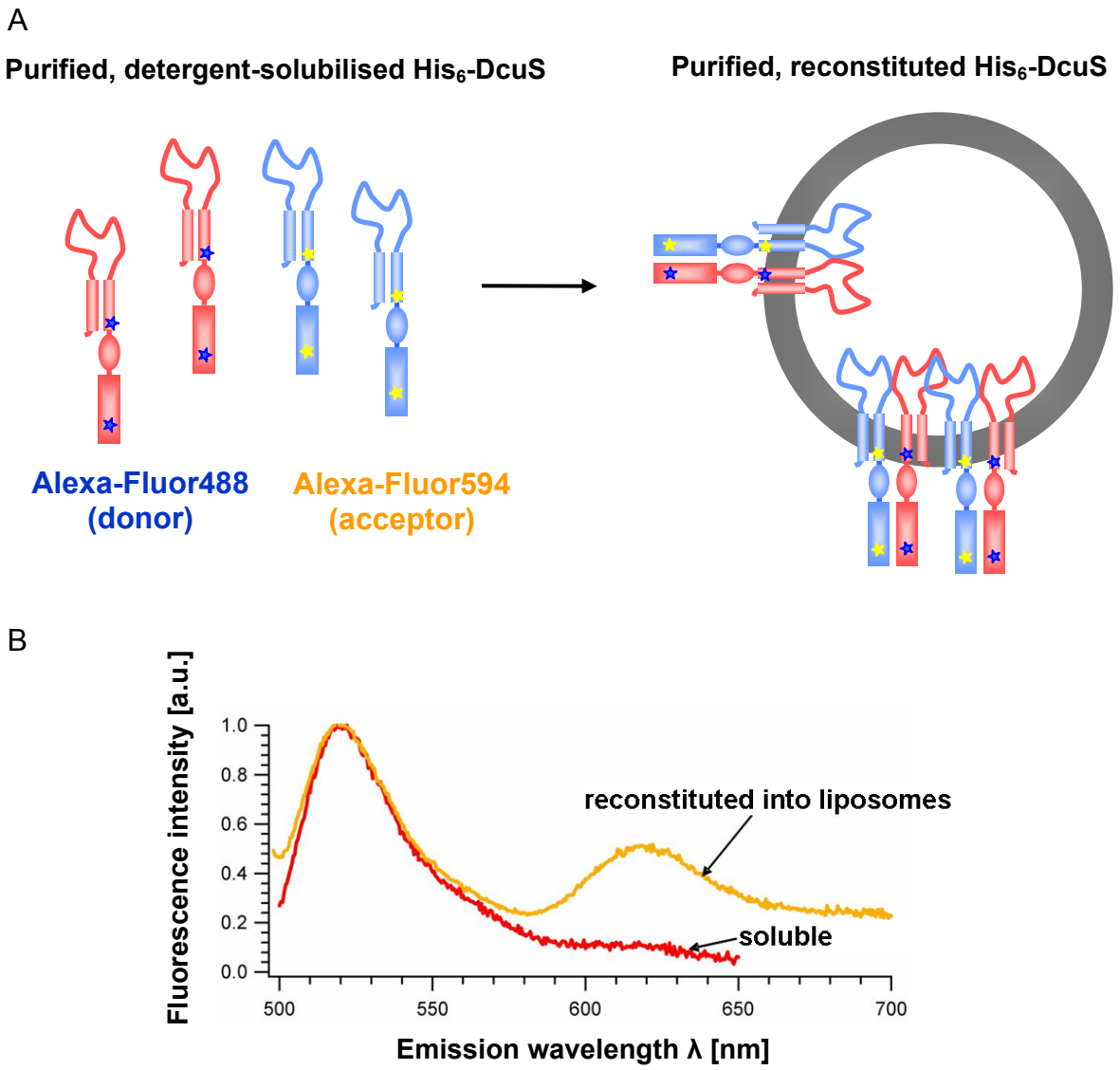

Figure 16: *In vitro* FRET measurements. A, Experimental setup. B, Experimental data. Emission spectra of a mixture of Alexa488-DcuS and Alexa 594-DcuS were recorded before and after reconstitution into liposomes after excitation at 493 nm. Spectra were normalised to unity while setting the highest fluorescence intensity to 1.0 after background subtraction (Rayleigh scattering originated from lipid or detergent micelles). The protein concentration was 0.1 mg in 1 ml of 50 mM Tris/HCl, pH 7.7. Reconstitution was performed at a phospholipid:protein ratio of 20:1 (mg/mg). The proteoliposomes after reconstitution exhibit an inside out orientation. Note that equally labelled DcuS monomers can also form oligomers, but do not contribute to FRET.

To confirm that the observed FRET signal was due to specific protein-protein interaction and not due to molecular crowding of DcuS in the liposomes, reconstitution of His_6-DcuS was performed at different phospholipid:protein ratios up to 160:1 (mg/mg) (Fig. 17). FRET was still detected at all tested phospholipid:protein ratios. The observed FRET is thus indicative for oligomer formation of His_6-DcuS after reconstitution into liposomes.

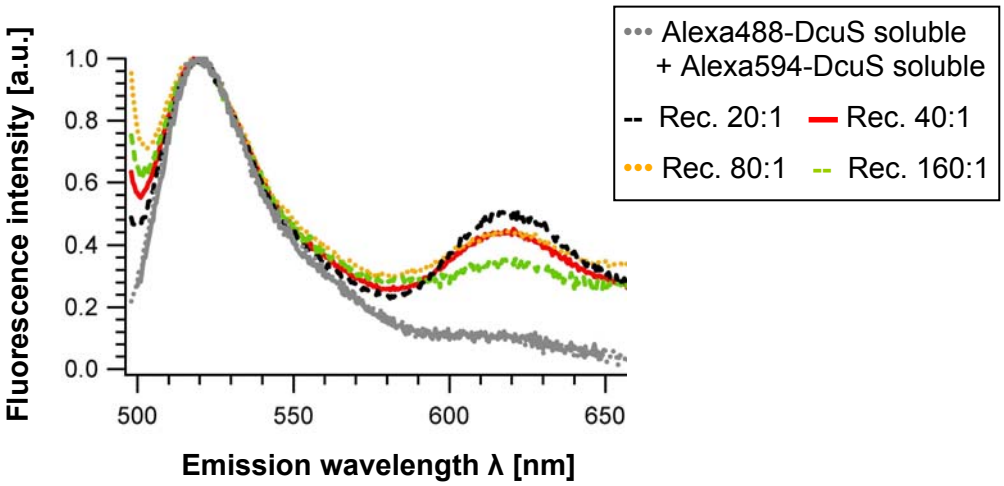

Figure 17: *In vitro* FRET measurements after reconstitution at various phospholipid:protein ratios. Emission spectra of a mixture of Alexa488-DcuS and Alexa 594-DcuS were recorded before (grey) and after reconstitution into liposomes after excitation at 493 nm. The mixture was diluted prior to reconstitution (Rec.) while keeping the amount of phospholipids constant, resulting in the following phospholipid:protein ratios (mg/mg): 20:1 (black), 40:1 (red), 80:1 (yellow), 160:1 (green). The protein concentration in 1 ml of 50 mM Tris/HCl pH7.7 was 0.1 mg/ml (Rec. 20:1), 0.05 mg/ml (Rec. 40:1), 0.025 mg/ml (Rec. 80:1), 0,0125 mg/ml (Rec. 160:1). Spectra were normalised to unity while setting the highest fluorescence intensity to 1.0 after background subtraction.

In vitro FRET measurements were also performed with His_6-DcuS labelled with iodacetamide fluorophores, i.e. 5-iodacetamidofluorescein (IAF) as donor and tetramethylrhodamine-5-iodacetamide (TMRIA) as acceptor, leading to similar results (not shown).

4.1.3 Chemical crosslinking of His_6-DcuS *in situ*

Proteins that are close together within a protein complex can be covalently crosslinked. The link remains stable upon SDS-PAGE. Proteins containing cysteine residues can be crosslinked by intermolecular disulfide bond formation under oxidative conditions. Besides, crosslinking is performed with chemical crosslinkers which connect subunits within a protein complex, mostly by formation of stable amide bonds after reaction of NHS esters with primary amines.

Influence of oxidising conditions on the oligomerisation of DcuS

DcuS (referred to as $DcuS_{WT}$) contains two cysteine residues, a membranous cysteine (C199) situated in the second transmembrane helix and a cytosolic cysteine (C471) located in the kinase domain (Fig. 18, left). Crosslinking by cysteine disulfides under oxidising conditions was tested with purified His_6-DcuS. Single cysteine mutants (referred to as $DcuS_{C199S}$ and $DcuS_{C471S}$) and a double cysteine mutant (referred to as $DcuS_{Cys-}$) were used, which were created by mutation of each cysteine to serine (Kneuper, 2005). The functional state of the DcuS cysteine mutants was tested by their capability to induce *dcuB'-'lacZ*

expression *in vivo*. All plasmid-encoded DcuS cysteine mutants were able to complement *dcuB'-'lacZ* expression anaerobically in the presence of fumarate up to 70 % of wild-type activity, demonstrating that all cysteine mutants were functional (Kneuper, 2005). Detergent-solubilised wild-type His_6-DcuS and cysteine mutants of His_6-DcuS, which were over-expressed and purified under aerobic conditions, were loaded on a SDS gel in the presence or absence of the reducing agent dithiothreitol (DTT) and subsequently detected by immunostaining (Fig. 18).

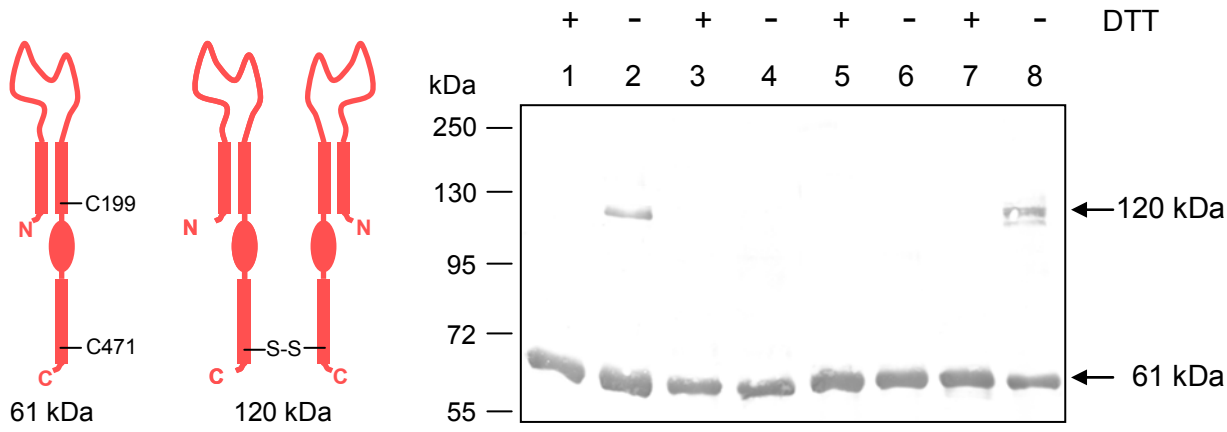

Figure 18: Influence of oxidising conditions on the oligomerisation of purified His_6-DcuS. Aerobically purified and detergent-solubilised cysteine mutants of His_6-DcuS (1 µg) were subject to SDS-PAGE in the presence or absence of dithiothreitol (DTT) and detected by Western blotting with antiserum against the periplasmic domain of DcuS. Lanes, 1+2: $DcuS_{WT}$, 3+4: $DcuS_{Cys}$-, 5+6: $DcuS_{C471S}$, 7+8: $DcuS_{C199S}$. On the left hand, the location of the two native cysteine residues in wild-type DcuS is illustrated.

All DcuS variants revealed a band of approximately 61 kDa, corresponding to the molar mass of a DcuS monomer. $DcuS_{WT}$ and $DcuS_{C199S}$ exhibited an additional dimeric band of about 120 kDa when loaded without DTT (Fig. 18, lanes 2 and 8). The dimerisation was due to intermolecular C471-disulfide bond formation. For $DcuS_{Cys-}$ no aggregation was detected under oxidising conditions because of the lack of oxidisable cysteine residues (Fig. 18, lane 4). Interestingly, $DcuS_{C471S}$, comprising C199, only revealed a monomeric band, indicating that C199 is not accessible to disulfide bond formation (Fig. 18, lane 6). For reconstituted $DcuS_{WT}$ and reconstituted DcuS cysteine mutants, the same band patterns were observed as for the detergent-solubilised proteins (not shown).

The specificity of DcuS dimerisation due to disulfide crosslinking was further investigated. Wild-type His_6-DcuS was purified in the presence of DTT in every step of the preparation. One aliquot was withdrawn and subsequently subjected to SDS-PAGE, a second aliquot was dialysed against DTT-less buffer prior to SDS-PAGE (Fig. 19).

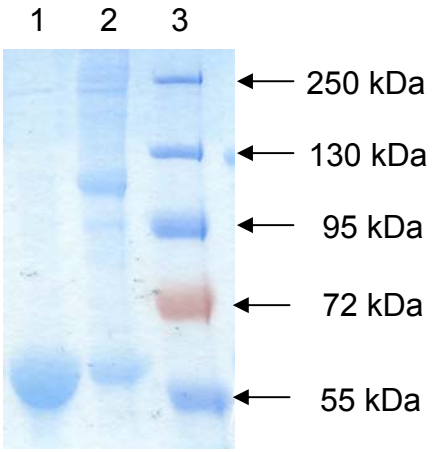

Figure 19: SDS-PAGE of His_6-$DcuS_{Wt}$ after purification under reducing conditions. Proteins (5 µg) were separated by SDS-PAGE and stained with Coomassie Blue. Lanes, 1: His_6-$DcuS_{WT}$ purified in the presence of DTT, 2: His_6-$DcuS_{WT}$ purified in the presence of DTT and dialysed against DTT-less buffer (4 °C, 2 x 2 h and overnight). Both samples were loaded without DTT in the sample buffer. Lane 3: PageRuler Plus Prestained Protein Ladder (Fermentas).

Both samples were loaded without DTT in the sample buffer. In lane 1 (Fig. 19), the monomeric band of His_6-DcuS was visible. No dimeric band was observed. Lack of disulfide formation may be due to transfer of DTT in the SDS-PAGE buffer from the protein sample. After removing DTT completely from the second aliquot by dialysis, an additional distinct dimeric band appeared (Fig. 19, lane 2). Hence, the observed crosslinking of His_6-DcuS is due to unspecific oxidative crosslinking and occurs when two monomers interact by chance. Moreover, all cysteine mutants can complement the function of wild-type DcuS *in vivo*, indicating that the cysteine residues in DcuS are not physiologically or functionally relevant, especially under the reducing conditions prevailing within the cytosol of the bacterial cell. In particular, the cysteine residues have no role in dimerisation.

Determination of the oligomeric state of DcuS by chemical crosslinking

To determine the oligomeric state of DcuS, detergent-solubilised, reconstituted and membrane-embedded His_6-DcuS was crosslinked with 30 µM disuccinimidyl suberate (DSS) (Fig. 20). DSS is a homobifunctional, non-cleavable and membrane-permeable crosslinker reacting with amide groups. Low concentrations of DSS were used to reduce unspecific crosslinking reactions owing to abundant crosslinker. Furthermore, crosslinking experiments were predominantly performed with $DcuS_{Cys-}$ to avoid unspecific DcuS aggregation due to oxidisation as observed for detergent-solubilised $DcuS_{WT}$ crosslinked in the absence of DTT (Fig. 20, lane 2). The presence of DTT turned out to disturb the crosslinking reaction (not shown). After crosslinking, detergent-solubilised $DcuS_{Cys-}$ was still found with the molecular mass of monomeric DcuS (61 kDa) (Fig. 20, lane 4), whereas reconstituted and membrane-embedded $DcuS_{Cys-}$ revealed a monomeric band, a weak band with the molecular mass corresponding to a dimer (120 kDa), and a distinct band of approx. 240 kDa corresponding to

a tetramer (Fig. 20, lanes 6 and 8). The weak band of the dimer might represent partially crosslinked tetrameric DcuS.

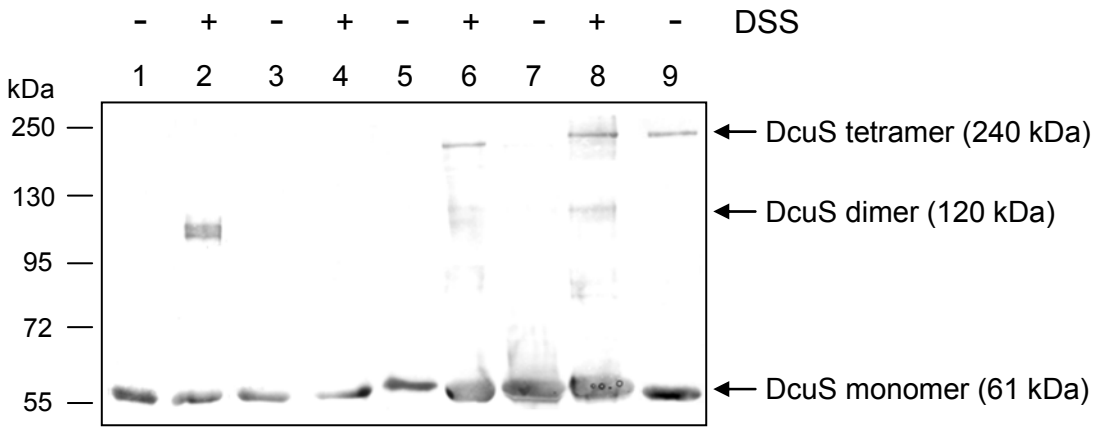

Figure 20: Determination of the oligomeric state of DcuS by chemical crosslinking. Detergent-solubilised, reconstituted or membrane-embedded His_6-DcuS was crosslinked with 30 µM disuccinimidyl suberate (DSS) in the absence of DTT. Samples were subject to SDS-PAGE in the presence of DTT and immunostained with anti-DcuS. Lanes, 1+2: solubilised $DcuS_{WT}$ (3 µg), 3+4: solubilised $DcuS_{Cys}$- (3 µg), 5+6: reconstituted $DcuS_{Cys}$- (3 µg), 7+8: membranes containing $DcuS_{Cys}$- (20 µg), 9: solubilised $DcuS_{Cys}$- (7 µg).

A distinct tetrameric band was also observed for detergent-solubilised $DcuS_{Cys-}$ without crosslinking when subjected to SDS-PAGE in great quantity (Fig. 20, lane 9); this is also the case for all the other variants of detergent-solubilised and reconstituted DcuS (not shown). The fact that a portion of purified DcuS was still tetrameric after application to denaturising SDS-PAGE suggests that the DcuS tetramer might be partially stable.

Taken together, biochemical studies imply that DcuS is present as a tetramer in the membrane of *E. coli*. The oligomerisation of DcuS *in vivo* and of reconstituted DcuS *in vitro* was also confirmed by FRET analysis.

4.1.4 Freeze-fracture electron microscopy and cw-EPR measurements with His_6-DcuS

Construction and functional state of His_6-DcuS Q83C

Site-specific labelling of proteins is a prerequisite for EPR measurements. For EPR studies, His_6-DcuS should be labelled with a thiol-specific spin-label at a fixed position in the protein and reconstituted into liposomes. The labelling site was introduced into the periplasmic domain of DcuS due to its known structure (Pappalardo *et al.* 2003; Cheung and Hendrickson, 2008). The single cysteine mutant $DcuS_{Q83C}$, containing one cysteine residue in the periplasmic domain, was constructed by site-directed mutagenesis. From the distance of the labelled cysteine residue between each monomer, the orientation of the DcuS monomers within the oligomer in the membrane should be determined by EPR measurements.

The functional state of $DcuS_{Q83C}$ was tested *in vivo* by *dcuB'-'lacZ* reporter gene fusion (Tab. 7). The plasmid-encoded DcuS cysteine mutant was able to complement *dcuB'-'lacZ* expression in a *dcuS* deletion strain (IMW260). After anaerobic growth in the presence of fumarate at least 80 % of wild-type activity was obtained, demonstrating that $DcuS_{Q83C}$ was functional. As a control for site-specific labelling, functional $DcuS_{Cys-}$ was used.

Table 7: Functional test of $DcuS_{Q83C}$ by induction of *dcuB'-'lacZ* expression. *E. coli* IMW260 was grown anaerobically in eM9 medium with 50 mM glycerol and 20 mM DMSO, with and without the addition of 20 mM fumarate as effector (Rauschmeier, unpublished data).

Strain (relevant genotype)	Expression of *dcuB'-'lacZ* (Miller units)	
	Fumarate	H_2O
IMW260 (*dcuS*)	14 ± 10	10 ± 4
IMW260 pMW151 (*dcuS*$^+$)	482 ± 60	6 ± 3
IMW260 pMW452 (*dcuS* C199S C471S Q83C)	387 ± 48	8 ± 3

Freeze-fracture electron microscopy of reconstituted His_6-DcuS

Purified His_6-$DcuS_{Q83C}$ and His_6-$DcuS_{Cys-}$ were labelled with methanethiosulfonate (MTSSL) spin label for EPR measurements and reconstituted into liposomes. The degree of reconstitution was examined by freeze-fracture electron microscopy.

Freeze-fracture is a method well-suited to examine lipid membranes and incorporated proteins. Rapidly frozen proteoliposomes were fractured, resulting in an upper and a lower fragment of proteoliposome vesicles, and visualised by electron microscopy (Fig. 21).

Reconstituted His_6-$DcuS_{Q83C}$ revealed dots located sporadically in the upper and in the lower fragment of the liposome vesicles, representing reconstituted protein (Fig. 21A). The reconstitution of His_6-$DcuS_{Q83C}$ was repeated several times leading to similar results. All protein was found inside the liposome vesicles. Reconstituted His_6-$DcuS_{Cys-}$ exhibited many dots incorporated into the liposome vesicles (Fig. 21B). Despite the same magnification of the images, the dots appeared bigger than those for reconstituted His_6-$DcuS_{Q83C}$, indicating a more efficient reconstitution of cysteine-less His_6-DcuS into liposomes.

Due to the cysteine-specific labelling of His_6-$DcuS_{Q83C}$, no reducing agent such as DTT was applied during purification of His_6-$DcuS_{Q83C}$. Possibly, an unspecific aggregation of His_6-$DcuS_{Q83C}$ based on cysteine disulfide formation, as observed for His_6-DcuS (Fig. 19, lane 2), might have occurred with a negative impact on the reconstitution efficiency.

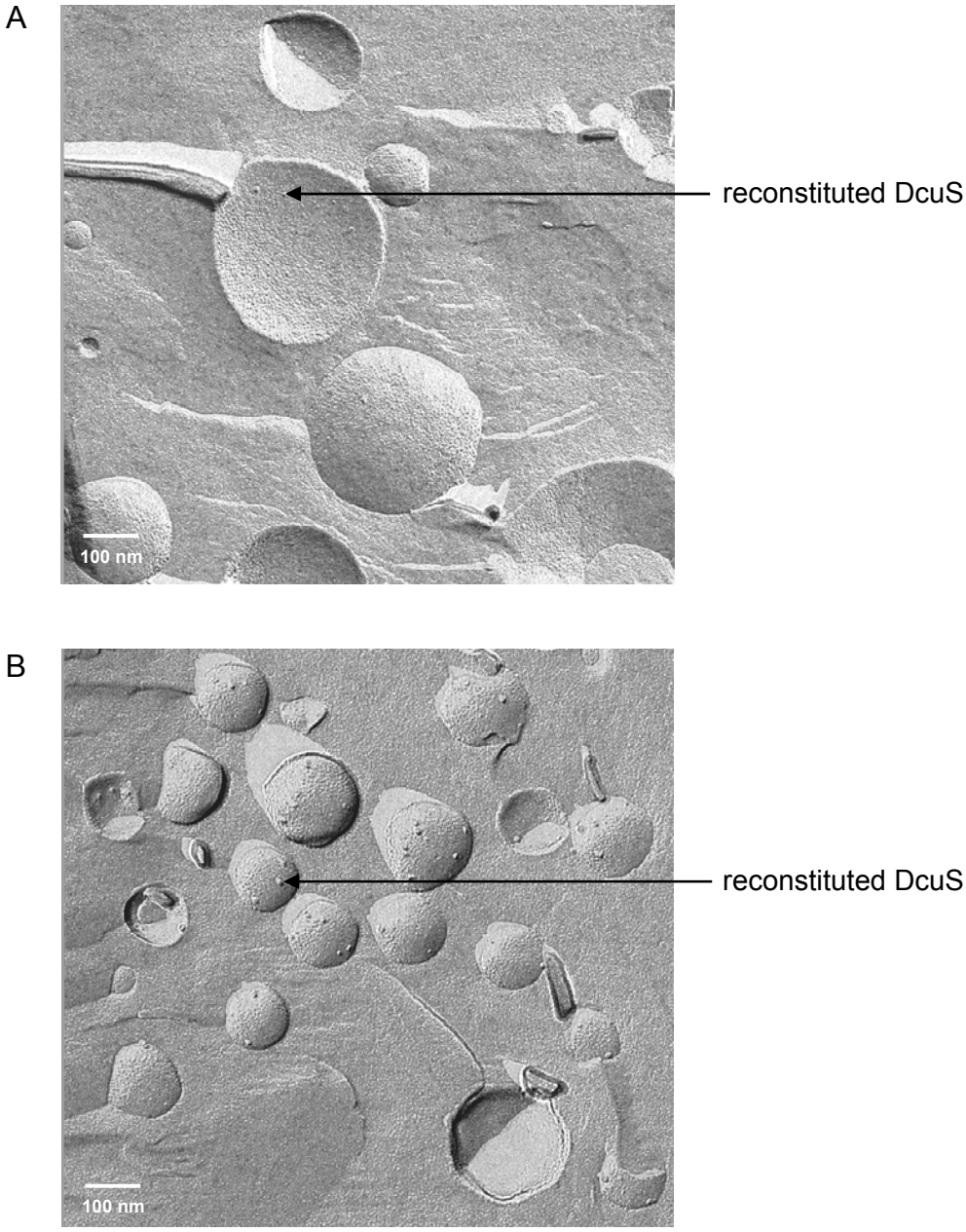

Figure 21: Freeze-fracture electron microscopy of reconstituted $DcuS_{Q83C}$ (A) and $DcuS_{Cys-}$ (B) (each 0.1 mM). Dots located in the fragmented liposome vesicles represent reconstituted DcuS. Magnification 1:160,000.

The labelling efficiency of His_6-$DcuS_{Q83C}$ would also have been diminished if not all cysteine residues were accessible for the spin label because of disulfide formation, thus the labelling efficiency of His_6-DcuS was examined by cw-EPR measurements.

Continuous wave (cw)-EPR measurements with cysteine variants of His_6-DcuS

Electron Paramagnetic Resonance (EPR) spectroscopy is a method to study the oligomeric state of proteins. Continuous wave (cw)-X-band EPR measurements were performed to determine the labelling efficiency of His_6-DcuS prior to detailed EPR investigations. cw-EPR measurements were performed with purified His_6-DcuS cysteine variants labelled with

methanethiosulfonate spin label (MTSSL). MTSSL is a small spin label, which is supposed to bind specifically to cysteine residues (Vileno *et al.*, 2005). Hence, $DcuS_{Cys-}$ was not expected to be spin-labelled by MTSSL. Nevertheless, the protein was labelled to an extent amounting to 62 % or 34 % of detergent-solubilised or reconstituted $DcuS_{Q83C}$, respectively (Fig. 22 and Tab. 8).

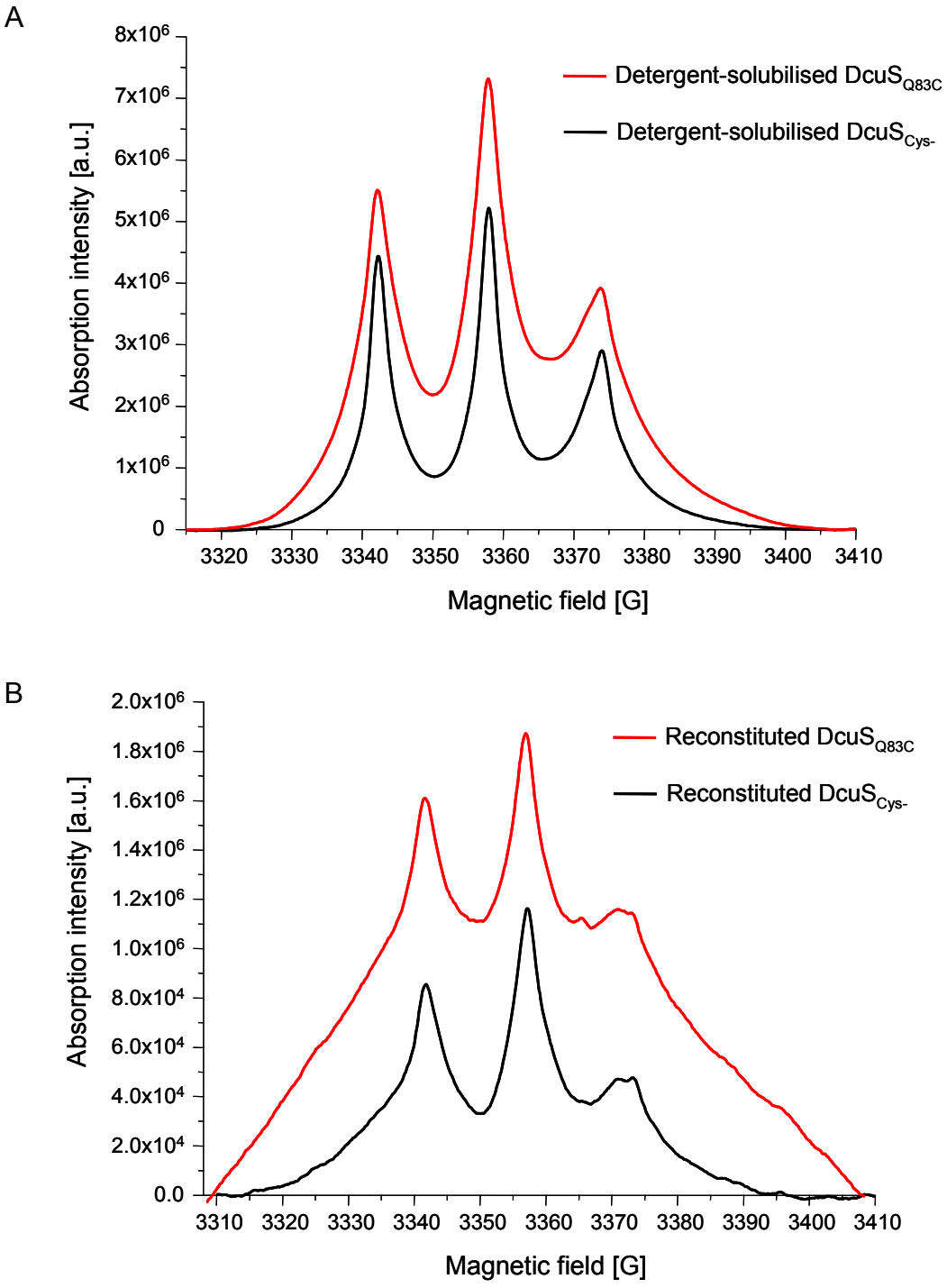

Figure 22: cw-X-band EPR spectra of DcuS cysteine variants at room temperature. A, Spectra of detergent-solubilised $DcuS_{Q83C}$ and $DcuS_{Cys-}$. B, Spectra of reconstituted $DcuS_{Q83C}$ and $DcuS_{Cys-}$. The absolute absorption intensity was measured after excitation of spin-labelled DcuS cysteine mutants with a microwave pulse. The integral of the signal represents the amount of spin labels in the sample.

The absence of cysteine residues in $DcuS_{Cys-}$ was confirmed by repeated DNA sequencing of the gene encoding $DcuS_{Cys-}$ in pMW336. To further test if MTSSL binds to components of the buffer, a sample containing labelling buffer without protein was labelled and purified equally to the protein containing samples. Dialysed labelling buffer harboured only 1 % of spin labels compared to the sample with $DcuS_{Q83C}$ (Tab. 8). Thus, accumulation of MTSSL to the detergent in the buffer could be neglected, and dialysis of labelled DcuS seems to be an adequate method to get rid of free, unbound MTSSL.

Table 8: Integrals of cw-EPR spectra in Fig. 22. The integral of a cw-EPR spectrum reflects the amount of nitroxide spin label in the sample. Integrals of the spectra of detergent-solubilised proteins and of the sample containing dialysed labelling buffer were measured for 155 scans, whereas integrals of the spectra of reconstituted proteins were measured for 465 scans.

Sample	absolute integral	relative integral [%]
Detergent-solubilised $DcuS_{Q83C}$	1.702 e^7	100
Detergent-solubilised $DcuS_{Cys-}$	1.059 e^7	62
Dialysed labelling buffer	1.77 e^5	1
Reconstituted $DcuS_{Q83C}$	7.893 e^6	100
Reconstituted $DcuS_{Cys-}$	2.654 e^6	34

The vast amount of spin label in the sample containing $DcuS_{Cys-}$ indicates unspecific labelling of DcuS with MTSSL. A sample of detergent-solubilised and dialysed $DcuS_{Cys-}$ was concentrated by filter centrifugation (Molecular weight cutoff 30 kDa). The flow-through and the retained supernatant were tested for the spin-label concentration by cw-EPR. The flow-through contained no spin label, which had to be retained in the supernatant in the DcuS-detergent micelles.

The membrane-embedded chemotaxis receptor Tar is also reported to be unspecifically labelled by MTSSL for EPR measurements (Ottemann *et al.*, 1998).

Due to the unspecific labelling of His_6-DcuS, no detailed EPR measurements could be performed. Unspecific labelling of His_6-DcuS was also observed for other labels, as reported for the *in vitro* FRET measurements in section 4.1.2.

4.1.5 Determination of the kinase activity of His_6-DcuS by a cyclic enzymatic test

Reconstituted His_6-DcuS catalyses autophosphorylation by [γ-^{33}P]ATP with an approximate K_D of 0.16 mM for ATP, whereas the detergent-solubilised sensor shows no kinase activity (Janausch *et al.*, 2002).

The kinetics of DcuS autophosphorylation should be determined by a cyclic enzymatic test as an alternative method to autoradiography. The enzymatic cascade of the assay is illustrated (Fig. 23). Purified His_6-DcuS, phosphoenol pyruvate (PEP), nicotinamide-adenine dinucleotide (NADH), PHP-phosphatase, pyruvate kinase (PK), lactate dehydrogenase (LDH) and adenosine triphosphate (ATP) were added to the reaction mixture. Functional DcuS exhibits kinase activity leading to the hydrolysis of ATP to ADP and inorganic phosphate. ADP is subsequently phosphorylated through PK activity with PEP as phosphor-donor, resulting in the regeneration of ATP and the formation of pyruvate. Pyruvate is then reduced to lactate through LDH activity, while NADH is oxidised to NAD^+. The decrease of NADH is determined photometrically by recording an absorption spectrum at 365 nm. The kinase activity of DcuS represents the limiting step of the enzymatic cascade. The decrease of NADH is proportional to the kinase activity and thus a direct measure of DcuS autophosphorylation. To prevent stagnation of the kinase activity due to accumulation of phosphorylated DcuS, unphosphorylated DcuS is regained through PHP-histidine phosphatase activity.

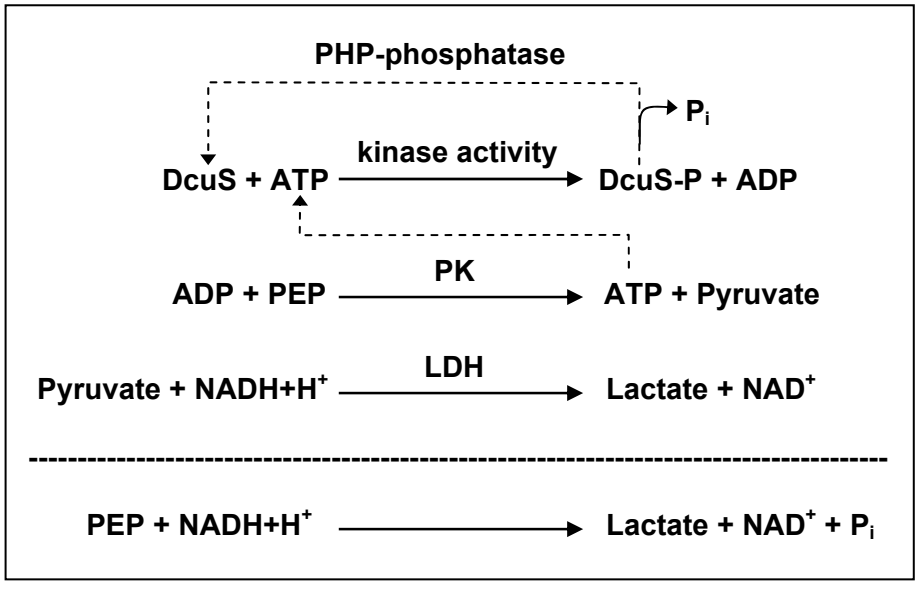

Figure 23: Cyclic enzymatic test to determine the kinase activity of His_6-DcuS. The reaction cascade is started with the addition of ATP. Eukaryotic PHP histidine phosphatase was added to regain unphosphorylated DcuS in the cyclic test. LDH, lactate dehydrogenase; PEP, phosphoenol pyruvate; PK, pyruvate kinase.

Enzymatic control test with glucose and hexokinase

The applicability of the enzymatic kinase test was first checked by the addition of glucose and hexokinase instead of DcuS (Fig. 24). The initiation step of the enzymatic cascade, i.e. the hydrolysis of ATP to ADP, is thereby accomplished by the phosphorylation of glucose through hexokinase (HK) activity. The stepwise addition of the components to the reaction mixture demonstrated that solely NADH contributed to absorption at 365 nm. The enzymatic cascade was started with the addition of hexokinase resulting in the immediate decrease of NADH. The high enzymatic activity of hexokinase was further observed after repeated addition of NADH. The enzymatic test should thus be adequate to determine DcuS kinase activity, which is assumed to be substantial slower than hexokinase activity.

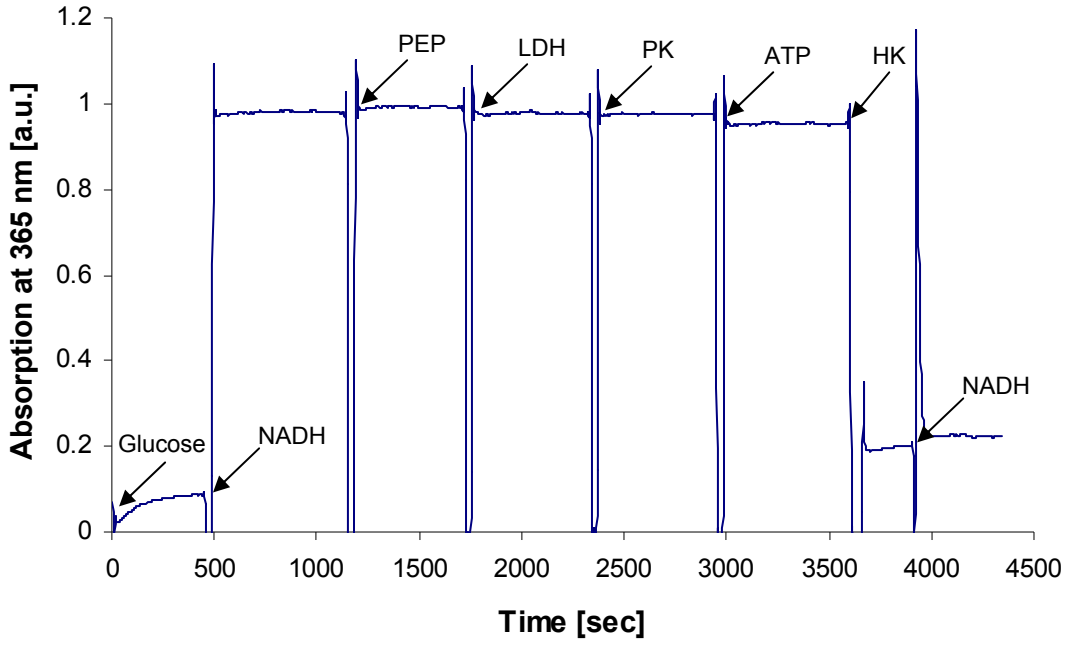

Figure 24: Absorption spectrum of NADH in the enzymatic control test at 37 °C. Glucose and hexokinase (HK) were supplied to the reaction mixture, but neither DcuS nor phosphatase were added. The absorption at 365 nm was detected every 5 seconds. Arrows indicate the addition of the corresponding component.

Enzymatic kinase test with detergent-solubilised and reconstituted His_6-DcuS

Detergent-solubilised or reconstituted His_6-DcuS was added to the reaction mixture (Fig. 25). The reaction cascade was started with the addition of ATP. As control, the absorption spectrum of the reaction mixture without DcuS or with phospholipids, respectively, was recorded. The absorption spectrum of the sample without DcuS as well of the sample containing detergent-solubilised His_6-DcuS remained constant. Detergent-solubilised His_6-DcuS thus exhibited no kinase activity. This is in accordance with the findings of Janausch *et al.* (2002).

The absorption of the samples containing phospholipids or reconstituted His_6-DcuS was approximately twice as high as that of the other samples. Both spectra decreased continuously, even before the addition of ATP. This could be attributed to the phospholipids, whose absorption masked the absorption of NADH. The same was withal observed for absorption spectra of Alexa488-labelled DcuS in liposomes (Liao, 2008).

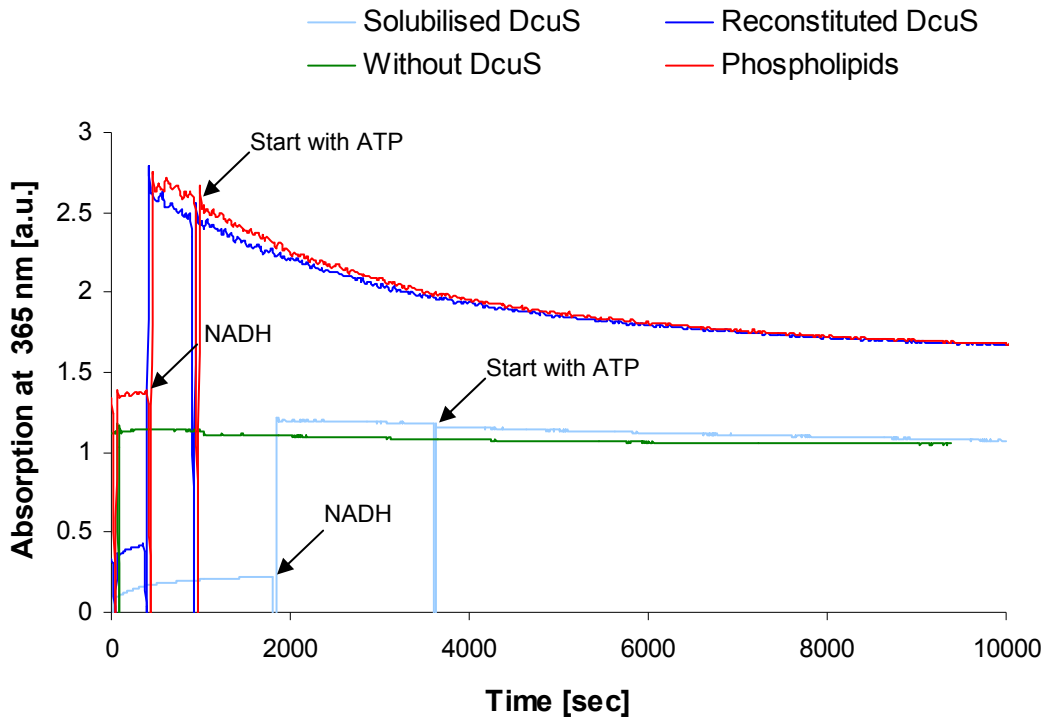

Figure 25: Absorption spectrum of NADH in the enzymatic test with His_6-DcuS at 37 °C. 20 µg of detergent-solubilised (light blue) or reconstituted His_6-DcuS (dark blue) were added. Reaction mixtures without DcuS (green) or with phospholipids (red) served as control. The absorption at 365 nm was detected every 5 seconds and measured for approximately 3 hours. Arrows indicate the addition of the corresponding component.

Various concentrations of the proteoliposomes were tested, but the high absorption of the phospholipids could not be diminished. Even when the reaction was started after 3 h at a constant absorption spectrum, no decrease of NADH was observed, presumably due to the still high liposome absorption of about 2. The kinase activity of reconstituted His_6-DcuS could thus not be determined by the enzymatic test.

4.2 Subcellular localisation of DcuS and CitA within the cell membrane of *E. coli*

Some proteins involved in chemotaxis, cell division and virulence show polar, helical or homogeneous localisation in the cell membrane (Sourjik and Berg, 2000; Shapiro *et al.*, 2002; Shiomi *et al.*, 2006). Little is known about distribution of membrane-bound metabolic sensor histidine kinases in the cell.

4.2.1 Localisation of DcuS-YFP and CitA-YFP in *E. coli*

The related sensor histidine kinases DcuS and CitA were each fused with the enhanced variant of the yellow fluorescent protein (YFP) and expressed in *E. coli* under the control of the *araBAD* promoter in the low-copy vector pBAD30, to ensure low- or moderate-level expression of the fusion gene (Guzman *et al.*, 1995). Localisation of DcuS-YFP and CitA-YFP fusion proteins within the cell membrane of *E. coli* was studied by means of confocal fluorescent microscopy (Scheu *et al.*, 2008).

Functional state of DcuS-YFP and CitA-YFP

The DcuS-YFP fusion protein used for the localisation studies was the same as described and which was shown to be functional (section 4.1.1).

CitA is a citrate-specific sensor histidine kinase closely related to DcuS (Kaspar and Bott, 2002; Mascher *et al.*, 2006). The functional state of CitA-YFP was confirmed in a similar way as for DcuS-YFP. Although *dcuB'-'lacZ* expression was mainly dependent on active DcuS, inactivation of CitA (IMW280) led to a decrease of *dcuB* induction by a factor of 1.7. This response of *dcuB'-'lacZ* expression to CitA will be discussed in detail in section 4.3. IMW280 expressing CitA-YFP (pMW557) restored the function of wild-type CitA (IMW237) to 89 % in the presence of citrate (Tab. 9). Therefore, CitA-YFP can be regarded as functional as well.

Table 9: Functional test of CitA-YFP by induction of *dcuB'-'lacZ* expression. *E. coli* strains were grown anaerobically in eM9 medium with 50 mM gluconate and 20 mM DMSO, with and without the addition of 20 mM citrate as effector.

Strain (relevant genotype)	Expression of *dcuB'-'lacZ* (Miller units)	
	Citrate	H_2O
IMW237 (wt)	35 ± 5	7 ± 2
IMW280 (*citA*)	21 ± 6	9 ± 2
IMW260 (*dcuS*)	5 ± 4	2 ± 2
IMW280 pMW557 (*citA-yfp*)	31 ± 3	4 ± 4

The relatively low stimulation of *dcuB'-'lacZ* under given conditions was due to catabolite repression by gluconate, which was added to the medium as carbon source to enhance bacterial growth.

Distribution of DcuS-YFP in cellular compartments of *E. coli*

To ensure that YFP fluorescence was derived from membrane-integral DcuS-YFP, the presence of DcuS-YFP inclusion bodies and their contribution to the fluorescence of the cells was measured. Sucrose step-gradient centrifugation, cell fractionation and Western blot analysis showed that less than 32 % of DcuS-YFP protein and maximally 10 % of the total fluorescence of the cells resided in inclusion bodies (Tab. 10). DcuS-YFP aggregates are thus not formed in significant amount. Based on the small contribution of the inclusion bodies, it can be concluded that the fluorescence in the bacteria corresponds to membrane-integral DcuS-YFP.

Table 10: Distribution and fluorescence of DcuS-YFP in cellular compartments of *E. coli*. The cell homogenate of *E. coli* IMW262pMW407 (*dcuS*$^-$, p*dcuS-yfp*) induced with 333 µM arabinose for 4 h was separated into supernatant and pellet fraction by low-speed centrifugation. Quantitative Western blot analysis was performed with both fractions using antibodies raised against the His_6-tag of the fusion protein, the average value of 3 independent preparations is shown. Besides, fluorescence of low-speed supernatant and low-speed pellet fraction was detected after excitation at 488 nm. (Scheu *et al.*, 2008)

Fraction	Western blot (Protein amount)	Fluorescence
Low-speed supernatant (soluble proteins and membranes)	68 %	90 %
Low-speed pellet (debris and inclusion bodies)	32 %	10 %

Fluorescence microscopy

The spatial distribution of DcuS-YFP and CitA-YFP within *E. coli* was studied by live imaging of immobilised cells in buffer using confocal fluorescence microscopy. Mid-log phase cells expressing fluorescent proteins were immobilised on polylysine-coated cover slides and excited at 488 nm with a confocal laser beam.

An overview image of *E. coli* cells expressing membranous DcuS-YFP (JM109pMW407) or cytosolic wild-type YFP (JM109pEYFP), respectively, is shown (Fig. 26). The light emitted by the samples was split into two beams which allowed the synchronous recording of microscopic images and fluorescence emission spectra (Fig. 26, upper row). The spectra matched very well the characteristic emission spectrum of YFP, confirming that the photons detected in the microscopic images were emitted by YFP.

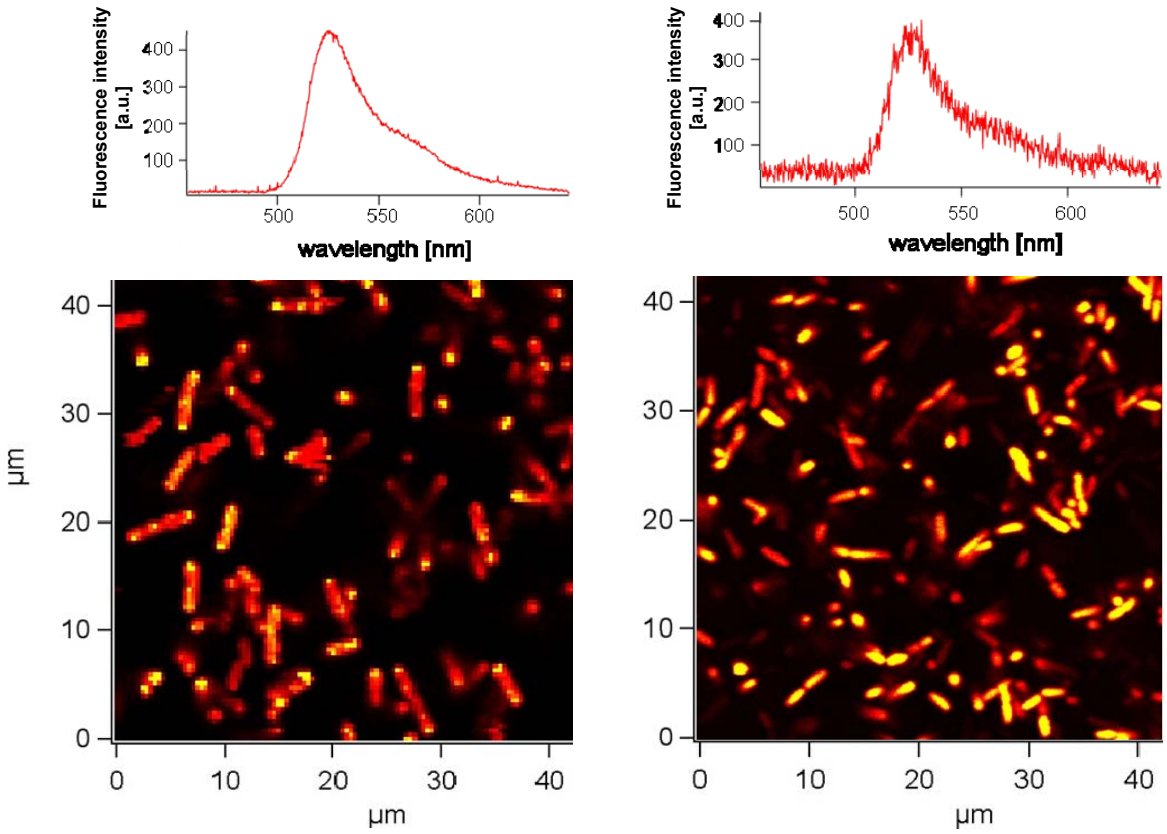

Figure 26: Fluorescence microscopy of *E. coli* expressing membranous DcuS-YFP (left) or cytosolic YFP (right). Cells expressing DcuS-YFP (JM109pMW407) or YFP (JM109pEYFP) were immobilised on a polylysine-coated cover slide and excited at 488 nm with a confocal laser beam.

The fluorescence intensity of most of the cells expressing membranous DcuS-YFP was not homogeneously distributed; instead there were bright spots located at the cell poles (Fig. 26, left). In contrast, cells expressing cytosolic YFP exhibited a homogeneous distribution in the cytoplasm (Fig. 26, right).

Fluorescence intensity profiles of single cells expressing DcuS-YFP and CitA-YFP

Individual *E. coli* cells expressing DcuS-YFP or CitA-YFP showed spots at the cell poles that were much brighter than the fluorescence intensity at the membrane of the cylindrical part of the cell (Fig. 27, upper row). Moreover, the fluorescence at the membrane was brighter than that in the cytosolic region. For quantitative evaluation of the fluorescence intensities within the cells, line profiles were generated along the cell axis (Fig. 27, lower row). The line profiles revealed two peaks corresponding to the bright spots at the cell poles. For the wild-type strain expressing DcuS-YFP (JM109pMW407) the ratio of fluorescence intensity of polar maximum to cytosol was 6.9 for the first polar peak and 3.6 for the second one. For the same peaks, the ratios of polar maximum to the cylindrical part of the cell membrane were 4.3 and 2.2, respectively. The latter ratio might reflect the situation of membrane proteins more directly. For other proteins with polar localisation mostly the former ratio is quoted (Liberman

et al., 2004). For reasons of comparability the former ratio (polar maximum / cytosol) will be hereafter used as well. Most of the cells investigated revealed peaks at both cell poles.

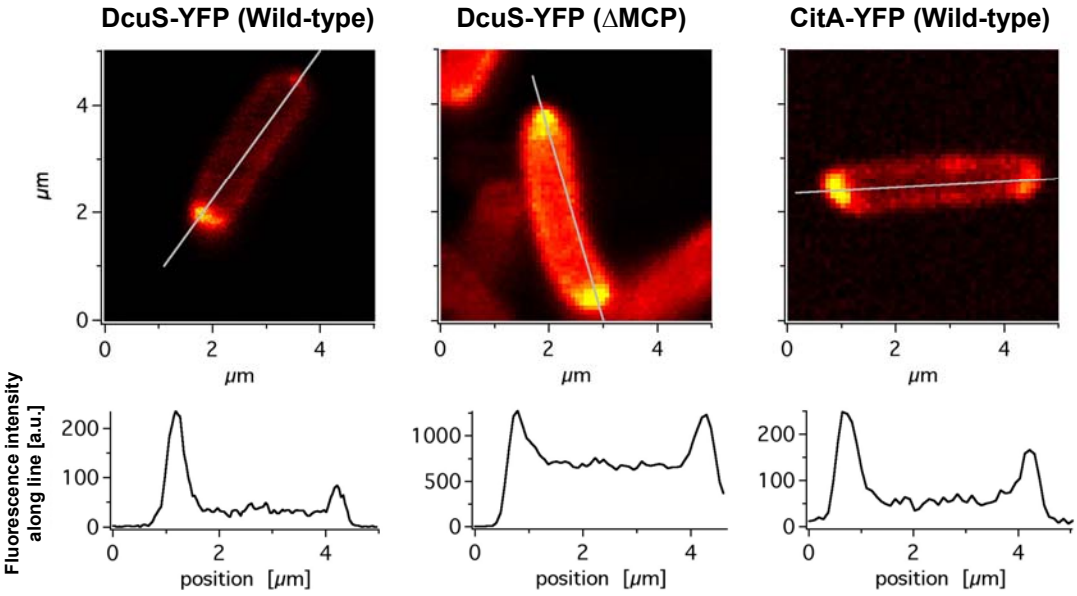

Figure 27: Profiles of single *E. coli* cells expressing DcuS-YFP or CitA-YFP. Fluorescence intensity profiles were recorded along the cell axis of single cells expressing DcuS-YFP (JM109pMW407 and UU1250pMW407) or CitA-YFP (JM109pMW442) after induction with 333 µM arabinose. In strain UU1250, all methyl-accepting chemotaxis sensor proteins are deleted (ΔMCP). (Scheu *et al.*, 2008)

Polar accumulation of the DcuS-YFP fusion protein was observed to the same extent not only in a DcuS-deficient strain (IMW262), but in a CheY-deleted strain (VS100) as well (not shown). A polar accumulation was also observed in the chemoreceptor-deleted strain (UU1250), in which the five genes encoding the methyl-accepting chemotaxis proteins (MCPs) had been deleted. The overall fluorescence intensity of the cells was, on average, 2.5-fold higher than that in the other strains (see line profiles in Fig. 27). DcuS-YFP localisation seems to be independent of the presence of MCPs, which exhibit polar accumulation themselves (Sourjik and Berg, 2000).

The localisation of CitA (JM109pMW442 or IMW279pMW442) was the same as that of DcuS, i.e. the fusion protein was detected in the cell membrane and accumulated at the cell poles (Fig. 27). The mean ratio (polar maximum / cytosol) obtained for CitA-YFP was in the range of 3.5-5.1.

Fluorescence microscopy with reference proteins

As a reference for a protein with known polar accumulation, CheY-YFP was tested (VS100pVS1). CheY is a water-soluble intracellular protein that associates with the MCPs, which are localised at the cell poles. The polar localisation of CheY is comparable with that of the MCPs (Sourjik and Berg, 2000). Images and line profiles of CheY-YFP showed the polar

accumulation of this protein (Fig. 28). The fluorescence intensity at the poles was three times higher than the intracellular level. Thus CheY, DcuS and CitA show polar accumulation to similar extents. Slight differences in the polar accumulation could be due to some differences in genetic background of the strains used for this experiments.

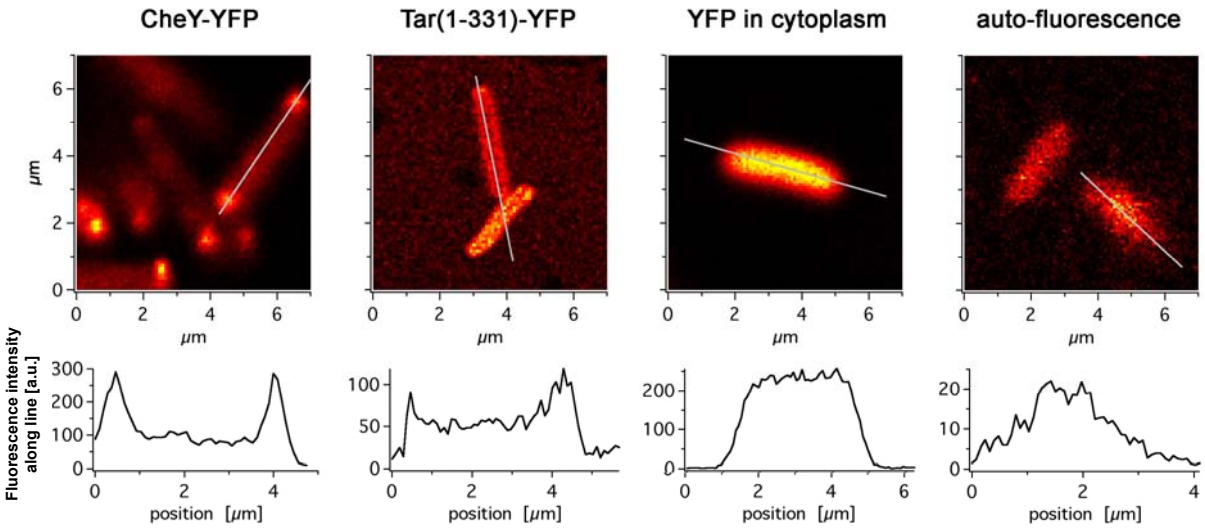

Figure 28: Reference proteins with polar, membranous or cytosolic localisation in *E. coli*. Fluorescence-intensity profiles of single cells expressing CheY-YFP (VS100pVS1), Tar(1-331)-YFP (JM109pDK108), wild-type YFP (JM109pEYFP), or without fluorescent protein (JM109). (Scheu *et al.*, 2008)

As a control for a protein with an even distribution over the cell membrane, a YFP fusion with truncated Tar(1-331) was used. Tar is a membrane-bound chemoreceptor which localises at the cell poles, whereas the C-terminal truncated Tar(1-331) is membrane bound, but without polar accumulation (Kentner *et al.*, 2006). Images of cells expressing the truncated Tar(1-331) fused to YFP (JM109pDK108) revealed a symmetrically distributed fluorescence over the entire cell membrane (Fig. 28). As a cytosolic protein, wild-type YFP was again used for comparison. Water-soluble YFP (JM109pEYFP) was homogeneously distributed in the cytoplasm, resulting in a line profile of roughly constant fluorescence level within the cell but with lower fluorescence at the membrane. This implies that YFP does neither contribute to membranous nor to polar localisation of the fusion proteins. *E. coli* cells expressing no fluorescent protein revealed only auto-fluorescence, with an intensity 10-fold lower than that of cells expressing YFP fusions (see line profiles). This auto-fluorescence resulted in relatively weak but not specifically localised fluorescence within the cells.

Dependence of DcuS-YFP localisation on the protein expression rate

Expression of the DcuS-YFP fusion protein (JM109pMW407) was induced by various concentrations of arabinose. The pBAD30 vector is generally used for moderate-level expression due to its low copy number. After induction with 133 µM or 333 µM arabinose,

high expression of DcuS-YFP was detected by Western blotting with anti-DcuS antiserum (Fig. 29, lanes 5 and 6). In the presence of 10 µM arabinose (Fig. 29, lane 4), the expression of DcuS-YFP sharply decreased by a factor of 10, but was still significantly higher than that of endogenously expressed DcuS (Fig. 29, lane 2). Compared to the expression level of endogenous DcuS (JM109), which was estimated to be maximally 0.004 % of the total cell protein, the amounts of DcuS-YFP induced by 10, 133 or 333 µM arabinose were estimated to be about 0.04 %, 0.4 % or 0.4 %, respectively, of the total cell protein. For comparison, 1 µg of purified His_6-DcuS or His_6-DcuS-YFP, respectively, was loaded (Fig. 29, lanes 1 and 7, respectively).

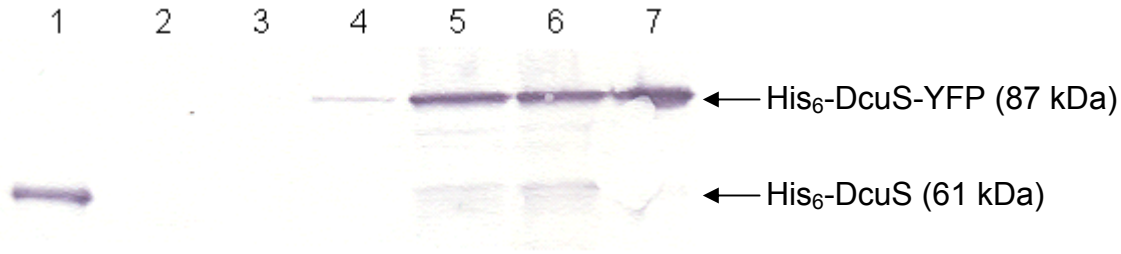

Figure 29: Detection of DcuS-YFP in lysed cells of *E. coli* by Western blotting with antiserum against the periplasmic domain of DcuS. *E. coli* expressing DcuS-YFP (JM109pMW407) was grown under aerobic conditions in LB broth in the presence of 0 µM (lane 3), 10 µM (lane 4), 133 µM (lane 5) and 333 µM arabinose (lane 6). For lane 2, *E. coli* wild-type (JM109) was grown anaerobically in M9 mineral medium with 50 mM glycerol and 20 mM fumarate to mid-log phase. Cells were sedimented and the pellet was dissolved in SDS sample buffer. 60 µg (lanes 3-6) or 120 µg (lane 2) of cell lysates were subjected to SDS-PAGE. Lanes 1 and 7 contain 1 µg of purified His_6-DcuS or His_6-DcuS-YFP, respectively. (Scheu *et al.*, 2008)

Further localisation studies were performed with cells induced by arabinose concentrations as low as 10 µM and up to 333 µM. With the induction by 10 µM arabinose, measurements could be performed at a low DcuS level as close as possible to the *in vivo* conditions, but at the fluorescence detection limit. On the other hand, induction by 333 µM arabinose resulted in DcuS levels which were higher than the endogenous levels, but the inducer concentration was still much lower than that commonly used for localisation studies.

The influence of inducer concentration on DcuS-YFP localisation was studied at the single cell level. The fluorescence intensity ratios of polar maximum to cytosol and polar maximum to membrane were plotted as a function of the arabinose concentration used for fusion protein expression (Fig. 30A). Despite some fluctuations in the two ratios, polar accumulation of DcuS-YFP already appeared at low concentrations of both inducer and DcuS-YFP and remained constant at higher concentrations. Images of single cells induced at low arabinose concentrations (10 µM or 100 µM, respectively) confirmed the polar localisation of DcuS-YFP at low expression levels, whereas uninduced cells showed no YFP-specific emission, but only weak auto-fluorescence (Fig. 30B). The polar accumulation of DcuS-YFP was thus independent of the expression level of the fusion protein.

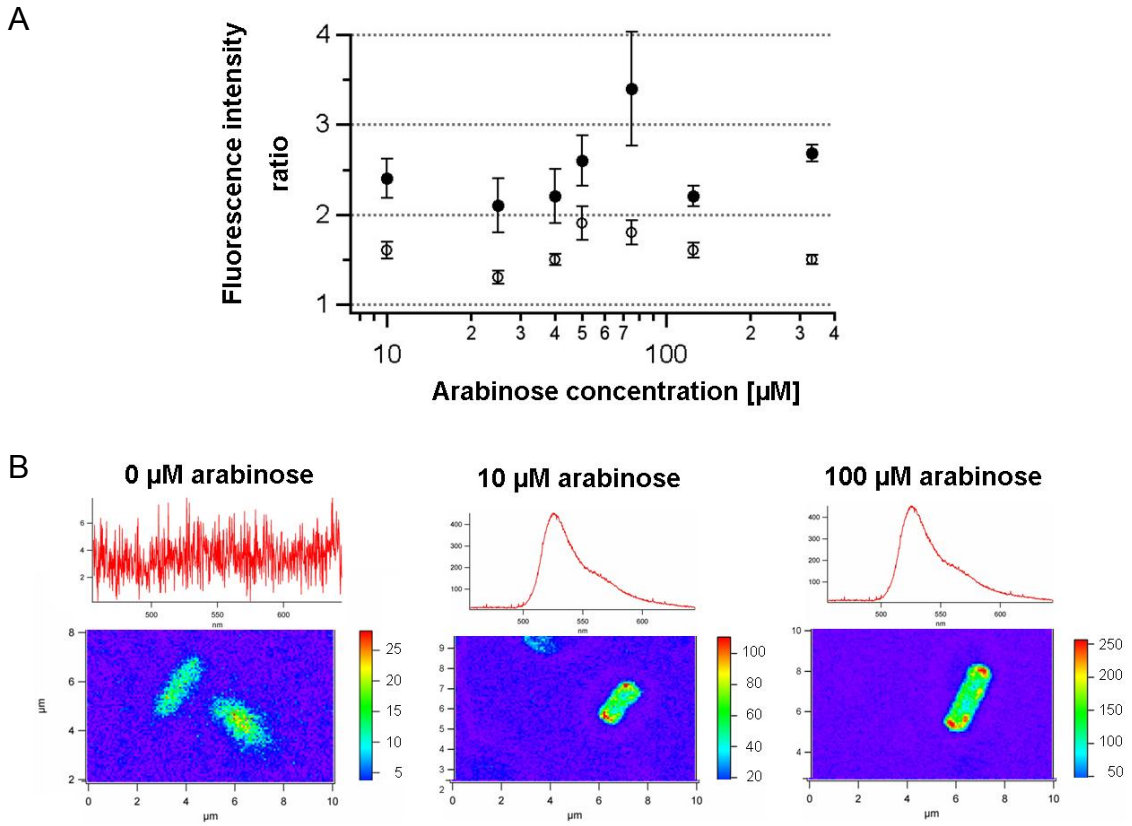

Figure 30: Dependence of DcuS-YFP localisation on inducer concentration. Expression of DcuS-YFP (IMW262pMW407) was induced with increasing concentrations of arabinose. Samples were harvested after 4.5 h. A, Fluorescence intensity ratios (●, polar maximum / cytosol; ○, polar maximum / membrane) are plotted against the arabinose concentration with average values ± standard deviations from 3-28 cells. B, Images of single cells induced at indicated arabinose concentrations. Different fluorescence intensities are illustrated by different colours. Upper row, emission spectra of the cells after excitation at 488 nm. (Figure A derived from Scheu *et al.*, 2008)

The time-course of DcuS-YFP and CitA-YFP localisation was also investigated. After induction of DcuS-YFP or CitA-YFP expression (IMW262pMW407 or JM109pMW442) from the beginning of incubation, cell samples were collected every 30 min and analysed for polar localisation of the fusion proteins at the single cell level. The maximum fluorescence intensity per cell and the ratio of polar maximum to cytosol are plotted as a function of time (Fig. 31). DcuS-YFP and CitA-YFP behaved very similarly with respect to their fluorescence-intensity kinetics (Fig. 31A). After a lag phase of about 1.5-2 h, fluorescence intensity and thus protein expression rate increased continuously. By contrast, with respect to their ratio kinetics, the two fusion proteins behaved differently (Fig. 31B). The fluorescence intensity ratio for DcuS-YFP was close to 2.0 after 30 min of induction and persisted for at least 2 h. The ratio for CitA-YFP was 2.5 after 30 min and slightly increased with time. Despite the different behaviour of their ratio kinetics, the polar accumulation of both DcuS-YFP and CitA-YFP was established already within the first 30 min after their expression, and their localisation persisted for several hours, being independent of the protein expression rate.

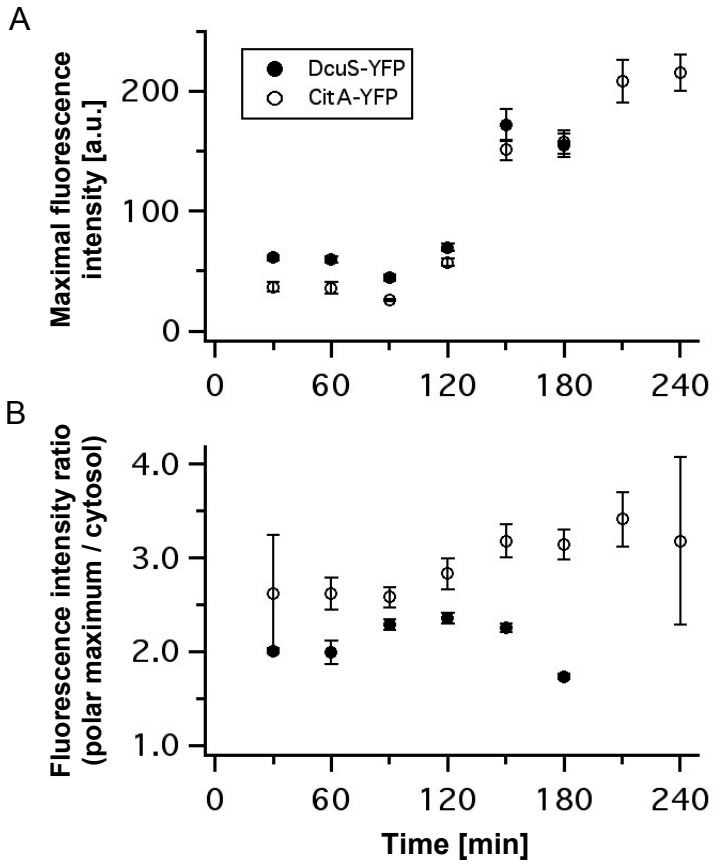

Figure 31: Dependence of DcuS-YFP and CitA-YFP localisation on protein expression rate. Expression of DcuS-YFP (IMW262pMW407, ●) and CitA-YFP (JM109pMW442, ○) was induced with 333 µM arabinose. Samples were collected every 30 min. The average values ± standard deviations of fluorescence intensities from 5-39 cells are plotted against the time after induction. A, Peak fluorescence intensity of the bright spots within the cells; B, Fluorescence intensity ratio of polar maximum to cytosol. (Scheu *et al.*, 2008)

Influence of effectors and DcuS-associated proteins on the polar accumulation

Polar accumulation of DcuS-YFP and CitA-YFP was studied in the presence or absence of the corresponding effector fumarate or citrate, respectively. As a control, DcuS-YFP localisation was also examined in the presence of acetate, which is not sensed by DcuS (Janausch *et al.*, 2002). The fluorescence intensity ratios of polar maximum to cytosol of individual cells from independent cultures were averaged (Tab. 11). The DcuS-YFP fusion protein in the DcuS-deleted strain (IMW262) revealed a significant increase in polar accumulation upon the presence of the effector fumarate. The same was observed for both the DcuB-deleted strain (IMW502) and various wild-type strains (MC4100, JM109). No increase in polar accumulation of DcuS-YFP was observed in the presence of acetate, suggesting that the effect of fumarate on polar accumulation of DcuS-YFP is specific. In the DcuR-deleted strain (IMW205), the polar accumulation of DcuS-YFP increased only to a very low extent in the presence of fumarate. Taken together, the data suggest that presence of fumarate increases the polar accumulation of DcuS-YFP, and the presence of DcuR is required for this effect.

Table 11: Influence of the effectors fumarate and citrate on polar accumulation of DcuS-YFP and CitA-YFP. *E. coli* wild-type (JM109 or MC4100) and mutant strains expressing DcuS-YFP (pMW407) or CitA-YFP (pMW442) were grown at 30 °C for 4 h with 133 µM arabinose in the presence or absence of 20 mM fumarate or citrate, respectively, as effector, or 20 mM acetate. Each value in the table represents the mean ratio of the fluorescence intensity of polar maximum to cytosol ± standard deviation obtained from 67-257 cells. No pre-selection was made, but all cells which gave a clear image were analysed. n.d., not determined. (Table derived from Scheu *et al.*, 2008)

Protein	Strain (relevant genotype)	Mean ratio with effector	Mean ratio without effector	Mean ratio with acetate
DcuS-YFP	Wild-type	3.2 ± 0.2	2.6 ± 0.2	2.8 ± 0.1
	IMW262 (*dcuS*$^-$)	3.4 ± 0.1	2.6 ± 0.1	2.7 ± 0.1
	IMW502 (*dcuB*$^-$)	3.6 ± 0.1	2.7 ± 0.1	n.d.
	IMW205 (*dcuR*$^-$)	2.9 ± 0.1	2.7 ± 0.1	n.d.
CitA-YFP	JM109 (wild-type)	5.1 ± 0.2	3.5 ± 0.2	n.d.

The polar accumulation of CitA-YFP in the wild-type strain (JM109) significantly increased upon addition of citrate. No increase was observed in the presence of fumarate (not shown), suggesting that the effect of citrate on polar accumulation of CitA-YFP is specific.

4.2.2 Construction of a chromosomal *dcuS-bs2* gene fusion

The physiological role of the polar accumulation of the sensor histidine kinases DcuS and CitA is unknown. Future investigations should elucidate, if DcuS might be trapped at the cell pole by the anionic phospholipid cardiolipin, as demonstrated for other proteins (Matsumoto *et al.*, 2006; Romantsov *et al.*, 2007, 2008). The mole fraction of cardiolipin in the cytosolic membrane of *E. coli* is 5 % of total lipids. Cardiolipin is enriched at the cell poles and septa of growing cells (Mileykovskaya and Dowhan, 2000).

To study the localisation of DcuS under physiological conditions in a cardiolipin-deficient strain, a *dcuS-bs2* gene fusion was constructed and inserted into the chromosome of *E. coli* JW1241 (*cls*$^-$) and into a wild-type strain (MC4100). *bs2* encodes the flavin mononucleotide (FMN)-based fluorescent protein Bs2 (Evoglow; Drepper *et al.*, 2007). Bs2 is, in contrast to GFP derivatives, oxygen-independent allowing localisation studies under aerobic and anaerobic growth conditions. The chromosomal insertion of *dcuS-bs2* was accomplished by homologous recombination using a suicide vector system (Fig. 32). This involves a two-step procedure. First, the recombinant vector is integrated within the chromosomal target gene sequence by homologous recombination. Secondly, the vector is excised via a second crossover event, resulting in allelic exchange. Prerequisite of a suicide vector is the presence of a conditional origin of replication, a positive selectable marker and a negative or counter-selectable marker.

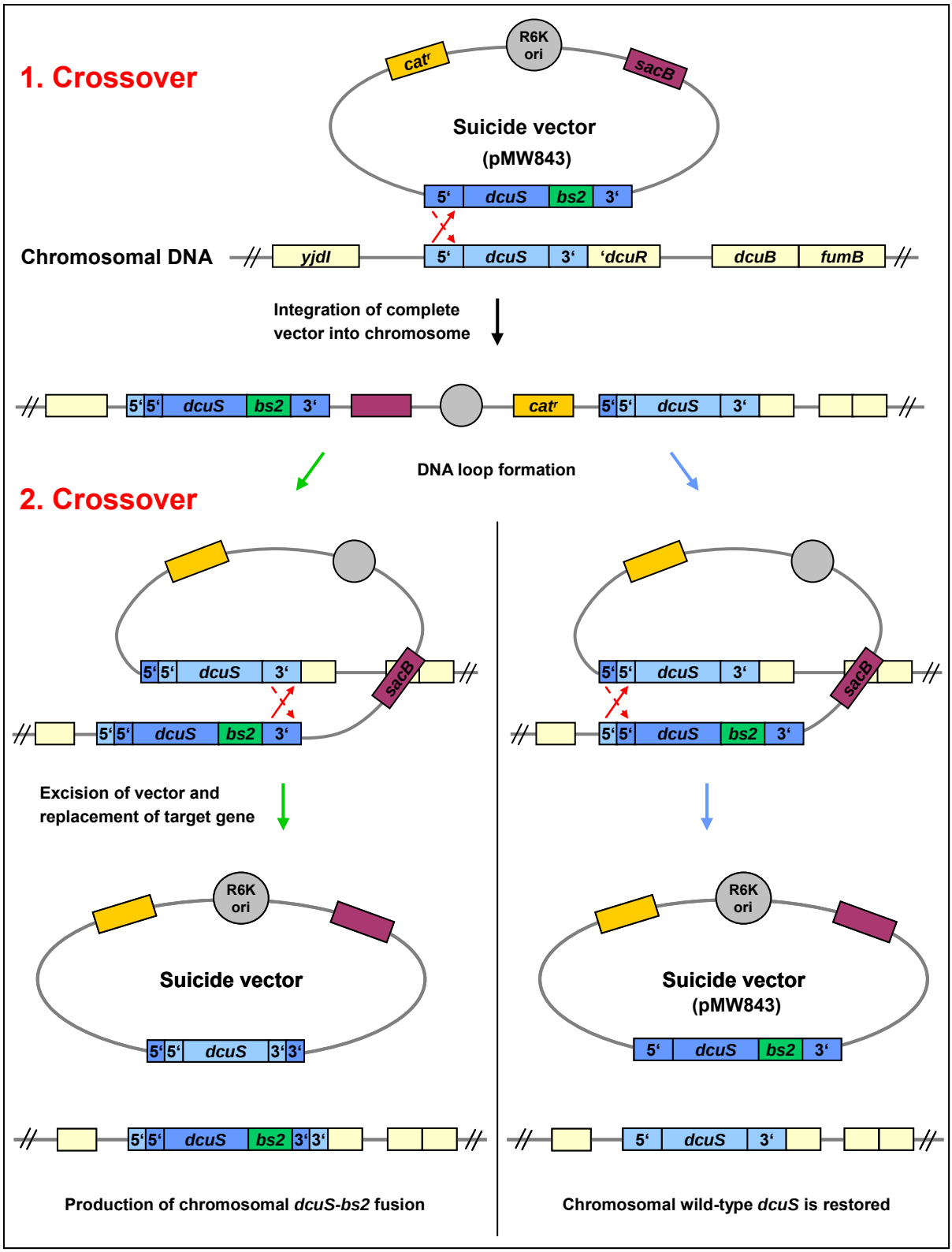

Figure 32: Scheme for homologous recombination of *dcuS-bs2* into the chromosome mediated by a suicide vector. The relevant selectable marker in the corresponding step of recombination is inscribed (*cat*^{r} for positive selection, *sacB* for negative selection, *oriR6K* as conditional origin of replication). The excised vector vanishes because it is not replicated in *pir*$^-$ strains. Resulting colonies have to be checked by PCR for the presence of chromosomal *dcuS-bs2*. Note that the 3'-end of *dcuS* overlaps with the 5'-end of *dcuR*.

dcuS-bs2 was cloned into the suicide vector pDS132 (pMW843). The gene fusion comprised the sequences adjacent to *dcuS* of about 800 bp on each side to allow homologous recombination into the chromosome. Integration of pMW843 into the chromosome via the first crossover was selected by a chloramphenicol resistance (Fig. 32). Excision of the vector via the second crossover was selected by the counter-selective *sacB* gene. *sacB* is originated from *Bacillus subtilis* and encodes the enzyme levansucrase, which catalyses transfructosylation from sucrose to fructose, resulting in levan synthesis and sucrose hydrolysis (Gay *et al.*, 1983). Expression of this enzyme is lethal in most gram-negative bacteria in the presence of 5 % sucrose. Hence, cells were grown in a sucrose-containing medium for vector excision. The resulting chromosomal product depended on the site of the second crossover. If it occurred at the opposite end of the first crossover, allelic exchange took place. If the second crossover happened at the same site as the first crossover, the wild-type gene was restored (Fig. 32). Statistically, 50 % of the cells carried the desired allele. The excised vector vanished because pMW843 contains the conditional R6K origin of replication, which is just able to replicate in strains producing the π protein, the product of the *pir* gene, which is absent in the *pir* negative strains JW1241 and MC4100.

Colonies carrying the chromosomal *dcuS-bs2* fusion were identified by PCR (Fig. 33). As expected, in 50 % of the colonies analysed the desired allelic exchange had occurred. JW1241 (*cls*$^-$, *dcuS-bs2*) and MC4100 (wt, Δ*lacZ*, *dcuS-bs2*) are hereafter referred to as IMW569 and IMW570, respectively.

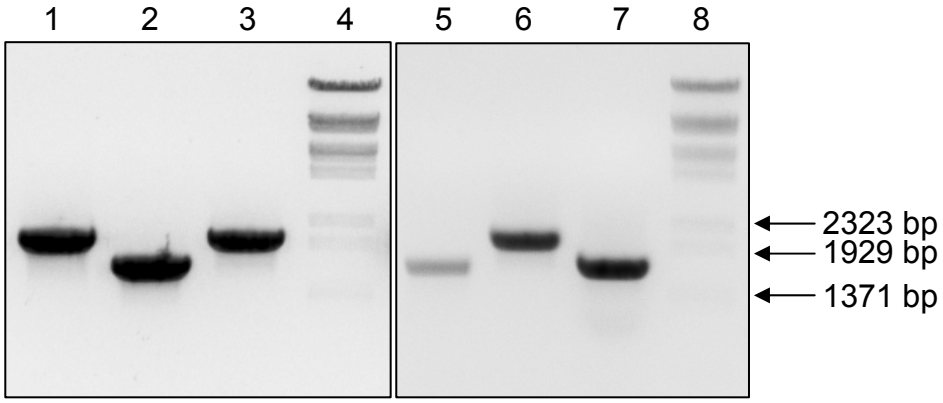

Figure 33: Screening for colonies bearing chromosomal *dcuS-bs2* after homologous recombination. Three colonies of strain JW1241 (*cls*$^-$) and MC4100 (Δ*lacZ*), respectively, were subjected to PCR with primers dcuS_for and dcuS_rev. Integration of *dcuS-bs2* into the chromosome led to a fragment of a size of 2094 bp (lanes 1, 3 and 6), whereas wild-type *dcuS* resulted in a fragment of 1695 bp (lanes 2, 5 and 7).

1: JW1241 (*cls*-) after homologous recombination, clone 1 → positive (IMW569)
2: JW1241 (*cls*-) after homologous recombination, clone 2
3: JW1241 (*cls*-) after homologous recombination, clone 3 → positive
4: λ-DNA digested with *Bst*EII
5: MC4100 (Δ*lacZ*) after homologous recombination, clone 1
6: MC4100 (Δ*lacZ*) after homologous recombination, clone 2 → positive (IMW570)
7: MC4100 (Δ*lacZ*) after homologous recombination, clone 3
8: λ-DNA digested with *Bst*EII

The λ-lysogenic strain IMW237 (*dcuB'-'lacZ*) was immune towards homologous recombination, presumably due to the expression of the λ repressor, and could not be used for chromosomal insertion of *bs2*. Therefore, the reporter-less strain MC4100 (Δ*lacZ*) was used for *dcuS-bs2*-insertion.The resulting strain IMW570 was tested by introducing the *dcuB'-'lacZ* fusion on plasmid. The functional state of *dcuS* in the chromosomal *dcuS-bs2* gene fusion was thus tested with plasmid-borne *dcuB'-'lacZ* reporter gene fusion (pMW99) (Tab. 12).

Table 12: Functional test of chromosomally encoded DcuS-Bs2 by induction of *dcuB'-'lacZ* expression. *E. coli* strains were grown anaerobically in eM9 medium with 50 mM glycerol, 20 mM DMSO and 20 mM fumarate as effector.

Strain (relevant genotype)	Expression of *dcuB'-'lacZ* (Miller units)
	Fumarate
MC4100 (wt, Δ*lacZ*) pMW99 (*dcuB'-'lacZ*)	12649 ± 177
IMW262 (*dcuS*$^-$, Δ*lacZ*) pMW99 (*dcuB'-'lacZ*)	418 ± 86
IMW570 (*dcuS-bs2*, Δ*lacZ*) pMW99 (*dcuB'-'lacZ*)	41 ± 5

The wild-type strain (MC4100) revealed a very high induction of *dcuB'-'lacZ* of about 12650 MU, which was due to the relatively high copy number of pMW99. The expression of the reporter gene fusion in the *dcuS* deletion strain (IMW262) was lower by a factor of 30, representing basal activity. In IMW570, *dcuB'-'lacZ* activity was even ten times lower than that observed in IMW262, implying that DcuS/R or DcuR were not functional. *dcuR* is located downstream of *dcuS* and the genes are arranged in one operon overlapping within 4 bp. The construction of the chromosomal *dcuS-bs2* gene fusion therefore inevitably resulted in the loss of function of *dcuR*.

To clarify if *dcuS* was functional upon fusion with *bs2* in the presence of active DcuR, *dcuS-bs2* was cloned into the low-copy vector pBAD30-Tet (Graf, 2009), which resulted in pMW875. *dcuS-bs2* in pMW875 is transcriptionally regulated by the *dcuS* promoter. ß-Galactosidase assays were performed with pMW875 and plasmid-encoded wild-type DcuS (pMW181) in the DcuS-deleted strain IMW260 harbouring a chromosomal *dcuB'-'lacZ* reporter gene fusion (Fig. 34). *dcuB'-'lacZ* expression in a strain with chromosomal wild-type *dcuS* (IMW237) was additionally compared. DcuS-Bs2 induced *dcuB'-'lacZ* expression to a similar extent as chromosomally encoded wild-type DcuS in the presence of fumarate. Expression levels obtained with the pET28a derivative pMW181 bearing *dcuS* with its own promoter were lower by a factor of approx. 2, presumably due to the unphysiological high copy-number of pMW181. DcuS can thus be regarded as functional in the fusion with Bs2.

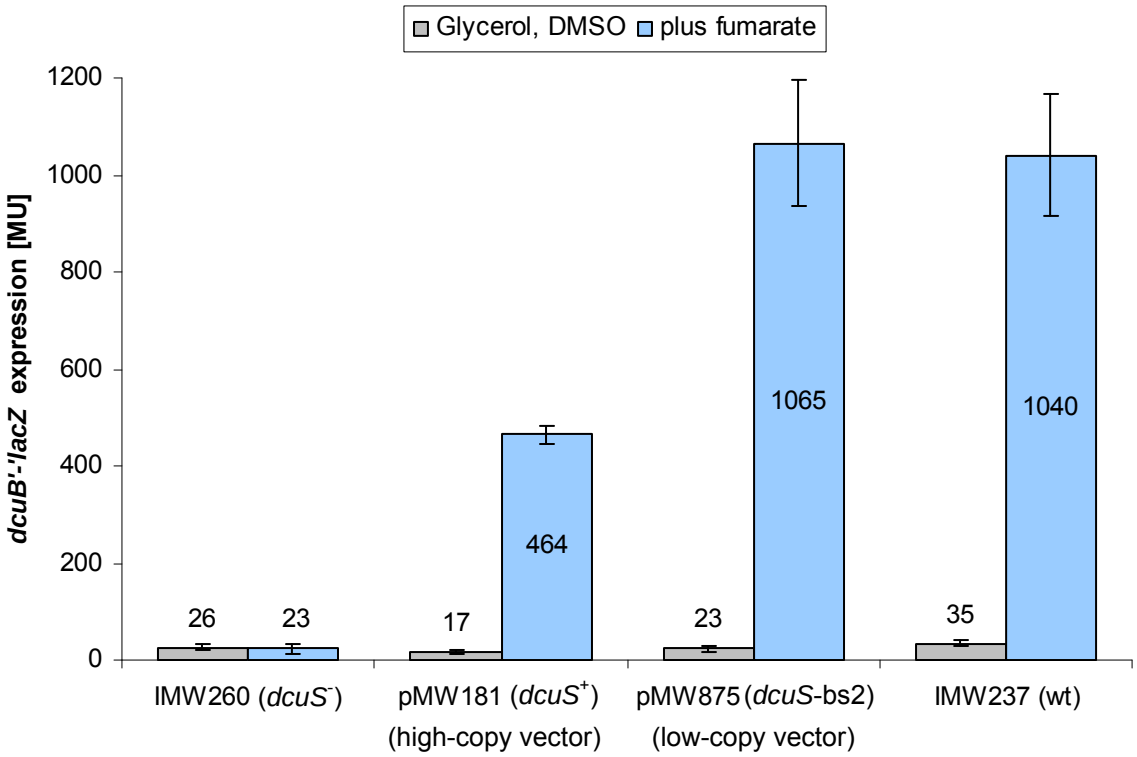

Figure 34: Functional test of plasmid-encoded DcuS-Bs2 by induction of *dcuB'-'lacZ* expression. Bacteria were grown anaerobically in eM9 medium with 50 mM glycerol, 20 mM DMSO and with 20 mM fumarate as effector.

As shown for the DcuS-YFP fusion protein, its polar localisation is still observed in a *dcuR*-negative strain (Tab. 11). In future studies, DcuS localisation within the cell membrane will be investigated under anaerobic conditions as well with chromosomally encoded DcuS-Bs2 as with low-copy plasmid-encoded DcuS-Bs2 in a wild-type *E. coli* strain (MC4100) and in a cardiolipin synthase-defective mutant (JW1241).

4.3 Studies of protein-protein interaction between DcuS and CitA in *E. coli*

DcuS and CitA belong to the CitA family of sensor histidine kinases and reveal a high topological, functional and structural similarity (Pappalardo *et al.*, 2003; Reinelt *et al.*, 2003). The metabolic pathways regulated by both sensors share common reactions during substrate degradation, including fumarate respiration (Fig. 2). A possible interaction of both sensors based on *dcuB'-'lacZ* expression assays is implied (Zientz, 2000; Krämer *et al.*, 2007) and was studied in detail.

4.3.1 Influence of CitAB on the induction of genes regulated by DcuSR

Expression of *dcuB* under anaerobic conditions is induced by the two-component system DcuSR in the presence of C_4-dicarboxylates and citrate. The citrate-specific CitAB two-component system of *E. coli* mediates gene regulation for anaerobic citrate fermentation (Yamamoto *et al.*, 2008; Rauschmeier, 2009). The contribution of CitAB to citrate regulation of *dcuB'-'lacZ* was examined. Therefore, a wild-type *E. coli* strain and a series of mutants, each lacking the kinase (DcuS or CitA) or the response regulator (DcuR or CitB) and harbouring a chromosomal *dcuB'-'lacZ* reporter gene fusion, were tested under anaerobic conditions in the absence or presence of citrate or fumarate as effector (Fig. 35).

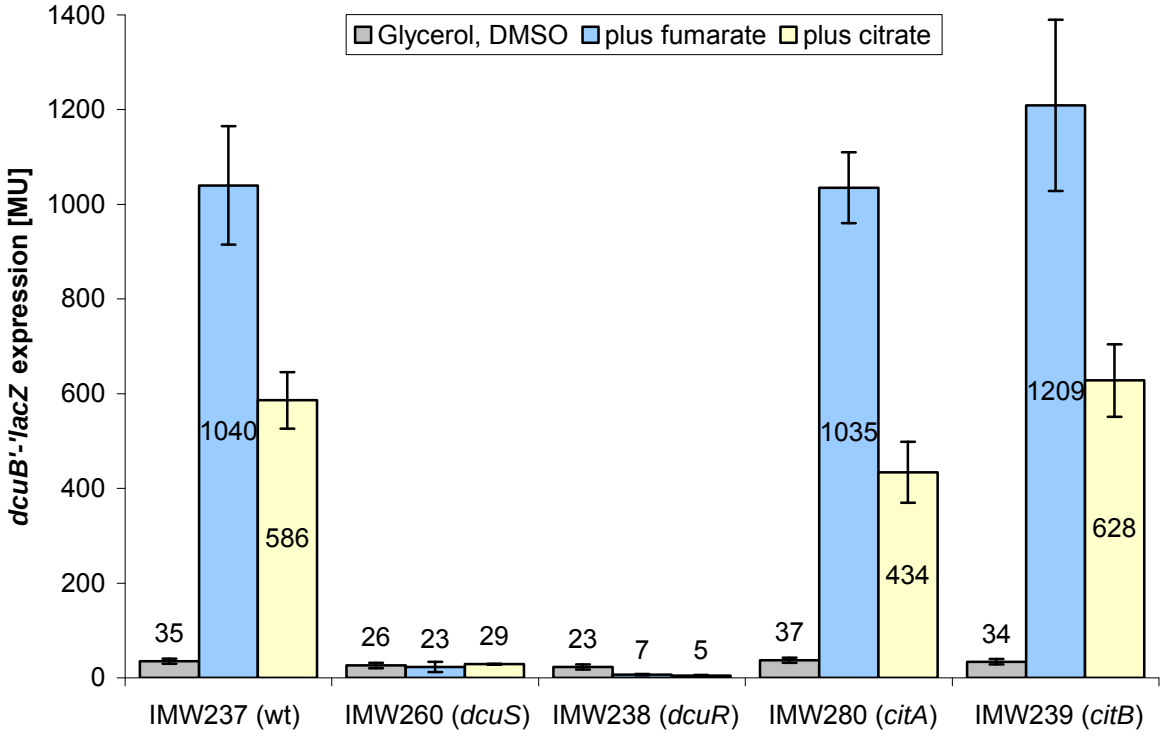

Figure 35: Influence of DcuSR and CitAB on *dcuB'-'lacZ* expression. *E. coli* strains were grown anaerobically in eM9 medium with 50 mM glycerol and 20 mM DMSO, with and without the addition of 20 mM fumarate or 20 mM citrate, respectively.

In the wild-type strain (IMW237), *dcuB'-'lacZ* expression was strongly induced in the presence of fumarate. With citrate as effector, *dcuB'-'lacZ* was also significantly induced, although the expression was half that of fumarate. In the *dcuS* or *dcuR* mutant (IMW260 or IMW238, respectively), the stimulation of *dcuB* expression by either effector was completely lost. This demonstrates that the induction of *dcuB* is mainly dependent on DcuSR. Nevertheless, deletion of CitA (IMW280) led to a decrease of *dcuB'-'lacZ* induction in the presence of citrate by a factor of 1.4. This result is comparable with that shown in Tab. 9, where a decrease of *dcuB'-'lacZ* expression by a factor of 1.7 was observed for IMW280 grown anaerobically with gluconate as carbon source. The decrease in *dcuB* activation was not observed with fumarate as effector and is thus citrate-specific. In contrast, inactivation of CitB (IMW239) had only small effect on *dcuB* expression resulting in a slight increase by a factor of 1.1 with citrate and a factor of 1.2 with fumarate as effector, although lying within the standard deviations. The findings that the induction of *dcuB'-'lacZ* is dependent on active DcuS and active DcuR, but requiring additional CitA for maximal induction upon growth on citrate, suggest a direct interaction of CitA and DcuS.

4.3.2 FRET measurements with CitA-YFP and DcuS-CFP

The supposed interaction between the sensor histidine kinases DcuS and CitA was further investigated via FRET measurements with cells co-expressing DcuS-CFP and CitA-YFP (JM109pMW408pMW442). FRET measurements were performed analogous to those described in section 4.1.1. The control measurements were again compared.

The resulting relative FRET efficiency of 35 % at a donor fraction of 0.4 ± 0.01 indicated specific FRET between DcuS-CFP and CitA-YFP (Fig. 36). The direct interaction of DcuS and CitA could thus be confirmed by an independent method.

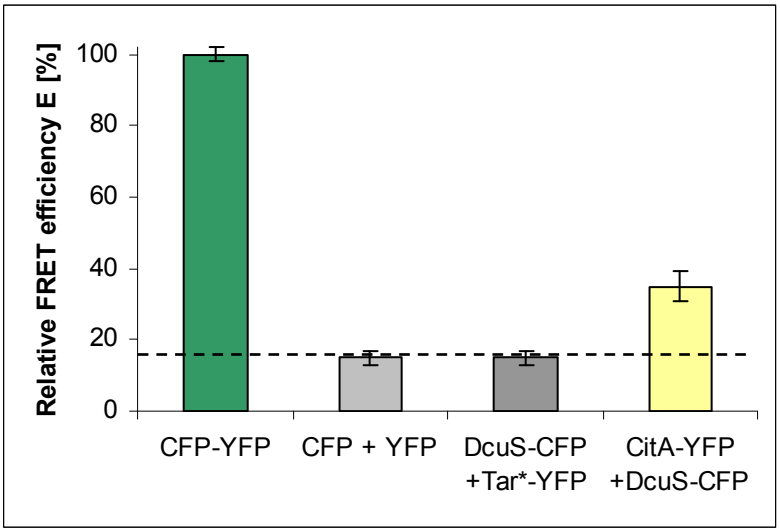

Figure 36: Detection of the interaction between CitA and DcuS via FRET measurements. The relative FRET efficiency of CFP-YFP fusion protein was set as 100 %. Dashed line indicates the threshold value of specific FRET. *Tar(1-331)-YFP.

Potential crosstalk between DcuSR and CitAB

CitAB induces the expression of the *citCDEFXGT* gene cluster, encoding the holo-citrate lyase and the citrate transporter CitT, in the presence of citrate under anaerobic conditions. A *citC'-'lacZ* reporter gene fusion was used to investigate CitAB dependent gene expression in *E. coli* (Rauschmeier, 2009). DcuSR dependent gene expression in the presence of citrate or fumarate was studied with the *dcuB'-'lacZ* reporter gene fusion (Fig. 35). The results were summarised and a potential crosstalk between the two related two-component systems DcuSR and CitAB of *E. coli* was analysed (Tab. 13, Fig. 37).

Table 13: Influence of DcuSR and CitAB on *dcuB'-'lacZ* and *citC'-'lacZ* expression. *E. coli* strains were grown anaerobically in eM9 medium with 50 mM glycerol, 20 mM DMSO and 20 mM fumarate or 20 mM citrate as effector, respectively. Expression studies with *dcuB'-'lacZ* (Fig. 35) were compared with expression studies with *citC'-'lacZ* summarised from Rauschmeier (2009).

Genotype	*dcuB'-'lacZ* (MU)		*citC'-'lacZ* (MU)	
	Citrate	Fumarate	Citrate	Fumarate
Wild-type	586	1040	251	3
dcuS	29 [a, g]	23 [a]	216 [j]	2
dcuR	5 [b, h]	7 [b]	95	2
citA	434 [i]	1035	5 [c, e]	12 [e]
citB	628	1209	8 [d, f]	11 [f]

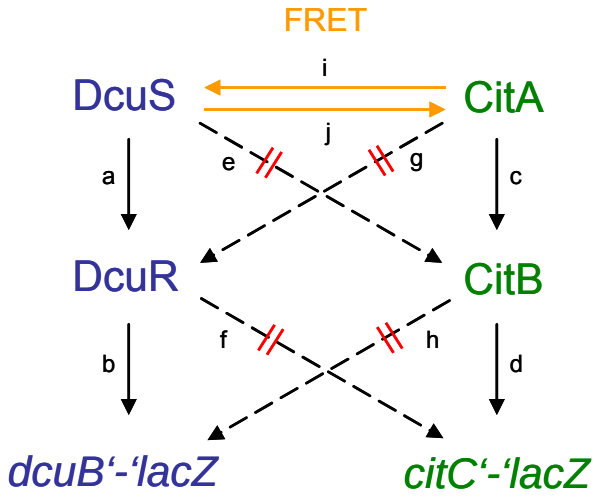

Figure 37: Potential crosstalk between the DcuSR and CitAB two-component systems (TCS). ß-Galactosidase assays were performed to study a potential crosstalk between the two related TCS. Small letters (a-j) relate the data from Tab. 13 to the arrows. Thereby expression levels of the mutant strains have to be compared to wild-type activity. a-d confirm the known activation cascade for each TCS (DcuSR = blue, CitAB = green; Zientz *et al.*, 1998; Yamamoto *et al.*, 2008 and Rauschmeier, 2009). e-h exclude a crosstalk between sensor and non-cognate response regulator or RR and non-cognate target gene, respectively (red dashes). A direct interaction between CitA and DcuS was detected as well by expression studies in the presence of citrate (i and j) as via FRET measurements (orange arrows).

dcuB'-'lacZ expression is dependent on DcuSR in the presence of citrate and in the presence of fumarate. Nevertheless, maximal induction of *dcuB'-'lacZ* in the presence of citrate was only attained when active CitA was additionally present. This implies a direct interaction between DcuS and CitA, which was also confirmed by FRET measurements (Fig. 36). No decrease of *dcuB'-'lacZ* induction was observed in a *citB* deletion strain, excluding a direct regulation of *dcuB* or the *dcuSR* operon by CitB. A phospho-transfer from the citrate-specific sensor CitA to DcuR can also be excluded, because in the DcuS-deleted strain *dcuB* expression was at a basal level, both in the presence of citrate or fumarate.

citC'-'lacZ was induced with citrate as effector but not in the presence of fumarate (Tab. 13). *citC* expression was completely lost in the absence of CitA or CitB. The direct induction of *citC'-'lacZ* was thus exclusively dependent on CitAB. Inactivation of DcuS led to a decrease of *citC'-'lacZ* expression by a factor of 1.2, which could be deduced from the interaction between CitA and DcuS. A drastic decrease of *citC'-'lacZ* induction by a factor of 2.6 was observed when DcuR was inactivated. The impact of DcuR on *citC* expression might be due to a direct transcriptional activation of *citAB* by DcuR.

Taken together, for the DcuSR and CitAB two-component systems, a crosstalk between sensor and non-cognate response regulator or RR and non-cognate target gene, respectively, was excluded *in vivo*. Protein-protein interaction between the sensor kinases CitA and DcuS was observed. Furthermore, DcuSR might be involved in the regulation of *citAB* expression.

5. Discussion

5.1 Oligomerisation of DcuS

Escherichia coli is able to grow under aerobic and anaerobic conditions in the presence of C_4-dicarboxylates. Fumarate functions as electron acceptor in anaerobic fumarate respiration. Expression of the genes for fumarate respiration and for the aerobic C_4-dicarboxylate transporter DctA is induced by the two-component system DcuSR through a phosphorelay (Zientz *et al.*, 1998; Janausch *et al.*, 2002). The stimulus is detected by the periplasmic domain of the sensor histidine kinase DcuS and the signal is then transduced across the membrane. For membrane-bound sensor proteins, the mechanism of signal transduction from the periplasm across the membrane into the cytosol is not fully understood. Oligomerisation appears to be obligatory for the function of sensor histidine kinases, where the catalytic domain of one subunit phosphorylates the conserved histidine residue of another subunit by ATP hydrolysis (Qin *et al.*, 2000). In contrast to eukaryotic membrane-bound receptor tyrosine kinases, whose oligomerisation is often triggered by their signal molecules, bacterial membrane-bound sensor histidine kinases are supposed to prevail oligomeric independent of the presence of effector (Gao and Stock, 2009). Signal transduction within the oligomer is exclusively mediated by conformational changes upon ligand binding. In the preformed oligomeric state, sensor histidine kinases are ready to transmit the stimulus as soon as the signal is detected. Probably this strategy was adopted by bacteria to allow a quick response to changing environmental conditions. Isolated periplasmic PAS domains of DcuS and related sensor histidine kinases like CitA and PhoQ are observed as dimers in the crystal structure with a protein concentration up to 44 mM (Cheung and Hendrickson, 2008; Sevvana *et al.*, 2008; Cheung *et al.*, 2008). However, the high protein concentrations are not physiological and might not reflect the native state of full-length sensor histidine kinases. Oligomerisation of the membrane-bound sensor histidine kinases EnvZ and VirA was also deduced from *in vivo* complementation studies (Yang and Inouye, 1991; Pan *et al.*, 1993). A dimeric state of the sensor kinases is assumed, although a higher oligomeric state is conceivable.

The oligomerisation of full-length DcuS was investigated using a combination of chemical crosslinking and quantitative FRET spectroscopy in proteoliposomes and in living cells. FRET measurements with fluorescently labelled DcuS *in vivo* and *in vitro* demonstrated effector-independent fluorescence resonance energy transfer and thus constitutive oligomerisation of DcuS in the membrane. The absence of changes in the energy transfer efficiency upon fumarate treatment suggests that the ligand-induced signal transduction is achieved exclusively by conformational changes rather than altering the oligomerisation state. The relevance of the *in vivo* FRET measurements was confirmed by control

experiments. A CFP-YFP tandem fusion was generated as a positive control. The constant and tight coupling of the FRET pair revealed the maximal energy transfer that could be obtained under given experimental conditions. Hence, the relative FRET efficiency of the CFP-YFP fusion was set as 100 %. As a negative control, CFP and YFP were co-expressed in the same cell as independent proteins, resulting in a minor relative FRET efficiency of 15 %. This value was set as threshold and only FRET efficiencies clearly above this value represented specific FRET between interacting proteins. When CFP and YFP were expressed in different cells, no FRET occurred. As a negative control for membrane-embedded proteins which are not expected to interact, a truncated membrane-bound variant of the chemotaxis receptor Tar fused with YFP was co-expressed with DcuS-CFP, again revealing a minor relative FRET efficiency of 15 %. The four control experiments helped to define the background FRET signal of the experimental system. The relative FRET efficiency of cells co-expressing DcuS-CFP and DcuS-YFP was clearly above the threshold value, proving DcuS-DcuS interaction.

The degree of DcuS oligomerisation was determined by chemical crosslinking with disuccinimidyl suberate (DSS). The crosslinking experiments gave clear evidence that DcuS is a tetramer in isolated bacterial membranes, and after reconstitution of purified His_6-DcuS into liposomes. There were also low amounts of dimeric DcuS detected in the membranes and in proteoliposomes, but the dimer is presumably a fraction of the tetramer that has not been completely crosslinked.

Intermolecular disulfide bond formation via Cys471 under oxidising conditions resulted in unspecific dimerisation of His_6-DcuS. The lack of tetramers is explained by the presence of only one site for disulfide formation per monomer (Cys471), which allows only dimer formation. This dimerisation was observed for detergent-solubilised as well for reconstituted His_6-DcuS and occurs when two monomers interact in the complex or by chance.

The DcuS oligomer is not very stable, and most of the detergent-solubilised His_6-DcuS was monomeric. However, a small portion of detergent-solubilised His_6-DcuS was present in the tetrameric state, which was even retained during SDS gel electrophoresis. Oligomeric forms of DcuS, i.e. those in bacterial cells and proteoliposomes, are capable of autophosphorylation, whereas monomeric DcuS in detergent lacks kinase activity (Janausch *et al.*, 2002). Thus the oligomeric state of DcuS in the membrane is essential for kinase function. The functional state is obviously not regulated by reversible oligomerisation of DcuS, since the protein is a permanent oligomer in the membrane independent of the presence of effector. Further, higher oligomeric states of DcuS can not be excluded.

Several approaches were carried out to determine the degree of oligomerisation of DcuS by intermolecular FRET to confirm the crosslinking results. Donor-labelled DcuS and acceptor-

labelled DcuS were mixed *in vitro* or expressed *in vivo* at various donor fractions. The degree of oligomerisation should thereby be determined by fitting the calculated donor fractions and FRET efficiencies to a model of oligomeric state (Adair and Engelman, 1994; Meyer *et al.*, 2006; Liao, 2008).

Unknown parameters in the *in vivo* and *in vitro* test systems complicated determining the oligomeric state of DcuS via FRET. The orientation and thus the distance between donor and acceptor could not be predicted, neither in the DcuS-GFP fusion proteins, nor in the unspecifically labelled His_6-DcuS. Additionally, *in vivo* donor fractions were limited to a range of 0.25-0.55 despite the use of different vector systems and different induction times. *In vitro*, the labelling efficiency could not be determined due to the unspecific labelling of His_6-DcuS. Finally, the model of oligomeric state was developed for proteins with uniform oligomeric states, whereas Cys471-containing His_6-DcuS exhibited mixed oligomeric states in detergent and in proteoliposomes, as shown by oxidative crosslinking.

In future studies, oligomerisation sites and domains of DcuS should be investigated by performing the chemical crosslinking experiments with truncated variants of DcuS and with full-length DcuS mutated at specific amino acid residues.

It could further be investigated, if cells co-expressing DcuS-CFP and CheY-YFP show fluorescence resonance energy transfer. Although the polar localisation of DcuS-YFP was independent of the presence of the methyl-accepting chemotaxis proteins, an interaction between the sensor kinase DcuS and the chemotaxis response regulator CheY can not be excluded and is even proposed (Yamamoto *et al.*, 2005).

5.2 Subcellular localisation of DcuS and CitA in *E. coli*

The subcellular localisation of the carboxylate sensor histidine kinases DcuS and CitA fused with YFP was studied by means of confocal laser scanning microscopy. DcuS-YFP and CitA-YFP were found to accumulate at one or both cell poles of *E. coli* (Scheu *et al.*, 2008). The polar accumulation depended solely on DcuS or CitA, whereas YFP contributed neither to membranous nor to polar localisation. The expression of recombinant proteins may result in the formation of non-specific aggregates in form of inclusion bodies, which are frequently located close to the cell poles, thus mimicking the polar localisation of proteins (Margolin, 2000). However, denatured GFP in inclusion bodies is not properly folded and therefore not fluorescent (Drew *et al.*, 2001). Nevertheless, potential problems with DcuS-YFP in inclusion bodies were tested by various experiments. The cell fraction of a homogenate that contains potential inclusion bodies exhibited only low fluorescence intensity with maximally 10 % of the total. DcuS-YFP localisation was also independent of the inducer concentration

controlling *dcuS-yfp* expression, and therefore of the protein expression level. Polar accumulation of DcuS-YFP or CitA-YFP became evident soon after induction at low levels of expression, implying that polar accumulation was not due to over-expression of the fusion proteins. Furthermore, the inducer L-arabinose was consumed by the *E. coli* strains as determined through HPLC (not shown). In the presence of L-arabinose, the bacteria generally grew slower showing a diauxic growth, also without containing a pBAD vector. Polar accumulation was quantified by a fluorescence intensity ratio of polar maximum to membrane. The ratio of either DcuS-YFP or CitA-YFP was 1.6 or above, implying that these proteins accumulated but were not exclusively located at the cell poles. Altogether, the polar accumulation of DcuS and CitA appears to represent the native state of the sensor kinases.

The polar accumulation of DcuS-YFP and CitA-YFP was increased in the presence of effector (fumarate or citrate, respectively). The increase of DcuS depended on the presence of its cognate response regulator DcuR, suggesting that the polar accumulation is related to the functional state of the DcuSR two-component system. Both, the polar accumulation at low concentrations of DcuS and its further increase in the presence of the effector fumarate indicate that the polar accumulation is of physiological relevance, and that DcuR might play a role in DcuS localisation.

Methyl-accepting chemotaxis proteins (MCPs) represent the paradigm for polar accumulated sensory proteins (Lybarger and Maddock, 2000; Sourjik and Berg, 2000). MCP-associated proteins, such as CheY, accumulate at the cell poles to a similar extent as DcuS and CitA. The fluorescence intensity ratios of polar maximum to cytosol for MCP-related proteins were reported to be in the range of 1.2-2.2, and for CheY about 1.6 (Sourjik and Berg, 2000). In this study, fluorescence intensity ratios of polar maximum to cytosol in the range of 2.6-3.6 were determined for DcuS, and a similar range was observed for CitA. Thus, the amount of DcuS that accumulated at the cell poles is comparable to that of the chemotaxis proteins, even if the methods to determine the ratios were slightly different in the two studies. However, the polar accumulation of DcuS did not depend on the presence of the MCP complex. In the absence of MCPs, DcuS still accumulated at the cell poles. Hence, there seems to be no direct interaction between DcuS and the MCPs.

For DcuS and CitA, the degree of polar accumulation increased in the presence of the corresponding effector (fumarate or citrate, respectively). This could indicate that the polar accumulation is functionally relevant and that it supports proper function of the two sensor kinases in an unknown way. Clusters of chemotaxis sensors together with the sensor-related proteins CheA and CheW are well documented (Lybarger and Maddock, 2000). The clusters are believed to support stimulus integration and the sensitivity of the sensors (Sourjik, 2004; Thiem *et al.*, 2007). Chemotaxis requires no asymmetric distribution for the function of the sensory complexes, and the role of polar localisation of the complexes is not understood. It

could be related to the diffusion restriction of cell envelope proteins in the polar region, which might extend to the cytosolic membranes (de Pedro *et al.*, 2004).

The spatial distribution of some sensor kinases is essential for their function, e.g. in controlling asymmetric processes in cell division and development (Shapiro *et al.*, 2002), whereas the reason for localisation of metabolic sensor kinases is not evident. As shown here for DcuS and CitA, polar or asymmetric localisation is also observed for sensory histidine kinases that control metabolic processes without predicted asymmetric distribution in the cell. It is possible that such a polar accumulation is not restricted to DcuS and CitA. Due to the small size of bacterial cells, polar localisation could reflect a mechanism for spatial compartmentalisation of proteins, which are expressed under prevailing conditions. Polar accumulation of sensors perceiving low molecular compounds as periplasmic signals could further be an advantage for swimming cells detecting the substrate primarily with the pole, as discussed for the chemotaxis receptors, which are predominantly located at one pole (Berg and Turner, 1995). *E. coli* cells swim with either end in forward direction without favouring one end of the cell over the other. The described mechanism could apply to receptors located at both cell poles as shown for DcuS and CitA.

Influence of phospholipids on the localisation of membranous proteins

It was proposed that bacterial membranes consist of microdomains of phospholipids, as a result of the intrinsic chemical characteristics of the different phospholipids (Matsumoto *et al.*, 2006). The cytosolic membrane of *E. coli* includes three major phospholipids, i.e. approximately 75 % phosphatidylethanolamine (PE), 20 % phosphatidylglycerol (PG) and 5 % cardiolipin (CL) (Cronan, 2003). The proportion of the phospholipids varies with growth phase and medium osmolality, thereby CL increases when *E. coli* enters the stationary phase or with increasing osmolality (Romantsov *et al.*, 2007). CL is enriched at the cell poles and septa of growing *E. coli* cells (Mileykovskaya and Dowhan, 2000). It is suggested that CL is concentrated at the cell poles because of its small headgroup, which is required for the small radius of the membrane curvature at the cell poles and division sites (Matsumoto *et al.*, 2006). The negative charge of CL recruits peripheral membrane proteins to the membranes, which has been shown for various proteins, such as DnaA, FtsY, GlpD, PssA and SecA (Dowhan, 1997; Matsumoto, 2001; Walz *et al*., 2002). Basic residues of these proteins are assumed to interact with the negative charge of the acidic cardiolipin.

Trapping of membranous proteins in polar cardiolipin patches is also feasible for DcuS and CitA. A cardiolipin-dependent polar localisation of a transmembrane protein is demonstrated for the osmosensory transporter ProP (Romantsov *et al.*, 2007). In contrast, the polar localisation of its paralogue lactose-H^+ symporter LacY is cardiolipin-independent

(Romantsov *et al.*, 2008). The influence of cardiolipin on DcuS localisation will be investigated in a cardiolipin synthase-defective *E. coli* strain in future studies.

Construction of a chromosomal *dcuS-bs2* gene fusion

For future localisation studies, DcuS was genetically fused with Bs2, a flavin mononucleotide-based fluorescent protein, which shows fluorescence under aerobic and anaerobic conditions. The *dcuS-bs2* gene fusion was inserted into the chromosome of a cardiolipin-defective mutant and into a wild-type strain. As a consequence, *dcuR*, that overlaps with *dcuS* by 4 bp, was inactivated. Since polar localisation of DcuS-YFP was only slightly affected in a *dcuR* mutant, the strain should be useful for the studies. In addition, DcuR could be supplied from a plasmid. The presence of active DcuR enhanced polar accumulation of DcuS-YFP in the presence of effector, but was not essential for it.

The use of a suicide vector system for the insertion of genetically altered genes, e.g. gene fusions or point mutations, via homologous recombination into the bacterial chromosome involves several advantages compared to other methods. The target gene is introduced into the physiological chromosomal context and without leaving scars, such as antibiotic resistance markers, allowing a combination of multiple mutations in the same genetic background.

Additionally, *dcuS-bs2* was cloned into a low-copy plasmid under the control of the *dcuS* promoter. The plasmid can be expressed in strains of interest without the influence of polar effects, and therefore in the presence of active DcuR. Expression of plasmid-encoded DcuS-Bs2 led to a similar induction level of the *dcuB'-'lacZ* reporter gene fusion as chromosomally encoded wild-type DcuS.

In future studies, plasmid-encoded and chromosomally encoded DcuS-Bs2 can be used to investigate the influence of polar cardiolipin patches on the localisation of DcuS under physiological conditions (cooperation with Prof. Peter Graumann, Freiburg).

Furthermore, it can be tested if the cytosolic portion of DcuS contributes to polar localisation, as observed for Tar^{1-331}-YFP (Kentner *et al.*, 2006). The experiments can be performed with a cytosolically truncated variant of DcuS lacking the PAS and the kinase domain and fused to a fluorescent protein (DcuS(TM1-PAS_P-TM2)-FP).

In addition, it is possible to investigate if DcuS and CitA are inserted into the membrane directly at the cell poles after protein synthesis, or if the sensors are inserted into lateral regions of the membrane and then actively or passively migrate to the poles. This type of question can be studied by means of time-lapse microscopy and inhibition of continuous transcription of the gene fusion by treatment with rifampicin.

5.3 Interaction between DcuS and CitA in *E. coli*

E. coli is able to perform citrate fermentation in the presence of an oxidisable co-substrate (Lütgens and Gottschalk, 1980). The CitAB two-component system regulates gene expression of citrate fermentation (Yamamoto *et al.*, 2008). The sensor histidine kinase DcuS of *E. coli* senses citrate in addition to C_4-dicarboxylates. Despite the high apparent K_d value of DcuS for citrate compared to CitA, regulation by citrate via DcuSR might be physiologically relevant, since the K_d value is in the same range as those for C_4-dicarboxylates (Krämer *et al.*, 2007). Interaction between CitA and the structurally related sensor histidine kinase DcuS was observed by expression studies and by *in vivo* FRET measurements. Since citrate fermentation includes the reactions of fumarate respiration, the induction of the fumarate respiratory system by citrate and its increased induction based on the interaction between DcuS and CitA is plausible.

The findings of tetrameric DcuS and its interaction and co-localisation with the related sensor kinase CitA raise the possibility, that the oligomeric structure observed in the crosslinking experiments could also involve DcuS-CitA heterotetramers. This should be examined by treatment of membranes containing over-expressed DcuS with antibodies raised specifically against the periplasmic domain of $CitA_{Ec}$. The periplasmic domain of $CitA_{Ec}$ can be purified and used for antiserum production. In the presence of DcuS-CitA heterotetramers, a distinct tetrameric band is expected after crosslinking of membranes containing over-expressed DcuS, which interacts with anti-DcuS and anti-CitA in immunoblots.

Transcriptional regulation of *citA* in *E. coli*

The *citCDEFXGT* operon of *E. coli* is induced under anaerobic conditions in the presence of citrate (Rauschmeier, 2009). The genes responsible for citrate fermentation are repressed in the presence of the alternative electron acceptors oxygen or nitrate. Hypothetic NarL binding sites were detected upstream of *citC* and *citA*, each on the respective coding strand, suggesting a direct regulation of *citC* and *citA* expression by NarL (Fig. 38). Furthermore, a potential FNR binding site lies upstream of *citA*. FNR might therefore directly induce *citA* expression and indirectly regulate *citC* expression. Direct regulation of *citC* by FNR can not be ruled out. ArcA might also be involved in the regulation of *citA*. In citrate fermentation of *E. coli*, glucose can be degraded as co-substrate and does not cause catabolite repression (Lütgens and Gottschalk, 1980). No functional CRP binding site is therefore expected upstream of genes regulated by CitAB. The CRP binding site detected by computational analysis might be a consequence of its high similarity with the FNR consensus sequence. The identification of CitB consensus sequences in the intergenic region of *citC* and *citA* is based on sequence comparison with experimentally determined binding sites of CitB in

Klebsiella pneumoniae (Ingmer *et al.*, 1998). The importance of the CitB binding sites in *E. coli* was confirmed experimentally by a *citC'-'lacZ* reporter gene fusion lacking these sites (Rauschmeier, 2009). The presence of CitB binding sites upstream of *citA* is also consistent with the proposed auto-regulation of the *citAB* operon by CitAB (Yamamoto *et al.*, 2008).

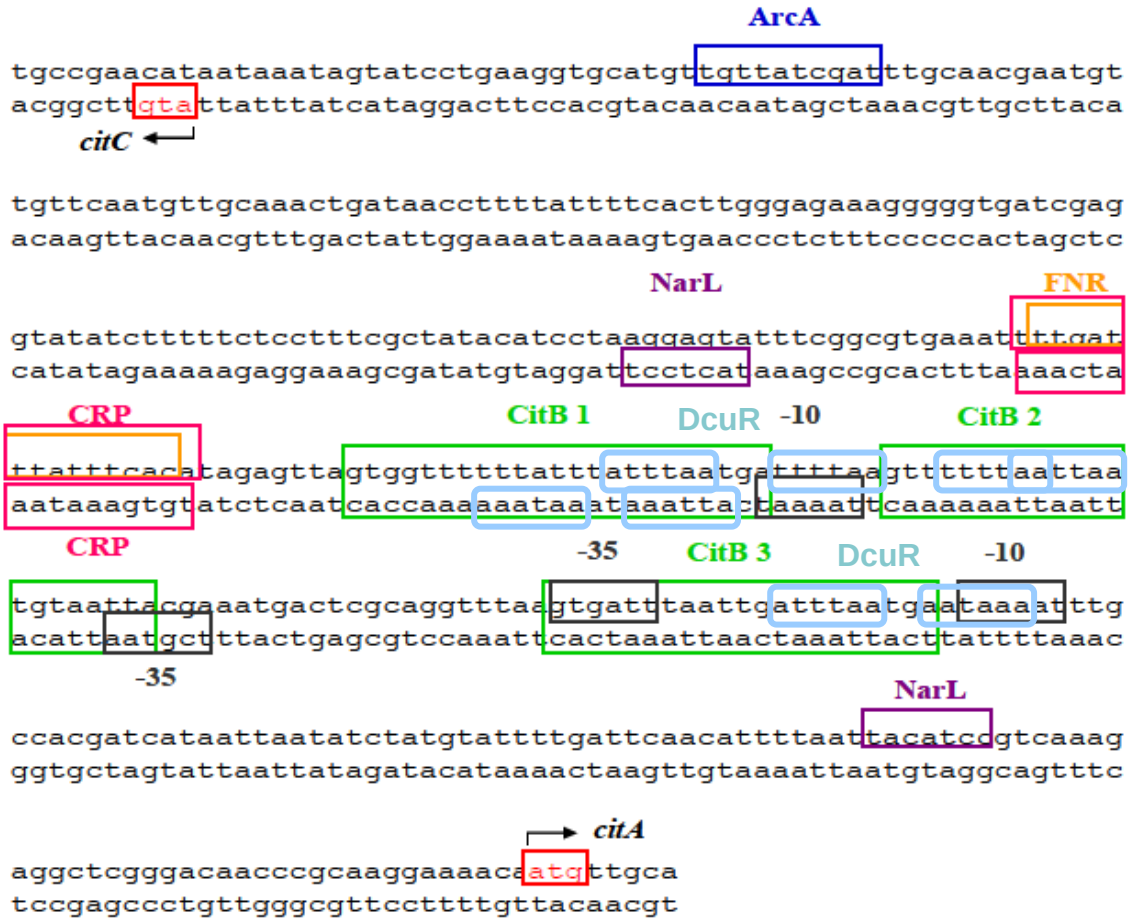

Figure 38: Putative DcuR-binding sites in the intergenic region of *citC* and *citA*. Potential DcuR-binding motifs (blue boxes), comprising a tandem repeat of (T/A)(A/T)(T/C)(A/T)AA (Abo-Amer *et al.*, 2004), were detected on the coding strand upstream of *citA*. A further consensus motif was found on the non-coding strand, possibly regulating *citC*. Note that putative binding sites of CitB (Ingmer *et al.*, 1998) and DcuR overlap. Potential binding sites of ArcA, CRP, FNR, NarL and promoter regions are based on computational analysis with the Prodoric software by Virtual Footprint (Münch *et al.*, 2005). (Figure derived from Rauschmeier, 2009)

The decreased induction of *citC'-'lacZ* by a factor of 2.6 in the absence of DcuR might be due to a direct regulation of *citA* by DcuR (Rauschmeier, 2009). Potential DcuR binding sites were detected upstream of *citA* by comparison of the DcuR tandem repeat motif, which was experimentally determined for several well-characterised DcuSR-induced genes (Abo-Amer *et al.*, 2004) (Fig. 38).

In future studies, a possible transcriptional regulation of *citAB* by DcuSR should be tested via the expression of a *citA'-'lacZ* reporter gene fusion in a wild-type strain and in a series of mutant strains defective in components of the DcuSR and CitAB systems.

5.4 Database research for domain organisation of histidine kinases with periplasmic sensing PAS domains

Periplasmic or extracellular sensing histidine kinases represent a subgroup of the membrane bound sensor kinases and contain an extracellular sensing domain (Mascher *et al.*, 2006). During transmembrane signalling, the signal has to pass the membrane across several domains. Sensors of this type are used for the response to many extracellular nutrients and other solutes that are hydrophilic and not able to cross the membrane. The sensing domain of the periplasmic sensing histidine kinases is generally framed by one transmembrane helix on either side (TM1 and TM2), followed by the C-terminal kinase or transmitter domain. The transmitter domain comprises a region with the conserved histidine residue for autophosphorylation and a highly conserved catalytic domain at the C-terminal end. The domain with the conserved histidine residue typically consists of two α-helices, which serve in dimerisation (DHp, dimerisation and histidine phosphotransfer; or HisKA domain). The catalytic domain (HATPase) catalyses autophosphorylation of the sensor kinase in the HisKA domain. Hybrid kinases contain one or more additional receiver domains typical for response regulators at the C-terminal end with a conserved aspartate residue for phosphorylation, and an additional transmitter (HPt) domain (Zhang and Shi, 2005). The phosphoryl transfer from the sensor kinase to the response regulator is catalysed by the response regulator, using the phosphoryl-sensor kinase as the phospho-donor (Wolanin and Stock, 2003).

The minimal domain organisation of a periplasmic sensing histidine kinase consists of a periplasmic sensor and a cytosolic kinase domain (TM1, sensor domain, TM2, HisKA-HATPase domain) (Fig. 39). It can be modified by inclusion of 'linker' regions between TM2 and the HisKA-HATPase domain, such as the HAMP (prevailing in histidine kinases, adenylyl cyclases, methyl-carrier proteins, and phosphatases) or PAS (Per-Arnt-Sim) domain (Aravind and Ponting, 1999; Galperin *et al.*, 2001). The linker domains apparently have an important role in signal transduction from the sensor domain along TM2 to the kinase domain, and vary considerably in size and type.

Several periplasmic sensing histidine kinases use PAS domains as sensory devices. PAS is an acronym formed from the names of the proteins in which the domain was first recognised, the *Drosophila* period clock protein (Per), the vertebrate aryl hydrocarbon receptor nuclear translocator (Arnt), and the *Drosophila* single-minded protein (Sim) (Ponting and Aravind, 1997). PAS domains are ubiquitous sensory domains responding to a wide range of signals including light, oxygen, redox potential and small molecules (Taylor and Zhulin, 1999). Although they are not well conserved at the level of the primary sequence, they share a common three-dimensional fold. PAS domains are composed of an α-helical cap, the PAS core structure that includes the first strands of the characteristic central β-sheet, the helical connector and the β-scaffold that completes the central β-sheet. The central β-sheet is

flanked by the helical cap on one side and the helical connector together with parts of the PAS core on the other side.

PAS domains were originally thought to be exclusively cytosolic sensing domains (Taylor and Zhulin, 1999). However, the periplasmic domains of CitA from *Klebsiella pneumoniae* ($CitA_{Kp}$, Swiss-Prot: P52687, PDB: 1p0z) and DcuS from *E. coli* ($DcuS_{Ec}$, P0AEC8, 1ojg) were shown to belong to the PAS structural fold (Reinelt *et al.*, 2003; Pappalardo *et al.*, 2003). This demonstrated that PAS domains are also used for extracellular sensing. Periplasmic PAS domains (PAS_P) have been identified by structural, biochemical, molecular genetic studies or by secondary structure prediction as the sensory devices in a considerable number of periplasmic sensing kinases (Fig. 39).

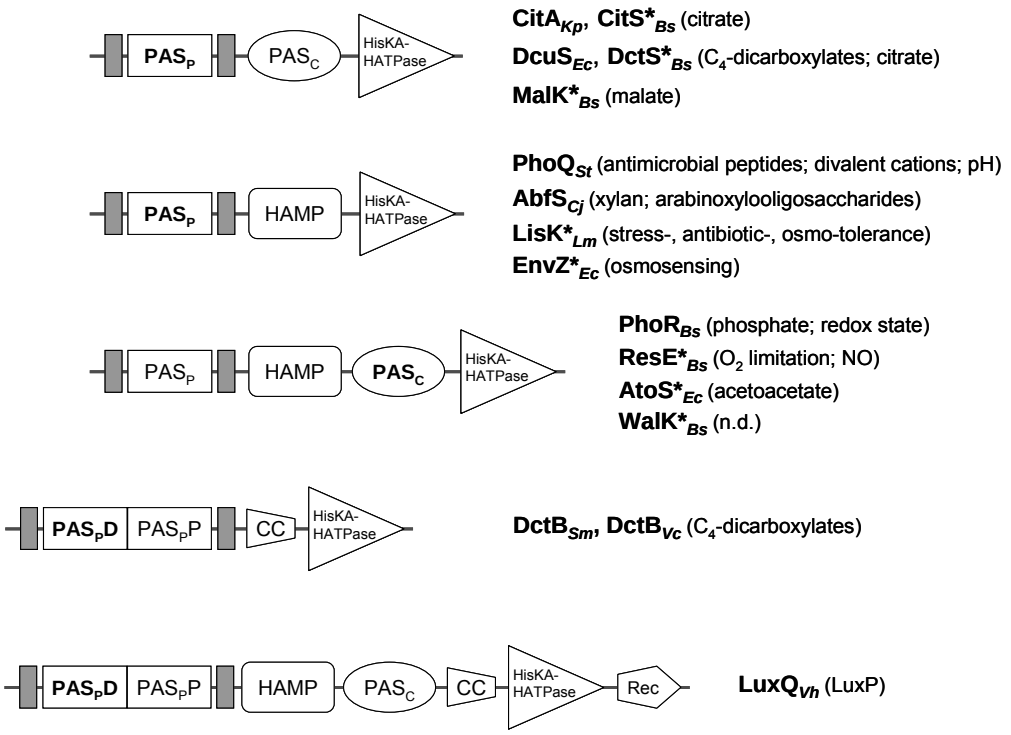

Figure 39: Domain organisation of histidine kinases containing a periplasmic sensing PAS (PAS_P) domain. Sensor kinases are depicted, for which the presence of PAS_P has been demonstrated experimentally by structural, biochemical, molecular genetic studies or by secondary structure prediction (PSIPRED, Jones, 1999; Bryson *et al.*, 2005). The PAS_P domain of EnvZ is hypothetical. In the tandem PAS domains the distal (PAS_PD) and proximal (PAS_PP) domains are indicated. Sensor kinases for which sensing of the stimulus (given in parenthesis) by PAS_P has not been verified experimentally are indicated (*). The PAS domain exerting the main sensory function is printed in bold letters. Transmembrane helices are marked in grey. CC, coiled-coil; Rec, receiver domain. *Bs, Bacillus subtilis; Cj, Cellvibrio japonicus; Ec, Escherichia coli; Kp, Klebsiella pneumoniae; Lm, Listeria monocytogenes; St, Salmonella typhimurium; Sm, Sinorhizobium meliloti; Vc, Vibrio cholerae; Vh, Vibrio harveyi*. WalK, alternative designation for YycG.

The PAS_P domains function by reversible binding of a stimulus molecule, and do not contain cofactors for sensing. A subgroup of the sensor kinases carry tandem PAS_p domains composed of two PAS domains. The PAS_P and the tandem PAS_P domains are framed by

one transmembrane helix on either side (TM1 and TM2). The sensor kinases with simple PAS_P domains each contain a signal transduction domain in the cytosol between TM2 and the HisKA-HATPase domain. Three groups can be identified according to the domain arrangement and composition of the signal transduction domains (Fig. 39). The signal transducing module is either a cytosolic PAS domain (PAS_C), a HAMP domain, or a combination of both. A PAS_C domain is found in $DcuS_{Ec}$ and $CitA_{Kp}$, and in the other members of the CitAB family, the CitA homologue $CitS_{Bs}$ (O34427), and the DcuS homologs $DctS_{Bs}$ (P96601) and $MalK_{Bs}$ (O05250) of *B. subtilis* (Yamamoto *et al.*, 2000; Asai *et al.*, 2000; Doan *et al.*, 2003). The sequence between TM2 and PAS_C in DcuS and CitA is very short (< 20 aa) and leaves no space for further domains. In $DcuS_{Ec}$ the PAS_C domain has been shown to be highly flexible and thus serve as a signal transducing module between TM2 and the kinase domain (Etzkorn *et al.*, 2008). The same presumably applies to $CitA_{Kp}$ and other members of the PAS_P/PAS_C containing sensor kinases.

$PhoQ_{St}$ (P14147, 1yax) of *Salmonella typhimurium*, $AbfS_{Cj}$ (B3PFT7, 2va0) of *Cellvibrio japonicus*, $LisK_{Lm}$ (Q9RPY9) of *Listeria monocytogenes*, $EnvZ_{Ec}$ (P0AEJ4) of *E. coli* and various other PAS_P containing sensor kinases possess a HAMP domain for signal transduction to the HisKA-HATPase domain (Cho *et al.*, 2006; Emami *et al.*, 2009; Cotter *et al.*, 1999; Kishii *et al.*, 2007). The role of PAS_P of $LisK_{Lm}$ is not known (Cotter *et al.*, 2002). For EnvZ, it is even not clear whether the periplasmic domain really forms a PAS domain, and the function of the supposed PAS_P is not known (Khorchid *et al.*, 2005). HAMP domains are small signal transducing modules of about 55 aa. A HAMP domain has been shown to effect rotational movement for reconfiguration of domain orientation in signal transduction by membrane bound sensors (Hulko *et al.*, 2006).

Sensor kinases $PhoR_{Bs}$ (P23545, 3cwf), $ResE_{Bs}$ (P35164), WalK $(YycG)_{Bs}$ (Q45614) of *B. subtilis* and $AtoS_{Ec}$ (Q06067) of *E. coli* contain both, HAMP and PAS_C domains as cytosolic linker modules of the proteins (Eldakak and Hulett, 2007; Baruah *et al.*, 2004; Szurmant *et al.*, 2008; Filippou *et al.*, 2008). The stimulus of $WalK_{Bs}$ is yet unknown, but the sensor kinase is essential for cell viability and controls the synthesis of proteins involved in cell wall remodelling and cell separation in *Bacillus subtilis* (Szurmant *et al.*, 2008; Dubrac *et al.*, 2008). The role of the HAMP domain in the HAMP/PAS_C containing proteins has not been studied. In $PhoR_{Bs}$, PAS_C has a sensory function, leaving a role for the HAMP domain in signal perception and transduction from the membrane (Eldakak and Hulett, 2007). In $PhoR_{Bs}$ and $ResE_{Bs}$, the PAS_C domains represent the primary sensory site sensing the intracellular redox status. The PAS_P domains of these proteins are proposed to represent a second signal input site for an additional stimulus or for signal amplification.

The DctB sensor kinases ($DctB_{Sm}$ P13633, 3e4o; $DctB_{Vc}$ Q9KQS3, 3by9) represent a family of sensor kinases with tandem PAS_P domains (Reid and Poole, 1998; Cheung and

Hendrickson, 2008; Zhou *et al.*, 2008). Some members of this family of sensor kinases contain a short hypothetical linker module (coiled-coil type) of about 100 aa in the cytosolic region between TM2 and the kinase domain. The LuxQ sensor (P54302, 2hje) of *Vibrio harveyi*, which also contains a tandem PAS_P domain, carries a complex cytosolic linker region comprising a HAMP, PAS_C, and a coiled-coil module (CC) of unknown function (Neiditch *et al.*, 2005). LuxQ is a hybrid sensor kinase, and the HisKA-HATPase domain is followed by a receiver (Rec) domain. The function of the domains in this combination is not clear. The tandem PAS_P of LuxQ differs from the other sensors with a PAS_P domain by its interaction with an accessory periplasmic protein (LuxP) rather than a low molecular weight stimulus. LuxP mediates the interaction of PAS_P from LuxQ with the primary stimulus of the system, auto-inducer AI-2 (Neiditch *et al.*, 2006).

Secondary structure elements of periplasmic and cytosolic PAS domains

With the increasing number of identified PAS_P domains and resolution of the corresponding structures, it was recognised that the periplasmic PAS_P domain of DcuS, DctB, CitA and PhoQ differs in the arrangement of the α-helical and β-sheet structures from common PAS domains, and the term PDC (for PhoQ, DcuS/DctB, CitA) domain was coined for this type of PAS domain topology (Cheung and Hendrickson, 2008). Analysis of the periplasmic PAS_P domains of other sensor histidine kinases reveals that the PDC-fold is a general feature (Fig. 40). Typically, the PAS_P domains contain three N-terminal helices, a central helical linker region, and one C-terminal α-helix, which are separated by two or three β-sheets (3α-2β-α-3β-α). The first N-terminal helix (α_1) is an extension of TM1. The central α helix is divided into two short α-helices in some of the periplasmic PAS domains. The same fold is also found in the distal PAS_P domains of the tandem PAS domains of DctB and $LuxQ_{Vh}$. The distal PAS_P of DctB is functionally homologous to the PAS_P domains of DcuS and CitA by binding of the effector molecule (Cheung and Hendrickson 2008; Zhou *et al.*, 2008). $PhoQ_{St}$, on the other hand, one of the original members of the PDC domain proteins, shows a significant variation of the PDC-fold by containing only one N-terminal α-helix (α_1) followed by 4 β-sheet structures, the first two of which replace α_2 and α_3 of the PDC-fold. The central β-sheets (β_5 β_6 β_7) of $PhoQ_{St}$ are separated by a largely extended loop between β5 and β6 (Fig. 40A).

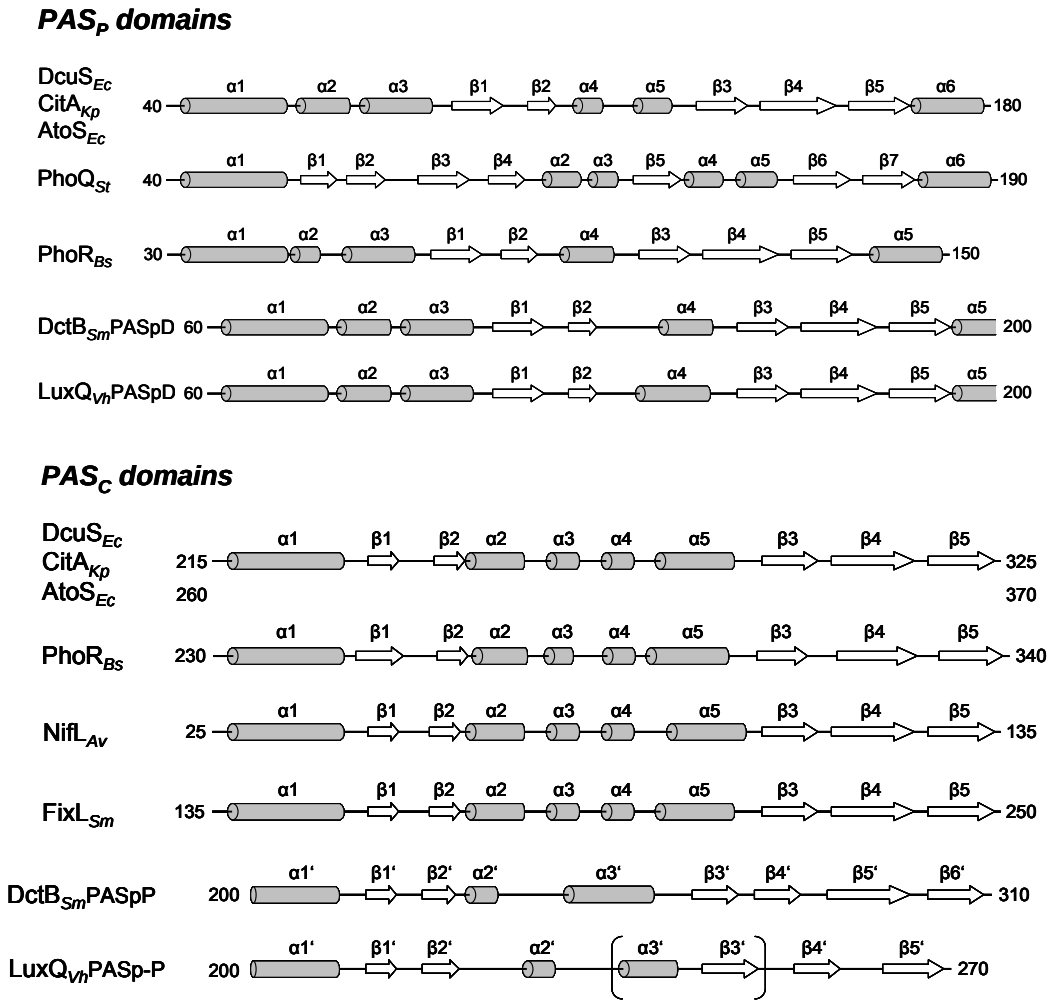

Figure 40: Secondary structure elements of periplasmic PAS_P and cytosolic PAS_C domains. Secondary structures were determined by structural studies or by secondary structure prediction (PSIPRED, Jones, 1999; Bryson *et al.*, 2005). A, PAS_P domains typically show a 3α-2β-α-3β-α structure (PDC-fold). B, PAS_C domains show a α-2β-4α-3β structure. Abbreviations are the same as for Fig. 39, and *Av*, *Azotobacter vinelandii*. The assignment of the α_3'-β_3' region of $LuxQ_{Vh}PAS_PP$ is unclear (in brackets). PAS_P and PAS_C stand for periplasmic or cytosolic PAS domain, PAS_PD and PAS_PP for distal or peripheral PAS_P domain.

The cytosolic PAS_C domain, on the other hand, typically shows a α-2β-4α-3β structure (Fig. 40B). Remarkably, this fold is not only found in PAS_C domains which carry cofactors for sensing, but also in PAS_C domains that function in signal relay. The sensing PAS_C domains are exemplified by the domains of $FixL_{Sm}$ (Swiss-Prot: P10955; PDB: 1d06, 1ew0), $NifL_{Av}$ (P30663; 2gj3) and $PhoR_{Bs}$, whereas the signal transducing domains are represented by those from $DcuS_{Ec}$ and $CitA_{Kp}$. The proximal of the tandem PAS domains of $DctB_{Sm}$ and of $LuxQ_{Vh}$ have similar arrangements as the cytosolic PAS_C domains. This is in agreement with the supposed function of the proximal PAS domains in signal transduction rather than sensing or binding of stimuli.

Mechanism of signal transduction by the citrate sensor CitA of *Klebsiella pneumoniae*

Binding of citrate by PAS_P of $CitA_{Kp}$ leads to a large movement of the minor loop (α_4 and α_5) that connects the β-sheets (Sevvana *et al.*, 2008). This results in a more compact structure of PAS_p and enhanced binding of citrate, which is proposed to lift the ends of the central β-sheet towards the citrate-binding site, while β5 pulls the C-terminal α-helix off the membrane (Fig. 41). As a result, TM2 is potentially lifted in the membrane in an axial direction towards the periplasmic side. The piston-type movement of TM2 could be directly transmitted according to this scheme to PAS_C, whereas TM1 stays in a fixed position in the membrane.

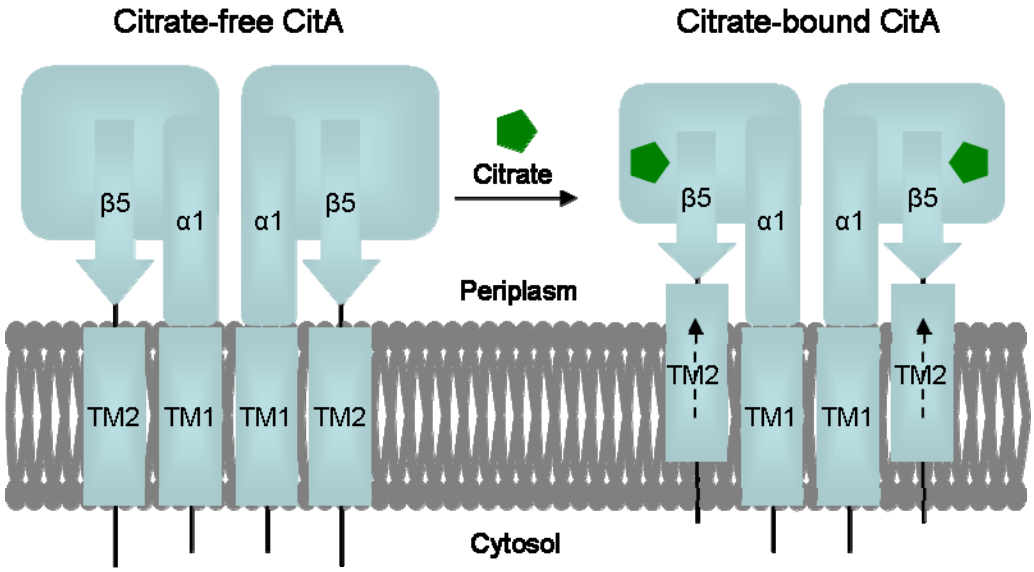

Figure 41: Model of the ligand-induced switch in the periplasmic domain of CitA. In the citrate-free state (left), the PAS_P domain is in the relaxed state. By binding of citrate (right) the PAS_P domain contracts by the postulated piston-type movement. The condensation of PAS_P triggers a vectorial movement of TM2 and thus the transduction of the signal to the PAS_C domain. (Figure modified from Sevvana *et al.*, 2008)

Such a piston-type displacement of TM2 relative to TM1 has also been identified as the signal transmitting step in chemoreceptor proteins like Tar (Ottemann *et al.*, 1999; Draheim *et al.*, 2006; Lai *et al.*, 2006).

It is assumed that signal perception by PAS_P of $DcuS_{Ec}$ is similar to that of $CitA_{Kp}$ due to their structural similarities, and due to the fact that $DcuS_{Ec}$ responds to binding of C_4-dicarboxylates and citrate by similar conformational changes to those observed in $CitA_{Kp}$ (Cheung and Hendrickson, 2008; Etzkorn *et al.*, 2008; Kneuper *et al.*, unpublished).

6. References

Abo-Amer, A.E., Munn J., Jackson, K., Aktas M., Golby, P., Kelly D.J., Andrews S.C. (2004)
DNA Interaction and Phosphotransfer of the C_4-Dicarboxylate-Responsive DcuS-DcuR Two-component Regulatory System from *Escherichia coli*.
J. Bacteriol. 186: 1879-89

Adair, B. D. and Engelman, D. M. (1994)
Glycophorin A helical transmembrane domains dimerize in phospholipid bilayers: a resonance energy transfer study.
Biochemistry, 33(18):5539-5544

Ames, P., Studdert, C. A., Reiser, R. H., and Parkinson, J. S. (2002)
Collaborative signaling by mixed chemoreceptor teams in *Escherichia coli*.
Proc Natl Acad Sci USA 99, 7060-7065

Aravind, L. and Ponting, C.P. (1999)
The cytoplasmic helical linker domain of receptor histidine kinase and methyl-accepting proteins is common to many prokaryotic signalling proteins.
FEMS Microbiol. Lett. 176, 111-116

Asai, K., Baik, S.-H., Kasahara, Y., Moriya, S. and Ogasawara, N. (2000)
Regulation of the transport system for C_4-dicarboxylic acids in *Bacillus subtilis*.
Microbiology 146: 263-271

Baba, T., Ara, T., Hasegawa, M., Takai, Y., Okumura, Y., Baba, M., Datsenko, K. A., Tomkita, M., Wanner, B. L., Mori, H. (2006)
Construction of *Escherichia coli* K-12 in-frame, single-gene knockout mutants: the Keio collection.
Molecular Systems Biology 2, 2006.0008

Baruah, A., Lindsey, B., Zhu, Y., Nakano, M. M. (2004)
Mutational Analysis of the Signal-Sensing Domain of ResE Histidine Kinase from *Bacillus subtilis*.
J. Bacteriol. 186: 1694-1704

Berg, H.C. and Turner, L. (1995)
Cells of *Escherichia coli* swim either end forward.
Proc. Natl. Acad. Sci. USA. 92, 477-479

Billinton, N. and Knight, A. W. (2001)
Seeing the Wood through the Trees: A Review of Techniques for Distinguishing Green Fluorescent Protein from Endogenous Autofluorescence.
Anal. Biochem. 291: 175-197

Blomfield, I.C., Vaughn, V., Rest, R.F., Eisenstein, B.I. (1991)
Allelic exchange in *Escherichia coli* using the *Bacillus subtilis* sacB gene and a temperature-sensitive pSC101 replicon.
Mol. Microbiol. 5: 1447-1457

Bott, M. (1997)
Anaerobic citrate metabolism and its regulation in enterobacteria.
Arch. Microbiol. 167: 78-88

Bradford, M. (1976)
A rapid and sensitive method for the quantitation of microgram quantities of protein utilizing the principles of protein-dye binding.
Anal. Biochem. 72: 248-254

Bryson, K., McGuffin, L.J., Marsden, R.L., Ward, J.J., Sodhi, J.S., and Jones, D.T. (2005)
Protein structure prediction servers at University College London.
Nucleic Acids Res. 33 (Web Server Issue), W36-38

Chang, A. C. Y. and Cohen, S. N. (1978)
Construction and characterization of amplifiable multicopy DNA cloning vehicles derived from the p15A cryptic miniplasmid.
J. Bacteriol. 134: 1141-1156

Cheung, J., Bingman, C.A., Reyngold, M.R., Hendrickson, W.A., and Waldburger, C.D. (2008)
Crystal Structure of a Functional Dimer of the PhoQ Sensor Domain.
J. Biol. Chem. 283(20), 13762-13770

Cheung, J. and Hendrickson, W. A. (2008)
Crystal Structures of C_4-Dicarboxylate Ligand Complexes with Sensor Domains of Histidine Kinases DcuS and DctB.
J. Biol. Chem. 283: 30256-30265

Cho, U.S., Bader, M.W., Amaya, M.F., Daley, M.E., Klevit, R.E., Miller, S.I., and Xu, W. (2006)
Metal bridges between the PhoQ sensor domain and the membrane regulate transmembrane signaling.
J. Mol. Biol. 356, 1193-1206

Cotter, P., Emerson, N., Gahan, C.G.M., and Hill, C. (1999)
Identification and disruption of *lisRK*, a genetic locus encoding a two-component signal transducing system involved in stress tolerance and virulence in *Listeria monocytogenes*.
J. Bacteriol. 181, 6840-6843

Cotter, P.D., Guinane, C., Hill C (2002)
The LisRK signal transduction system determines the sensitivity of *Listeria monocytogenes* to nisin and cephalosporins.
Antimicrob Agents Chemother 46: 2784-2790

Cronan, J.E. (2003)
Bacterial membrane lipids: where do we stand?
Annu Rev Microbiol 57: 203-224

Datsenko, K.A. and Wanner, B.L. (2000)
One-step inactivation of chromosomal genes in *E. coli* K-12 using PCR products.
PNAS 97: 6640-6645

de Pedro, M. A., Grunfelder, C. G., and Schwarz, H. (2004)
Restricted mobility of cell surface proteins in the polar regions of *Escherichia coli*.
J Bacteriol 186, 2594-2602

Doan, T., Servant, P., Tojo, S., Yamaguchi, H., Lerondel, G., Yoshida, K.-I., Fujita, Y. and Aymerich, S. (2003)
The *Bacillus subtilis ywkA* gene encodes a malic enzyme and its transcription is activated by the YufL/YufM two-component system in response to malate.
Microbiology 149: 2331-2343

Dower, W. J., Miller, J. F., and Ragsdale, C. W. (1988)
High efficiency transformation of *E. coli* by high voltage electroporation.
Nucleic Acids Res 16, 6127-6145

Dowhan, W. (1997)
Molecular basis for membrane phospholipid diversity: why are there so many lipids?
Annu Rev Biochem 66: 199-232

Draheim, R.R., Bormans, A.F., Lai, R.Z., and Manson, M.D. (2006)
Tuning a bacterial chemoreceptor with protein-membrane interactions.
Biochemistry 45, 14655-14664

Drepper, T., Eggert, T., Circolone, F., Heck, A., Krauß, U., Guterl, J.-K., Wendorff, M., Losi, A., Gärtner, W., and Jaeger, K.-E. (2007)
Reporter proteins for *in vivo* fluorescence without oxygen.
Nat. Biotechnol. 25: 443-445

Drew. D.E., von Heijne, G., Nordlund, P., de Gier, J.W. (2001)
Green fluorescent protein as an indicator to monitor membrane protein overexpression in *Escherichi coli*.
FEBS Lett. 507: 220-224

Dubrac, S., Bisicchia, P., Devine, K.M., and Msadek, T. (2008)
A matter of life and death: cell wall homeostasis and the WalKR (YycGF) essential signal transduction pathway.
Mol. Microbiol. 70, 1307-1322

Eldakak, A. and Hulett, F. M. (2007)
Cys303 in the histidine kinase PhoR is crucial for the phosphotransfer reaction in the PhoPR two-Component system in *Bacillus subtilis*.
J. Bacteriol. 189: 410-421

Emami, K., Topaskas, E., Nagy, T., Henshaw, J., Jackson, K.A., Nelson, K.E., Mongodin, E.F., Murray, J.W., Lewis, R.J., and Gilbert, H.J. (2009)
Regulation of the xylan degrading apparatus of *Cellvibrio japonicus* by a novel two-component system.
J. Biol. Chem. 284(2):1086-96. Epub 2008 Oct 15

Erker, W., Sdorra, S., and Basché, T. (2005)
Detection of single oxygen molecules with fluorescence-labeled hemocyanins.
J Am Chem Soc 127, 14532-14533

Etzkorn, M., Kneuper, H., Dünnwald, P., Vijayan, V., Krämer, J., Griesinger, C., Becker, S., Unden, G. and Baldus, M. (2008)
Plasticity of the PAS domain and a potential role for signal transduction in the histidine kinase DcuS.
Nat. Struct. Mol. Biol. 15: 1031-1039

Farinha, M. A. and Kropinski, A. M. (1990)
High efficiency electroporation of *Pseudomonas aeruginosa* using frozen cell suspensions.
FEMS Microbiol. Lett. 58: 221-225

Filippou, P.S., Kasemian, L.D., Panagiotidis, C.A., and Kyriakidis, D.A. (2008)
Functional characterization of the histidine kinase of the *E. coli* two-component signal transduction system AtoS-AtoC.
Biochim. Biophys. Acta. 1780, 1023-1031

Fukushima, T., Szurmant, H., Kim, E.J., Perego, M., and Hoch, J.A. (2008)
A sensor hiostidine kinase co-ordinates cell wall architecture with cell division in *Bacillus subtilis*.
Mol. Microbiol. 69, 621-632

Galperin, M.Y., Nikolskaya, A.N., and Koonin, E.V. (2001)
Novel domains of the prokaryotic two-component signal transduction systems.
FEMS Microbiol. Lett. 203, 11-21

Gao, R. and Stock, A. M. (2009)
Biological insights from structures of two-component proteins.
Annu. Rev. Microbiol. 63: 133-54

Gay, P., LeCoq, D., Steinmetz, M., Ferrari, E., and Hoch, J. A. (1983)
Cloning structural gene *sacB*, which codes for exoenzyme levansucrase of *Bacillus subtilis*: expression of the gene in *Escherichia coli*.
J. Bacteriol. 153: 1424-1431

Golby, P., Kelly, D. J., Guest, J. R. and Andrews, S. C. (1998)
Transcriptional regulation and organization of the *dcuA* and *dcuB* genes, encoding homologous anaerobic C_4-dicarboxylate transporters in *Escherichia coli*.
J. Bacteriol. 180(24):6586-6596

Golby, P., Davies, S., Kelly, D. J., Guest, J. R., Andrews, S. C. (1999)
Identification and characterization of a two-component sensor-kinase and response-regulator system (DcuS-DcuR) controlling gene expression in response to C_4-dicarboxylates in *Escherichia coli*.
J. Bacteriol. 181: 1238-1248

Gordon, G. W., Berry, G., Liang, X. H., Levine, B., Herman, B. (1998)
Quantitative fluorescence resonance energy transfer measurements using fluorescence microscopy.
Biophys J 74(5): 2702-2713

Graf, S. (Diplomarbeit 2009)
Der Fumaratsensor DcuS aus *Geobacillus kaustophilus*.
Johannes Gutenberg-Universität, Mainz

Guzman, L.-M., Belin, D., Carson, M. J., Beckwith J. (1995)
Tight Regulation, Modulation, and High-Level Expression by Vectors Containing the Arabinose pBAD Promoter.
J. Bacteriol. 177: 4121-4130

Heermann, R., Altendorf, K., Jung K. (1998)
The turgor sensor KdpD of *Escherichia coli* is a homodimer.
Biochim. Biophys Acta 1415: 114-124

Holloway, P.W. (1973)
A simple procedure for removal of Triton X-100 from protein samples.
Anal. Biochem. 53: 304-308

Hulko, M., Berndt, F., Gruber, M., Linder, J.U., Truffault, V., Schultz, A., Martin, J., Schultz, J.E., Lupas, A.N., and Coles, M. (2006)
The HAMP domain structure implies helix rotation in transmembrane signaling.
Cell. 126, 929-940

Ingmer, H., Miller, C. A., and Cohen, S. N. (1998)
Destabilized inheritance of pSC101 and other *Escherichia coli* plasmids by DpiA, a novel two-component system regulator
Mol. Microbiol. 29 (1): 49-59

Ishiguro, N. and Sato, G. (1985)
Nucleotide sequence of the gene determining plasmid-mediated citrate utilization.
J Bacteriol 164: 977-982

Iuchi, S. and Lin, E. C. C. (1988)
arcA (*dye*), a global regulatory gene in *Escherichia coli* mediating repression of enzymes in aerobic pathways.
Proc Natl Acad Sci USA 85:1888-1892

Iuchi, S., Cameron, D.C. and Lin, E.C.C. (1989)
A second global regulatory gene (*arcB*) mediating repression of enzymes in aerobic pathways of *Escherichia coli*.
J. Bacteriol. 171: 868-873

Janausch, I. G., Garcia-Moreno, I., Unden G. (2002)
Function of DcuS from *Escherichia coli* as a Fumarate-stimulated Histidine Protein Kinase *in vitro*.
J. Biol. Chem. 277: 39809-14

Jensen, K. F. (1993)
The *Escherichia coli* K-12 'wild types' W3110 and MG1655 have an *rph* frameshift mutation that leads to pyrimidine starvation due to low *pyrE* expression levels.
J. Bacteriol. 175:3401-3407

Jones, D.T. (1999)
Protein secondary structure prediction based on position-specific scoring matrices.
J. Mol. Biol. *292*, 195-202

Kaspar, S., Bott, M. (2002)
The sensor kinase CitA (DpiB) of *Escherichia coli* functions as a high-affinity citrate receptor.
Arch. Microbiol. 177: 313-321

Kentner, D., Thiem, S., Hildenbeutel, M., and Sourjik, V. (2006)
Determinants of chemoreceptor cluster formation in *Escherichia coli*.
Mol Microbiol 61, 407-417

Kentner, D. and Sourjik, V. (2006)
Spatial organization of the bacterial chemotaxis system.
Curr. Opin. Microbiol. 9, 1-6

Khorchid, A., Inouye, M., and Ikura, M. (2005)
Structural characterization of *Escherichia coli* sensor histidine kinase EnvZ: the periplasmic C-terminal core domain is critical for homodimerization.
Biochem. J. 385: 255-264

Kishii, R., Falzon, L., Yoshida, T., Kobayashi, H., and Inouye, M. (2007)
Structural and functional studies on the HAMP domain of EnvZ, an osmosensing transmembrane histidine kinase in *Escherichia coli*.
J. Biol. Chem. *282*, 26401-26408

Kleefeld, A. (Dissertation 2006)
Der Carrier DcuB als zweiter Sensor des Zweikomponentensystems DcuSR in *Escherichia coli*.
Johannes Gutenberg-Universität, Mainz

Kneuper, H., Janausch, I. G., Vijayan, V., Zweckstetter, M., Bock V., Griesinger, C., Unden, G. (2005)
The Nature of the Stimulus and of the Fumarate Binding Site of the Fumarate Sensor DcuS of *Escherichia coli.*
J. Biol. Chem. 280 (21): 20596-20603

Kneuper, H. (Dissertation 2005)
Struktur- und Funktionsuntersuchungen des C_4-Dicarboxylat-Sensors DcuS von *Escherichia coli.*
Johannes Gutenberg-Universität, Mainz

Kneuper, H., Scheu, P., Etzkorn, M., Sevvana, M., Dünnwald, P., Becker, S., Baldus, M., Griesinger, C., Unden, G. (2010)
Sensing ligands by periplasmic sensing histidine kinases with sensory PAS domains.
Book chapter. Editor: S. Spiro (in press)

Krämer, J., Fischer, J., Zientz, E., Vijayan, V., Griesinger, C., Lupas, A., Unden, G. (2007)
Citrate sensing by the C_4-dicarboxylate/citrate sensor kinase DcuS of *Escherichia coli*: binding site and conversion of DcuS to a C_4-dicarboxylate- or citrate-specific sensor.
J. Bacteriol. 189(11):4290-4298

Kulzer, F., Koberling, F., Christ, T., Mews, A., and Basché, T. (1999)
Terrylene in p-terphenyl: single-molecule experiments at room temperature.
Chem Phys 247, 23-34

Laemmli, U. K. (1970)
Cleavage of structural proteins during the assembly of the head of bacteriophage T4.
Nature 227: 680-685

Lai, W.C., Beel, B.D., and Hazelbauer, G.L. (2006)
Adaptional modification and ligand occupancy have opposite effects on positioning of the transmembrane signalling helix of a chemoreceptor.
Mol. Microbiol. 61, 1081-1090

Lakowicz, J. R. (2006)
Principles of Fluorescence Spectroscopy.
3rd Plenum, New York, 2006

Liao, Y.-F. (Dissertation 2008)
Oligomerization and Protein-Protein Interactions of the Sensory Histidine Kinase DcuS in *Escherichia coli*.
Johannes Gutenberg-Universität, Mainz

Liberman, L., Berg, H. C., and Sourjik, V. (2004)
Effect of chemoreceptor modification on assembly and activity of the receptor-kinase complex in *Escherichia coli*.
J Bacteriol 186, 6643-6646

Lütgens, M. and Gottschalk, G. (1980)
Why a co-substrate is required for anaerobic growth of *Escherichia coli* on citrate.
J. Gen. Microbiol. 119:63–70

Lybarger, S. R. and Maddock, J. R. (2000)
Differences in the polar clustering of the high- and low-abundance chemoreceptors of *Escherichia coli*.
Proc Natl Acad Sci USA 97, 8057-8062

Maier, K.S., Hubich, S., Liebhart, H., Krauss, S., Kuhn, A., and Facey, S.J. (2008)
An amphiphilic region in the cytoplasmic domain of KdpD is recognized by the signal recognition particle and targeted to the *Escherichia coli* membrane.
Mol. Microbiol. 68: 1471-1484

Margolin, W. (2000)
Green fluorescent protein as a reporter for macromolecular localization in bacterial cells.
Methods 20, 62-72

Mascher, T., Helmann, J.D., and Unden, G. (2006)
Stimulus perception in bacterial signal transducing histidine kinases.
Microbiol. Mol. Biol. Rev. 70, 910-938

Matsumoto, K. (2001)
Dispensable nature of phosphatidylglycerol in *Escherichia coli*: dual roles of anionic phospholipids.
Mol Microbiol 39: 1427-1433

Matsumoto, K., Kusaka, J., Nishibori, A., and Hara, H. (2006)
Lipid domains in bacterial membranes.
Mol Microbiol 61, 1110-1117

Maier, K.S., Hubich, S., Liebhart, H., Krauss, S., Kuhn, A., and Facey, S.J. (2008)
An amphiphilic region in the cytoplasmic domain of KdpD is recognized by the signal recognition particle and targeted to the *Escherichia coli* membrane.
Mol. Microbiol. 68: 1471-1484

Meile, J.C., Wu, L.J., Ehrlich, S.D., Errington, J. and Noirot, P. (2006)
Systematic localisation of proteins fused to the green fluorescent protein in *Bacillus subtilis:* Identification of new proteins at the DNA replication factory.
Proteomics 6, 2135-2146

Meyer, B.H., Segura, J.-M., Martinez, K.L., Hovius, R., George, N., Johnsson, K., and Vogel, H. (2006)
FRET imaging reveals that functional neurokinin-1 receptors are monomeric and reside in membrane microdomains of live cells.
Proc. Natl. Acad. Sci. USA 103: 2138-2143

Mileykovskaya, E., and Dowhan, W. (2000)
Visualization of phospholipid domains in *Escherichia coli* by using the cardiolipin-specific fluorescent dye 10-*N*-nonyl acridine orange.
J Bacteriol 182: 1172-1175

Miller, J. H. (1992)
A short course in bacterial genetics.
Cold Spring Harbor Laboratory, Cold Spring Harbor, N.Y.

Miroux, B. and Walker, J. E. (1996)
Over-production of proteins in *Escherichia coli*: mutant hosts that allow synthesis of some membrane proteins and globular proteins at high levels.
J. Mol. Biol. 260, 289-298

Müller, M. (Diplomarbeit 2007)
Funktionskomplementierung des Fumaratsensors DcuS von *Escherichia coli* durch Hybriddimere.
Johannes Gutenberg-Universität, Mainz

Mullis, K. B., Farone, F. A., Schar, S., Saiki, R., Horn, G., and Ehrlich, H. (1986)
Specific amplification of DNA *in vitro*: the polymerase chain reaction.
Cold Spring Harbor Symp. Quant. Biol. 51:263-273

Münch, R., Hiller, K., Grote, A., Scheer, M., Klein, J., Schobert, M., and Jahn, D. (2005)
Virtual footprint and PRODORIC: an integrative framework for regulon prediction in prokaryotes
Bioinformatics 21 (22): 4187-4189

Neiditch, M.B., Federle, M.J., Miller, S.T., Bassler, B.L., and Hughson, F.M. (2005)
Regulation of LuxPQ receptor activity by the quorum-sensing signal autoinducer-2.
Molecular Cell. 18, 507-518

Neiditch, M. B., Federle, M. J., Pompeani, A. J., Kelly, R. C., Swem, D. L., Jeffrey, P. D., Bassler, B. L., Hughson, F. M. (2006)
Ligand-induced asymmetry in histidine sensor kinase complex regulates quorum sensing.
Cell 126(6):1095-108

Novick, R. P. (1987)
Plasmid Incompatibility.
Microbiol. Rev. 51: 381-395

Ormö, M.; Cubitt, A. B.; Kallio, K.; Gross, L. A.; Tsien, R. Y., and Remington, S. J. (1996)
Crystal structure of the Aequorea victoria green fluorescent protein.
Science 273: 1392-1395

Ottemann, K.M., Thorgeirsson, T.E., Kolodziej, A.F., Shin, Y.K., and Koshland, D.E. (1998)
Direct measurement of small ligand-induced conformational changes in the aspartate chemoreceptor using EPR
Biochemistry 37 (20): 7062-7069

Ottemann, K.M., Xiao, W., Shin, Y.K., and Koshland, D.E. Jr. (1999)
A piston model for transmembrane signalling of the aspartate receptor.
Science. 285, 1751-1754

Pan, S. Q., Charles, T., Jin S., Wut, Z.-L., Nester; E. W. (1993)
Preformed dimeric state of the sensor protein VirA is involved in plant-*Agrobacterium* signal transduction.
Microbiol. Proc. Natl. Acad. Sci. 90: 9939-9943

Pappalardo, L., Janausch, I. G., Vijayan, V., Zientz, E., Junker, J., Peti, W., Zweckstetter, M., Unden, G., Griesinger, C. (2003)
The NMR structure of the sensory domain of the membranous two-component fumarate sensor (histidine protein kinase) DcuS of *Escherichia coli*.
J. Biol. Chem. 278: 39185-8

Paternostre, M.-T., Roux, M. and Rigaud, J.-L. (1988)
Mechanisms of membrane protein insertion into liposomes during reconstitution procedures involving the use of detergents. 1. Solubilization of large unilamellar liposomes (prepared by reverse-phase evaporation) by Triton X-100, octyl glucoside and sodium cholate.
Biochemistry 27:2668-2677

Patterson, G. H., Piston, D. W., Barisas, B. G. (2000)
Forster distances between green fluorescent protein pairs.
Anal Biochem 284: 438-440

Patterson, G., Day, R. N., Piston, D.
Fluorescent protein spectra (2001)
J. Cell Sci. 114: 837-838

Paul, R., Jaeger, T., Abel, S., Wiederkehr, I., Folcher, M., Biondi, E.G., Laub, M.T., and Jenal, U. (2008)
Allosteric regulation of histidine kinases by their cognate response regulator determines cell fate.
Cell 133, 452-461

Philippe, N., Alcaraz, J. P., Coursange, E., Geiselmann, J., and Schneider, D. (2004)
Improvement of pCVD442, a suicide plasmid for gene allele exchange in bacteria.
Plasmid 51: 246-255

Ponting, C.P. and Aravind, L. (1997)
PAS: a multifunctional domain family comes to light.
Curr. Biol. 7, R674-R677

Qin, L., Dutta, R., Kurokawa, H., Ikura, M., Inouye, M. (2000)
A monomeric histidine kinase derived from EnvZ, an *Escherichia coli* osmosensor.
Mol. Microbiol. 36: 24-32

Rauschmeier, M. (Diplomarbeit 2009)
Citratregulation in *Escherichia coli*.
Johannes Gutenberg-Universität, Mainz

Reid, C. J. and Poole, P. S. (1998)
Roles of DctA and DctB in signal detection by the dicarboxylic acid transport system of *Rhizobium leguminosarum*.
J. Bacteriol. 180: 2660-2669

Reinelt, S., Hofmann, E., Gerharz, T., Bott, M., Madden, D. R., (2003)
The structure of the periplasmic ligand-binding domain of the sensor kinase CitA reveals the first extracellular PAS domain.
J. Biol. Chem. 278: 39189-39196

Rigaud, J.-L., Paternostre, M.-T. and Bluzat, A. (1988)
Mechanisms of membrane protein insertion into liposomes during reconstitution procedures involving the use of detergents. 2. Incorporation of the light-driven proton pump bacteriorhodopsin.
Biochemistry 2:2677-2688

Rigaud, J.-L., Pitard, B. and Levy, D. (1995)
Reconstitution of membrane proteins into liposomes: application to energytransducing membrane proteins.
Biochim. Biophys. Acta 1231:223-246

Romantsov, T., Helbig, S., Culham, D. E., Gill, C., Stalker, L., and Wood, J. M. (2007)
Cardiolipin promotes polar localization of osmosensory transporter ProP in *Escherichia coli*.
Mol. Microbiol. 64: 1455-1465

Romantsov, T., Stalker, L., Culham, D.E., and Wood, J.M. (2008)
Cardiolipin Controls the Osmotic Stress Response and the Subcellular Location of Transporter ProP in *Escherichia coli*.
J. Biol. Chem. 283: 12314-12323

Sambrook, J. and Russel, D.W. (2001)
Molecular cloning: A Laboratory Manual (Third Edition), Volume 3
Cold Spring Harbor Laboratory Press, New York

Sasatsu, M., Misra, T.K., Chu, L., Laddaga, R., Silver, S. (1985)
Cloning and DNA sequence of a plasmid-determined citrate utilization system in *Escherichia coli*.
J Bacteriol 164: 983-993

Scheu, P. (Diplomarbeit 2005)
Der Fumaratsensor DcuS von *Escherichia coli*.
Johannes Gutenberg-Universität, Mainz

Scheu, P., Sdorra, S., Liao, Y.-F., Wegner, M., Basché, T., Unden, G., Erker, W. (2008)
Polar accumulation of the metabolic sensory histidine kinases DcuS and CitA in *Escherichia coli*.
Microbiology 154: 2463-2472

Sciara, M.I., Spagnuolo, C., Jares-Erijman, E., and Garcia Véscovi, E. (2008)
Cytolocalization of the PhoP response regulator in *Salmonella enterica*: modulation by extracellular Mg^{2+} and by the SCV environment.
Mol. Microbiol. 70, 479-493

Sevvana, M., Vijayan, V., Zweckstetter, M., Reinelt, S., Madden, D. R., Herbst-Irmer, R., Sheldrick, G. M., Bott, M., Griesinger, C. (2008)
A Ligand-Induced Switch in the Periplasmic Domain of Sensor Histidine Kinase CitA.
J. Mol. Biol. 377: 512-523

Shapiro, L., McAdams, H.H., and Losick, R. (2002)
Generating and exploiting polarity in bacteria.
Science 298, 1942-1946

Shaw, D.J. and Guest, J.R. (1982)
Nucleotide sequence of the *fnr* gene and primary structure of the Fnr protein of *Escherichia coli*.
Nucl. Acids Res. 10: 6119-6230

Shiomi, D., Yoshimoto, M., Homma, M., Kawagishi, I. (2006)
Helical distribution of the bacterial chemoreceptor via colocalization with the Sec protein translocation machinery.
Mol. Microbiol. 60: 894-906

Silhavy, T.J., Berman, M.L., Enquist, L.W. (1984)
Experiments with Gene Fusions.
Cold Spring Harbor Laboratory Press, Cold Spring Harbor, NY.

Sourjik, V. and Berg, H.C. (2000)
Localization of components of the chemotaxis machinery of *Escherichia coli* using fluorescent protein fusions.
Mol. Microbiol. 37, 740-751

Sourjik, V. (2004)
Receptor clustering and signal processing in *E. coli* chemotaxis.
Trends Microbiol 12, 569-576

Stewart, V. (1993)
Nitrate regulation of anaerobic respiratory gene expression in *Escherichia coli*.
Mol. Microbiol. 9: 425-434

Studier, F.W. and Moffatt, B.A. (1986)
Use of bacteriophage T7 RNA polymerase to direct selective high-level expression of cloned genes.
J. Mol. Biol. 189: 113-130

Szurmant, H., Bu, L., Brooks III, C.L., and Hoch, J.A. (2008)
An essential sensor histidine kinase controlled by transmembrane helix interactions with its auxiliary proteins.
Proc. Natl. Acad. Sci. U.S.A. 105, 5891-5896

Taylor, B. L. and Zhulin, I. B. (1999)
PAS domains: internal sensors of oxygen, redox potential, and light.
Microbiol. Mol. Biol. Rev. 63: 479-506

Thiem, S., Kentner, D., and Sourjik, V. (2007)
Positioning of chemosensory clusters in *E. coli* and its relation to cell division.
EMBO J 26, 1615-1623

Thiem, S. and Sourjik, V. (2008)
Stochastic assembly of chemoreceptor clusters in *Escherichia coli*.
Mol. Microbiol. 68, 1228-1236

Towbin, H., Staehelin, T. and Gordon, J. (1979)
Electrophoretic transfer of proteins from polyacrylamide gels to nitrocellulose sheets: procedure and some applications.
Proc. Natl. Acad. Sci. USA 76: 4350-4354

Truong, K. and Ikura, M. (2001)
The use of FRET imaging microscopy to detect protein–protein interactions and protein conformational changes *in vivo.*
Struc. Biol. 11: 573-578

Tseng, C.P. (1997)
Regulation of fumarase (*fumB*) gene expression in *Escherichia coli* in response to oxygen, iron and heme availability: role of the *arcA, fur* and *hemeA* gene products.
FEMS Microbiology Letters 157: 67-72

Tsien, R.Y. (1998)
The Green Fluorescent Protein.
Annu. Rev. Biochem. 67: 509-544

Vileno, B., Lekka, M., Sienkiewicz, A., Marcoux, P., Kulik, A.J., Kasas, S., Catsicas, S., Graczyk, A., and Forró,L. (2005)
Singlet oxygen (1∆g)-mediated oxidation of cellular and subcellular components: ESR and AFM assays.
J. Phys. Condens. Matter 17: 1471-1482

Walz, A.-Ch, Demel, R.A., de Kruijff, B., and Mutzel, R. (2002)
Aerobic *sn*-glycerol-3-phosphate dehydrogenase from *Escherichia coli* binds o the cytoplasmic membrane through an amphipathic α-helix.
Biochem J 365: 471-479

West, A. H. and Stock, A. M. (2001)
Histidine kinases and response regulator proteins in two-component signaling systems.
T. Biochem. Scien. 26 No.6

Wolanin, P.M. and Stock, J.B. (2003)
Transmembrane signalling and the regulation of histidine kinase activity. In: Inouye, M., and Dutta, R. (eds). Histidine kinases in signal transduction.
Academic Press, San Diego, Calif., pp. 73-122

Yamamoto, H., Murata, M. and Sekiguchi, J. (2000)
The CitST two-component system regulates the expression of the Mg-citrate transporter in *Bacillus subtilis*.
Mol. Microbiol. 37: 898-912

Yamamoto, K., Hirao, K., Oshima, T., Hirofumi, A., Ryutaro, U., Ishihama, A. (2005)
Functional characterization *in vitro* of all two-component signal transduction systems from *Escherichia coli*.
J. Biol. Chem. 280: 1448-1456

Yamamoto, K., Matsumoto, F., Oshima, T., Fujita, N., Ogasawara, N., Ishihama, A. (2008)
Anaerobic regulation of citrate fermentation by CitAB in *Escherichia coli*.
Biosci. Biotechnol. Biochem. 72: 3011-3014

Yang, Y. and Inouye, M. (1991)
Intermolecular complementation between two defective mutant signal-transducing receptors of *Escherichia coli*.
Biochem. Proc. NatI. Acad. Sci. 88:11057-11061

Yang, F., Moss, L. G., and Phillips, G. N. (1996)
The molecular structure of green fluorescent protein.
Nat Biotechnol 14: 1246-1251

Yanisch-Perron, C., Vieira, J., Messing, J. (1985)
Improved M13 phage cloning vectors and host strains: nucleotide sequences of the M13mp18 and pUC19 vectors.
Gene 33:103-19

Zhang, W. and Shi, L. (2005)
Distribution and evolution of multi-step phosphorelay in prokarytes: lateral domain recruitment involved in the formation of hybrid-type histidine kinases.
Microbiology. 151, 2159-2173

Zhou, Y.F., Nan, B., Nan, J., Ma, Q., Panjikar, S., Liang, Y.H., Wang, Y., and Su, X.D. (2008)
C_4-dicarboxylate sensing mechanisms, revealed by the crystal structures of DctB sensor domain.
J. Mol. Biol. 383, 49-61

Zientz, E., Bongaerts, J., Unden, G. (1998)
Fumarate regulation of gene expression in *Escherichia coli* by the DcuSR (*dcuSR* genes) two-component regulatory system.
J. Bacteriol. 180 (20): 5421-5425

Zientz, E. (Dissertation 2000)
Identifizierung und Charakterisierung des Fumaratregulationssystems DcuSR in *Escherichia coli.*
Johannes Gutenberg-Universität, Mainz

7. Publications and Presentations

Publications

Scheu, P., Sdorra, S., Liao, Y.-F., Wegner, M., Basché, T., Unden, G., Erker, W. (2008)
Polar accumulation of the metabolic sensory histidine kinases DcuS and CitA in *Escherichia coli*.
Microbiology 154: 2463-2472

Scheu, P., Liao, Y.-F., Bauer, J., Kneuper, H., Basché, T., Unden, G., Erker, W.
Tetrameric sensor kinase DcuS in the membrane of *Escherichia coli* and proteoliposomes: Chemical Crosslinking and FRET Spectroscopy.
Manuscript in preparation

Kneuper, H., Scheu, P., Etzkorn, M., Sevvana, M., Dünnwald, P., Becker, S., Baldus, M., Griesinger, C., Unden, G. (2010)
Sensing ligands by periplasmic sensing histidine kinases with sensory PAS domains.
Book chapter, Editor: S. Spiro (in press)

Posters

P. Scheu, W. Erker, Y.-F. Liao, S. Sdorra, T. Basché, G. Unden
Dimerization of the sensor kinase DcuS of *E. coli* in the membrane.
Annual Conference of VAAM, Jena, 2006; Poster prize

P. Scheu, W. Erker, S. Sdorra, Y.-F. Liao, T. Basché, G. Unden
Polar localization of the sensory histidine kinases DcuS and CitA in *E. coli*.
27th Symposium on Mechanisms of Gene Regulation, Jugendburg Ludwigstein, 2008

Talks

P. Scheu, W. Erker, Y.-F. Liao, S. Sdorra, T. Basché, G. Unden
Oligomerization and Localization of the Fumarate Sensor DcuS in *E. coli*.
26th Symposium on Mechanisms of Gene Regulation, Königswinter, 2006

P. Scheu, W. Erker, S. Sdorra, Y.-F. Liao, T. Basché, G. Unden
Polar Localization of the C_4-Dicarboxylate Sensor DcuS in *E. coli*.
Joint Annual Conference of VAAM and GBM, Frankfurt/Main, 2008